STUDIES OF THE EFFECTS OF ELECTROSTATIC FIELDS ON FLUID FLOWS

Henry R. Velkoff

Department of Mechanical Engineering

The Ohio State University
Aeronautical Foundation
Columbus, Ohio

Interim Summary Report
Report No. 10

DISTRIBUTION OF THIS DOCUMENT IS UNLIMITED

U. S. ARMY RESEARCH OFFICE - DURHAM
Box CM, Duke Station
Durham, North Carolina, 27706

Contract No. DA-31-124-ARO-D-446

DISCLAIMER

The views in this report are not to be construed as an official Department of the Army position unless so designated by other authorized documents.

The citation of trade names and names of manufacturers in this report is not to be construed as official Government endorsement or approval of commercial products or services referenced.

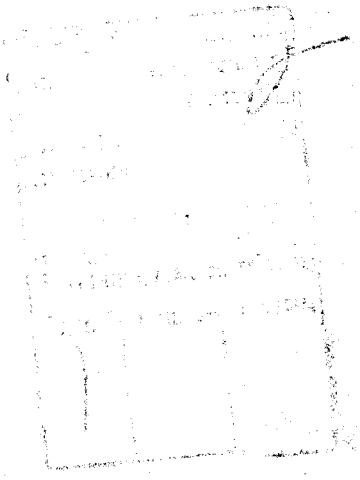

DISCLAIMER NOTICE

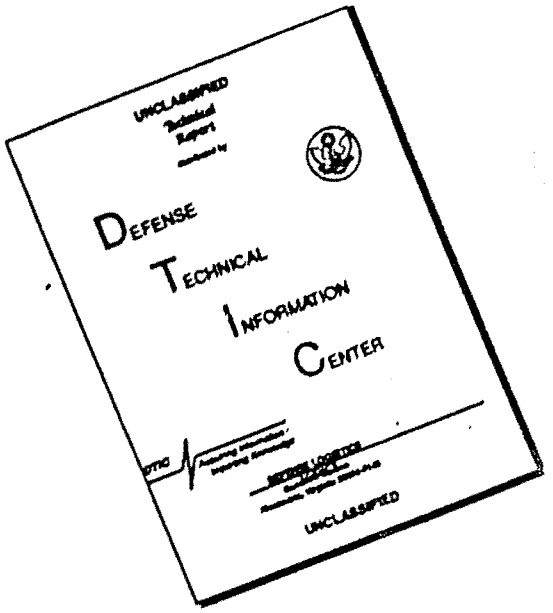

THIS DOCUMENT IS BEST QUALITY AVAILABLE. THE COPY FURNISHED TO DTIC CONTAINED A SIGNIFICANT NUMBER OF PAGES WHICH DO NOT REPRODUCE LEGIBLY.

STUDIES OF THE EFFECTS OF ELECTROSTATIC FIELDS ON FLUID FLOWS

Henry R. Velkoff

Department of Mechanical Engineering

The Ohio State University
Research Foundation
Columbus, Ohio

Interim Summary Report
Report No. 10

DISTRIBUTION OF THIS DOCUMENT IS UNLIMITED

U. S. ARMY RESEARCH OFFICE - DURHAM
Box CM, Duke Station
Durham, North Carolina, 27706

Contract No. DA-31-124-ARO-D-246

ABSTRACT

An overall review of studies of electrostatic interactions with fluid flows is presented. Review of prior studies involving ions with free convection, and channel flows is presented along with prior studies of field effects on condensation. The cause of large changes in laminar channel flow with ionization was studied both analytically and experimentally. The changes were determined to result from an electrically induced destabilization of the flow. External ion-flow boundary layer actions were studied and some influence on transition was found. Significant changes to frost formation and flame heat transfer under the action of an impressed E field were found. The possible use of ions injected into a gas stream as a flow diagnostic technique was explored and is considered a very logical area for future exploration.

TABLE OF CONTENTS

LIST OF FIGURES

LIST OF FIGURES (continued)

LIST OF FIGURES (continued)

LIST OF FIGURES (continued)

I. INTRODUCTION

This report presents a broad summary of the work that was conducted under the project sponsored by the U. S. Army Research Office - Durham. The specific area of investigation is the interaction of electrostatic fields on fluid flows and boundary layers. Since a broad range of interactions is possible, the scope of this report is wide, ranging from laminar channel flows through ion-diagnostic techniques.

The report itself presents some background material accomplished by the principal investigator prior to this program to indicate the overall continuity of effort in this particular field of endeavor. The report consists of several sections. Prior work is discussed in the sections on free convection, dielectrophoresis, condensation, and the initial work on channel flows. The more complete reports or papers summarizing each of these areas are listed in the references. The remaining work discussed herein was accomplished under this project with the exception of a portion of the ion-flow diagnostic tests. The use of ions as a diagnostic tool in the channel flow tests was done under this program, as well as the study and planning of the use of ion-flow diagnostics in external flow. The actual preliminary tests of the external flow diagnostics was accomplished by the principal investigator at the U. S. Army Aeronautical Research Laboratory, Moffett Field, California.

Specific work conducted under this program included an evaluation of the ion-channel flow interaction found, study of electrostatically induced secondary flows in channels, ion effects on external boundary layers using an interfereometer technique and also a traversing probe technique, electrostatic effects on flip-flop fluidic devices, effects of fields on flame heat transfer, and effects of fields on frost formation. The complete reports prepared on the above topics are indicated in the list of references.

II. BACKGROUND

A. TYPES OF ELECTROSTATIC FORCES

The study of the effects of electrostatic fields on fluid flows centers on the possible ways in which electrical-fluid interactions can exist. Two broad categories can be delineated, charge effects and nonuniform or gradient influences. In the first category fall all the usual coulomb force effects which depend on the existence of a free charge, and in the second category are more subtle influences in which gradients of properties of the fluid medium or the field are important. If one considers the body forces which can arise due to electrostatic effects, then the following equation depicts the body force[1]:

$$\bar{F} = \rho_c \bar{E}_{ext} + \tfrac{1}{2} \text{ grad } E^2 \rho \left[\left(\frac{\partial \epsilon}{\partial \rho}\right)_T\right] - \frac{E^2}{2} \text{ grad } \epsilon \qquad (1)$$

The charge force is the first term on the right hand side, and the nonuniform effects are given by the remaining two terms. In the case of a gas, the above relation assumes the more familar form:

$$\bar{F}_{gas} = \rho_c \bar{E}_{ext} + \left(\frac{\epsilon - \epsilon_0}{2}\right) \text{grad } E^2 \qquad (2)$$

The interesting term in Eq. (2) is the grad E^2. A similar term is found as an approximation in the case of liquids. The grad E^2 terms implies that a body force can exist on a electrically neutral fluid particle if a nonuniform electrical field exists. The other category of forces involved in electrostatics are the surface stresses due to a field and are of the form:

$$\sigma_n = \tfrac{1}{2} \epsilon E_n^2 \qquad (3)$$

The nature of the charge involved in the term $\rho_c \bar{E}$ of Eq. (1) (where ρ_c is the charge density) depends upon the medium as well as the means of generating the charge. That is, in an ordinary gas at low temperatures (below 1000°F) the ions will consist of those produced by external radiation, or impressed fields. They will include O_2 and N_2 ions in ordinary air as well as electrons. Existent impurities will also become charged and act as massive ions. In flames a host of nonequilibrium combustion ions are present including such specie as H_3O^+. In liquids the charged particles of importance to these studies generally are the impurities which exist as contaminants

in the liquid medium. Such impurities, (minute particles) can acquire a charge either because of induced ionization by an external field or through the natural double layer charging process familar to electrochemistry. When considering the charge effects on fluids one of the singularly most important factors is the mobility of the ions involved. Mobility is a measure of the rate at which a charged particle will move through a fluid under the action of an impressed field. Typically an electron has an extremely high mobility, whereas a charged colloid particle has a very low mobility. The mobility also serves as an indicator of the ability of a charged particle to couple with the fluid medium. An electron does not couple well with the fluid whereas the colloid ion does. Hence one can expect the interactions of electric fields with the fluids to be strongly dependent on the mobilities of the particles involved.

III. POSSIBLE INTERACTIONS

Based upon the nature of the electrostatic forces which can be exerted it is possible to hypothesize various fluid phenomena which could be affected by electrostatic fields or charges. The actions include the surfaces or interfaces of various liquids, change of phase such as boiling and condensation, boundary layer flows, convective heat transfer, flow attachment, and fluid orientation. Considerable study has been accomplished in the area of fluid surface effects by Melcher wherein he has shown that both liquid surfaces and streams can be destabilized using electrostatic fields.[2] The other possible interactions will be considered in greater detail in this report.

A particularly fascinating possibility which arises with these interactions is their use in fluid flow diagnostics. Since the ions have relatively little inertia, it is considered likely that they can be used as tracers to follow the fluid particles in the stream. Illustrations of the use of the ions in this fashion also are given later in this report.

A. EXPERIMENTAL FINDINGS

The electrostatic-fluid interactions which have been studied are grouped in areas of free convection, internal flows, external flows, flow attachment, change of phase, flame heat transfer, and ion-flow diagnostics.

1. Free Convection

The initial tests conducted to explore the possible use of the electrostatic fields on fluid flows were directed at studying the influences on free convection from a flat plate.[3] The test arrangement consisted of mounting an isothermally heated flat plate in a Mach Zehnder interferometer and stuyding the effects of various applied electrical actions. The particular arrangement was chosen to use a very sensitive instrument to observe small changes to a very sensitive phenomena, free convection. The arrangement is shown in Fig. 1, where the heated plate is shown along with a typical electrode. In this case the electrode was a single wire mounted horizontally at the center of the plate. Voltage was applied between the wire and the plate. In most runs the electrode was positive, but runs were also made with the heated plate positive. Figure 2 illustrates the action of the field on the thermal free convection boundary layer. It can readily be seen that as the corona current begins to flow, severe distortion to the thermal boundary layer occurs. At high currents the pattern is symmetrical about the centerline directly under the wire. It should be noted in each interferogram that the fine 0.004-inch corona wire is located

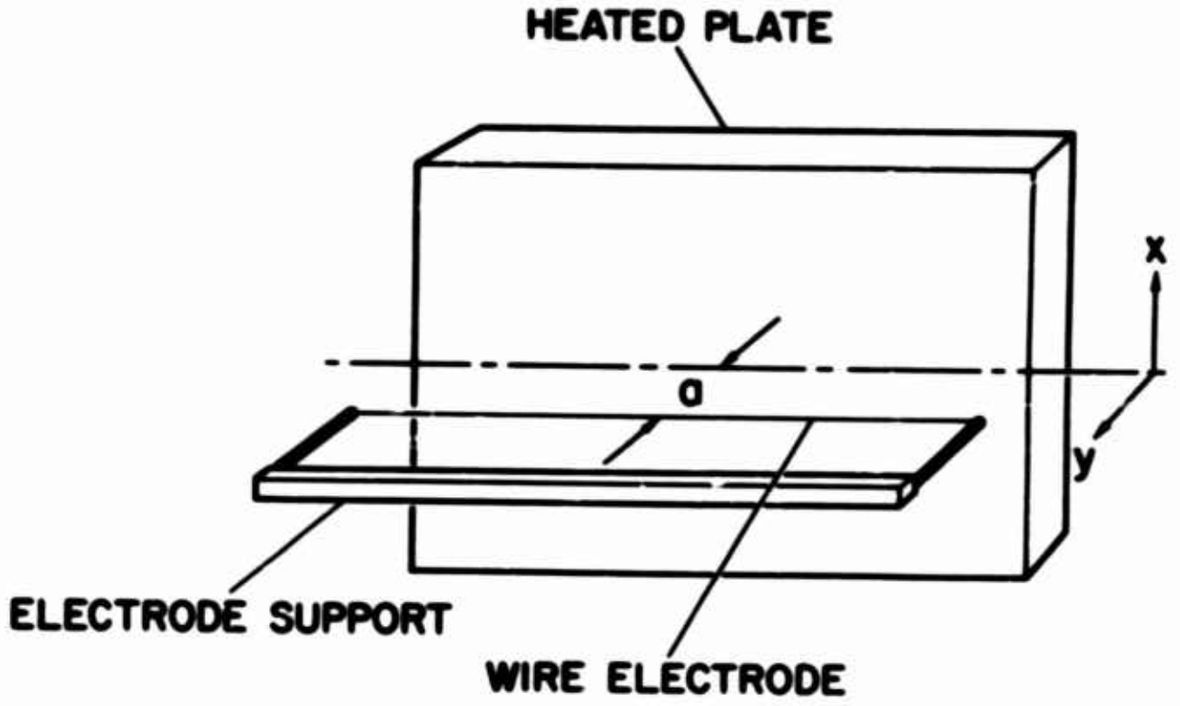

Fig. 1 - Plate and wire electrode schematic illustrating coordinates

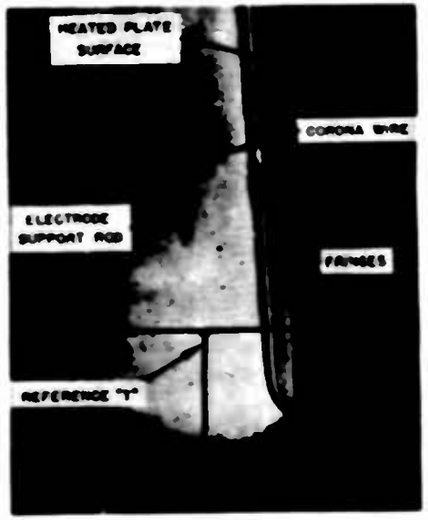

INTERFEROMETER PICTURE SHOWING VERTICAL HEATED PLATE WITH INTERFERENCE FRINGES AT RIGHT. NO APPLIED FIELD; 0.004 INCHES CORONA WIRE SPACED 2 cm FROM PLATE AT CENTERLINE.

VERTICAL PLATE; 2 cm SPACING; 5.8 kv, 1.85 MICROAMP

VERTICAL PLATE; 2 cm SPACING; 6.7 kv, 19.9 MICROAMP

Fig. 2

at the right end of the support rods which protrude from the lift side of the interferogram. The wire direction is perpendicular to the plane of the picture. On the right hand side the straight vertical dark surface is the heated plate and the interference fringes exist in front of the plate.

The severe distortions which were observed were considered to be due to the electric wind induced by the corona discharge. To test this hypothesis, runs were made with the plate in a horizontal position with the heated side facing down. Figure 3 illustrates the results. The wire is horizontal and is at the centerline 2 cm below the plate. The "T" shaped rod provides reference distance for data reduction. From this figure it can be seen that the severe distortion previously found is absent and a symmetric well-behaved pattern exists. It was concluded that the previous distortion was caused by the interaction of heated air up the plate with the corona wind flowing to the plate.

An analysis was conducted of the downward facing case, assuming the action was due to the electric wind. Using the electrostatic equations for the electric wind, and the momentum - integral method for the heat transfer analysis, an explicit solution was obtained,

$$p - p_\infty = \frac{2\epsilon \left(\frac{V}{2}\right)^2}{\left[\ln\left(\frac{2a}{r_a}\right)\right]^2}\left[1 + Z^2\right]^{-2} \qquad \text{electrostatic pressure eq.}$$

$$\frac{\partial}{\partial x}\int_0^\delta \rho u^2 dy - u_\infty \frac{\partial}{\partial x}\int_0^\delta \rho u dy \qquad \text{momentum eq.}$$

$$= \delta\frac{\partial p}{\partial y} - \mu\left(\frac{\partial u}{\partial y}\right)_{y=0}$$

$$\rho_\infty c_p\left[\frac{\partial}{\partial x}\int_0^{\delta_T} \rho u T dy - T_\infty \frac{\partial}{\partial x}\int_0^{\delta_T} \rho u dy\right] \qquad \text{energy eq.}$$

$$- \int_0^{\delta_T} u \frac{\partial p}{\partial x} dy = k_{\rho\infty}\left(\frac{\partial T}{\partial y}\right)_{y=0}$$

where $Z = x/a$ and r_a is the wire radius. The results are shown in Fig. 4 where reasonable agreement between theory and experiment is shown. The primary conclusion from this work is that the electrostatic actions are predictable and controllable.

HORIZONTALLY MOUNTED PLATE; NO APPLIED FIELD; 0.004 INCHES CORONA WIRE MOUNTED 2 cm BELOW CENTER-LINE OF PLATE.

HORIZONTAL PLATE; 2 cm SPACING WITH APPLIED FIELD; 5.0 kv, 1.05 MICROAMP.

Fig. 3 - Interferometer picture with horizontal plate

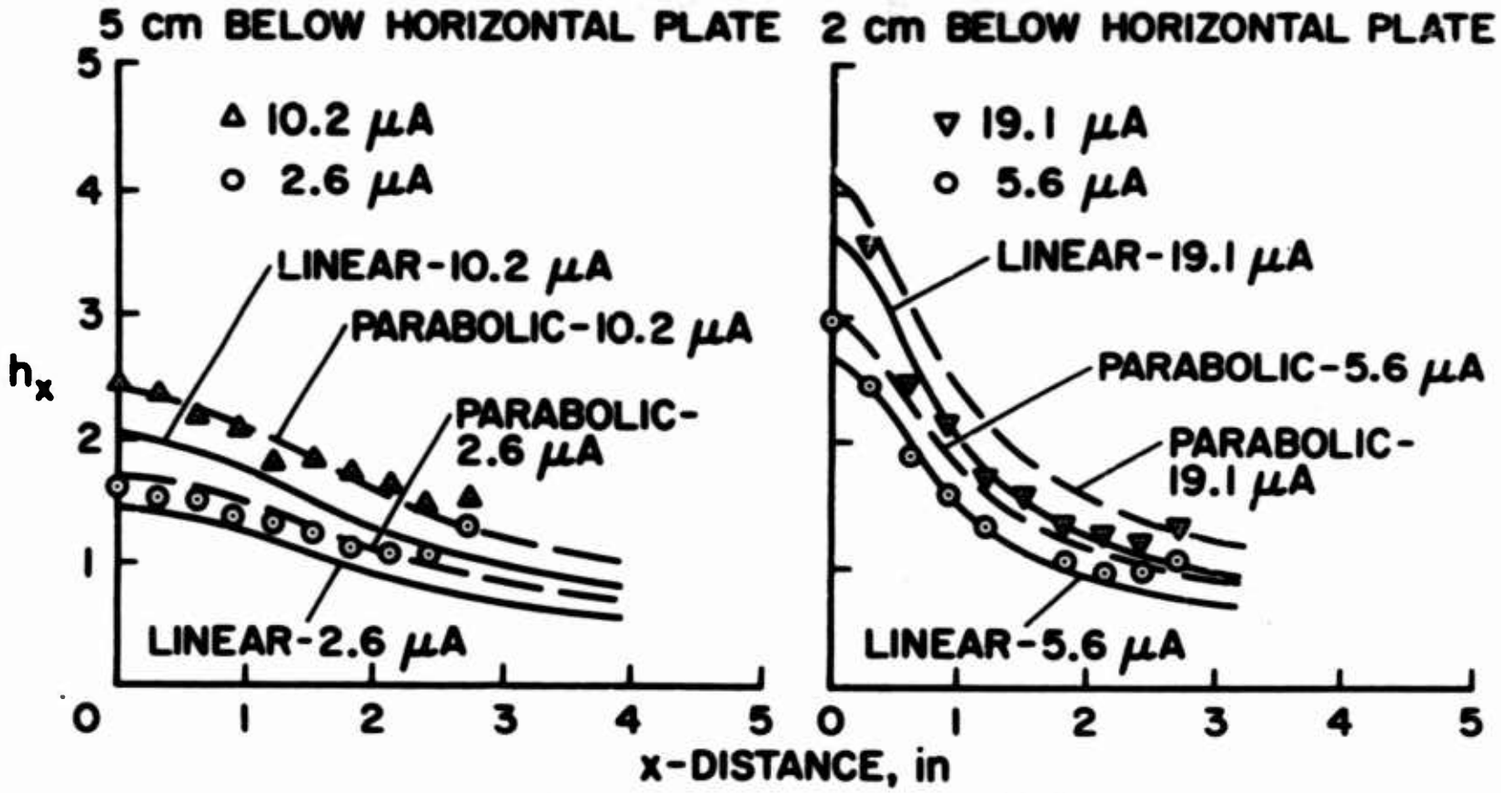

Fig. 4 - Comparison of test data with theory

Subsequent work in the area of free convection effects has been undertaken at the Air Force Institute of Technology and has been directed towards the actions of electric wind at low pressures and forced convective cells induced by electric wind.[4,5]

2. Dielectrophoresis

An exploratory study was made of the grad E^2 effects using a simulated zero gravity model.[3] Droplets of water were suspended at the interface of two nonconducting liquids. The arrangement is shown in Fig. 5. The central electrode just protrudes into the top of the liquid. The ground electrode is on the outside of the container. After the field (4,000 volts a.c.) is applied it can be seen that the final position of the water droplets is at the center electrode (Fig. 6). Thus the potential utility of the nonuniform field term is demonstrated. Work utilizing this principle has been carried out by various groups in an attempt to provide for "zero-G" fluid orientation.

3. Channel Flow

A fundamental aspect of a study of fluid flows is the influence of the viscous effects, leading, for example, to boundary layer flows. Because of the critical nature of boundary layers to practical fluid mechanic problems, study was initiated on the possible effects of electrostatic actions on viscosity and viscous flows. A simple experiment was conducted using channel gas flow in which ions were caused to flow transverse to the main stream in a radial direction.[6] The arrangement is shown in Fig. 7. Gas is passed into the plenum at the left, passes through the round channel and exhausts at the right. Pressure taps are located to measure the pressure drop in the channel. The ions are obtained by impressing a suitable voltage between the wire and the cylinder wall. Typical ion densities are 1×10^{10} ions per cubic centimeter in air at N.T.P. Results of the tests are presented in Fig. 8 where a typical friction factor-Reynolds number plot is presented. Although study of the ion-molecule interactions and the Navier Stokes equations had indicated only a very small influence of viscosity, the test results show that the friction factor has doubled in the laminar flow regime. The velocity profile associated with this action is shown in Fig. 9. At low Reynolds numbers the profile changes from a "modified parabolic" shape due to the presence of the corona wire and no ion flow to a profile which is similar to slug flow. It can be seen from a study of both figures that the ion influence tends to disappear in the turbulent regime. Heat transfer tests indicated an increase which corresponded to the increase in friction factor. The results implied an increase in effective viscosity similar to that reported for liquids with applied fields.[7,8]

4. Channel Flow-Approximate Analysis

If direct solution of all of the electrical field, current

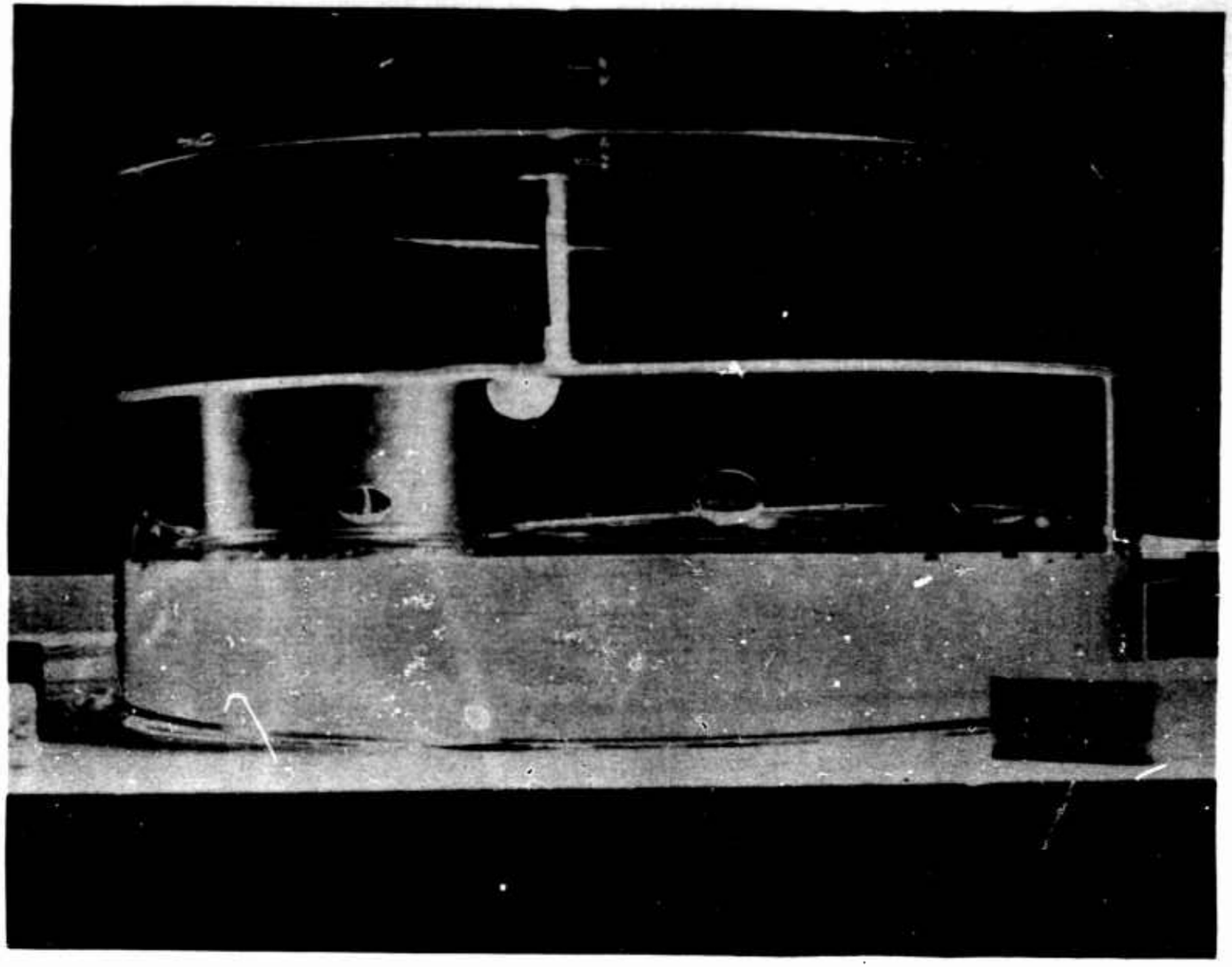

Fig. 5 - Dielectric influence on water droplets suspended in a nonconducting liquid. No applied field

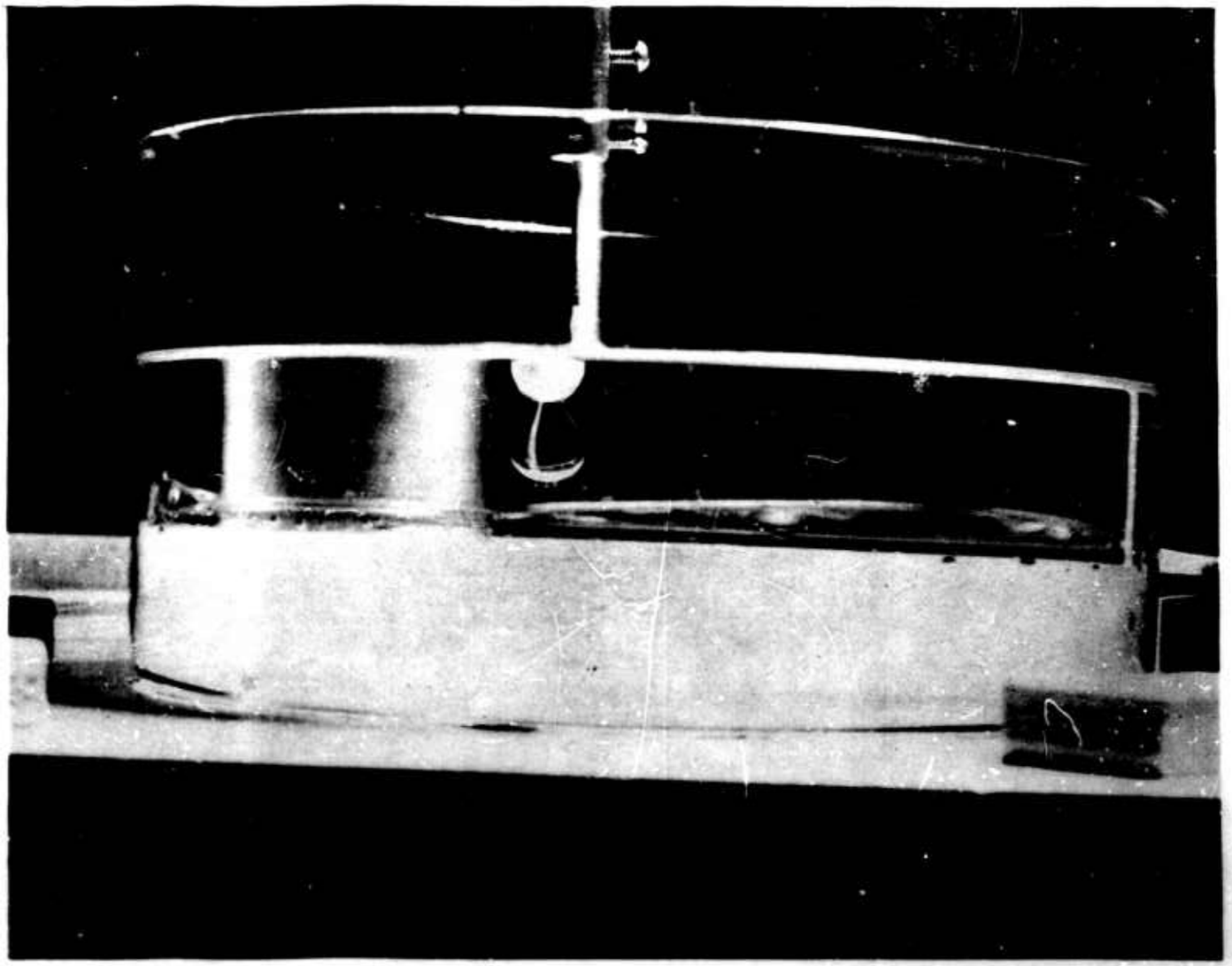

Fig. 6 - Dielectric influence on suspended water droplets, after application of electric field

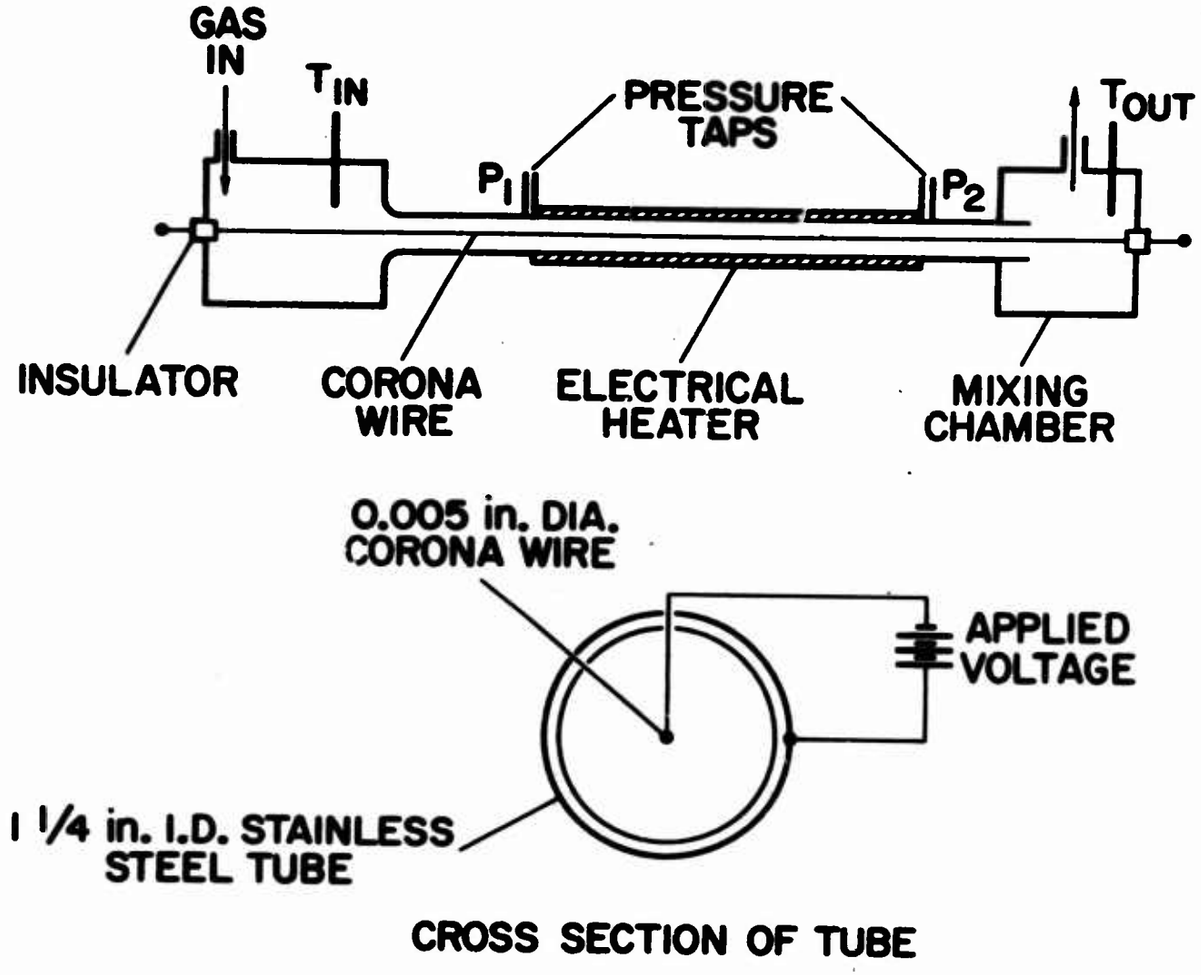

Fig. 7 - Experimental arrangement of tube and flow equipment

T = 80° F, p = 29.23 INCHES Hg, STARTING LENGTH 24 DIAMETERS, WIRE POSITIVE

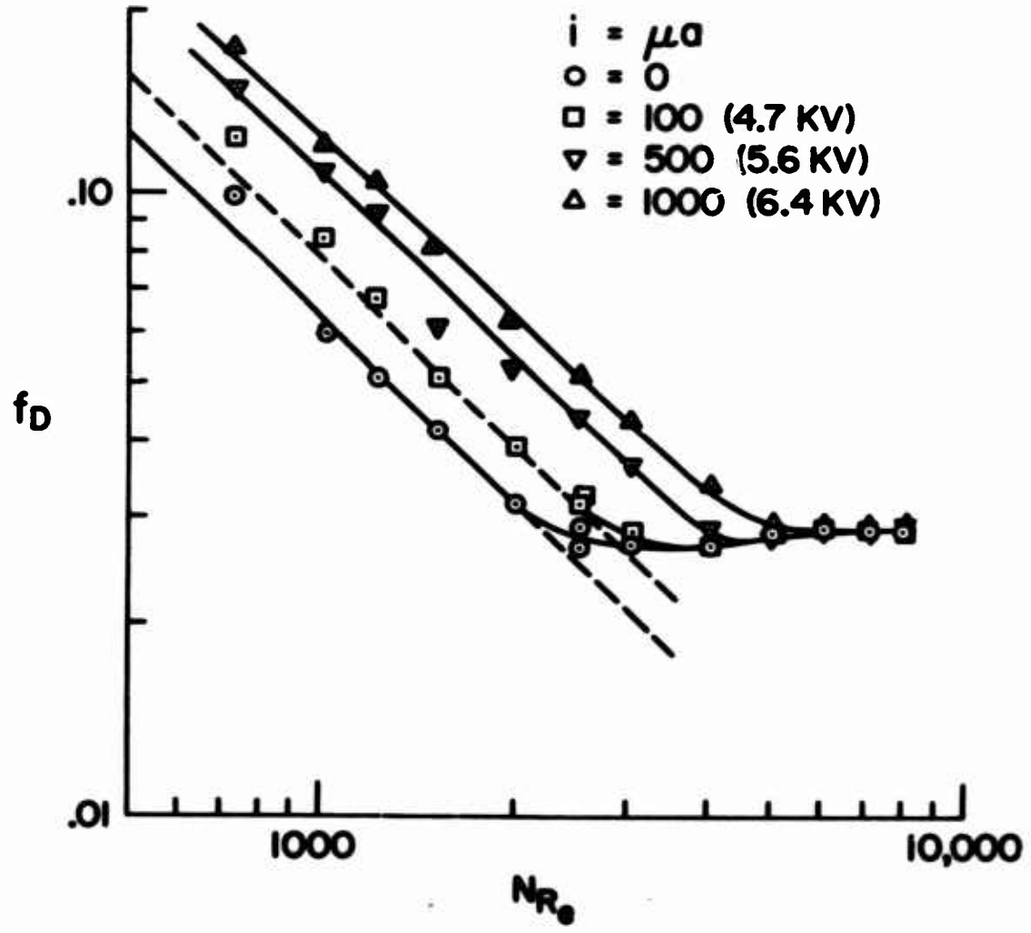

Fig. 8 - Effect of field on friction factor with air

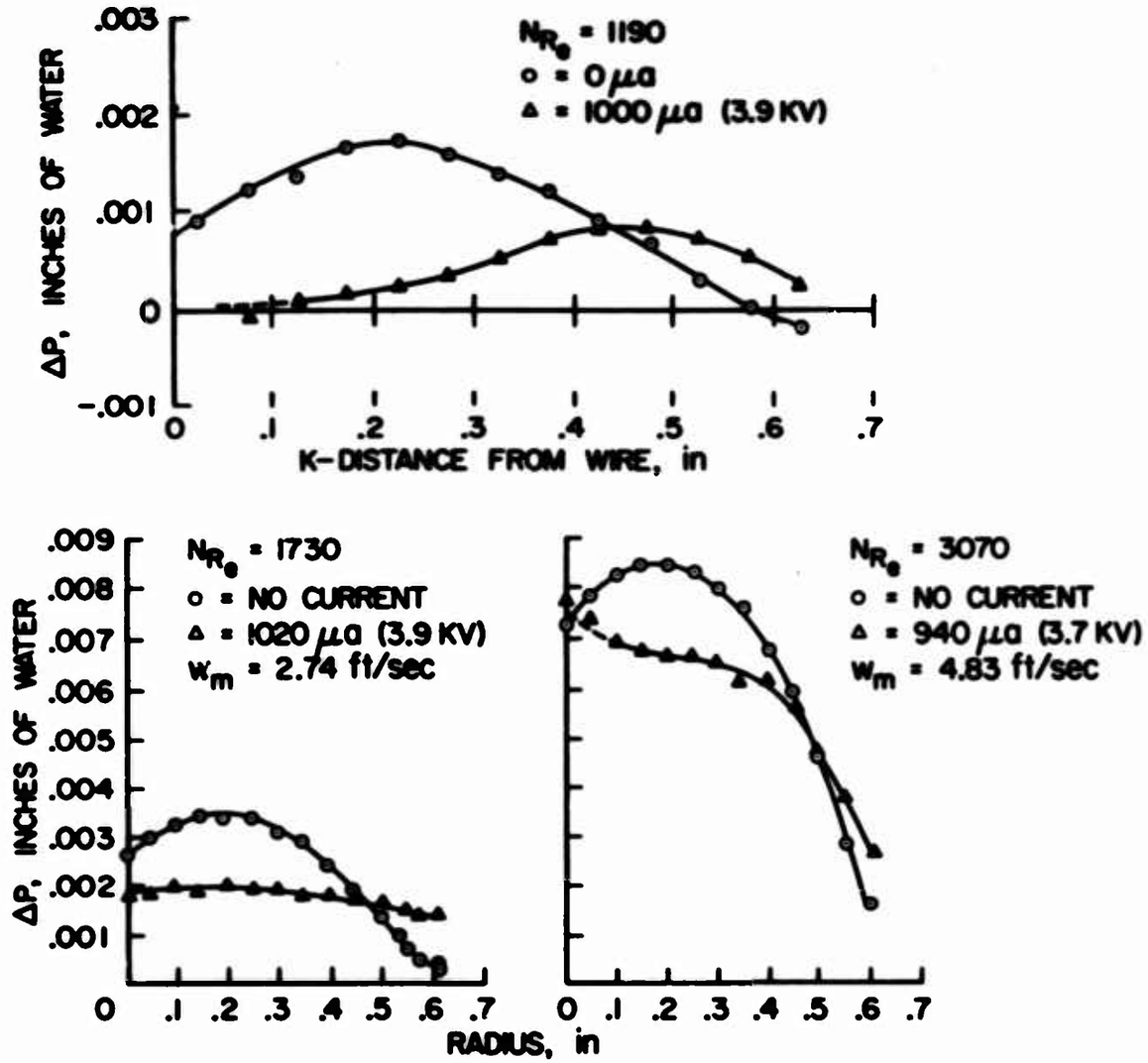

Fig. 9 - Effects of electrical field on velocity profile in tube

and flow equations is attempted, it leads to a complex nonlinear equation. Another approach based upon the actual experimental problem is possible. It can be assumed that the low velocity flow does not affect the mechanism of the corona discharge materially and consequently the corona charge density can be treated independently from the flow. In addition, because of the length of the channel used in the tests, it can also be assumed that the transverse charge density distribution is essentially constant along the axis of the channel. Figure 10 illustrates the coordinates used.

The current equation along the axis of the channel can be written as:

$$J_z = \rho_c w + \rho_c K E_z \tag{4}$$

The boundary conditions on the problem require that the current path must close in the system and that all charge that leaves the wire must reach the channel wall. This condition requires that no net current flows out of the channel, $i_z = 0$ at the end of the channel. Hence

$$\int_A J_z \, dA = 0 \tag{5}$$

For the cylindrical case the radial current density is given by

$$J_r = i_r / 2 \pi r l \tag{6}$$

Using div $\bar{J} = 0$, for cylindrical coordinates,

$$\frac{1}{r} \frac{\partial r J_r}{\partial r} + \frac{\partial J_z}{\partial z} = 0 \tag{7}$$

and substituting J_r from Eq. (14)

$$\frac{\partial J_z}{\partial z} = 0 \tag{8}$$

since i_r must be a constant.

ROUND TUBE CHANNEL WITH CENTRAL WIRE

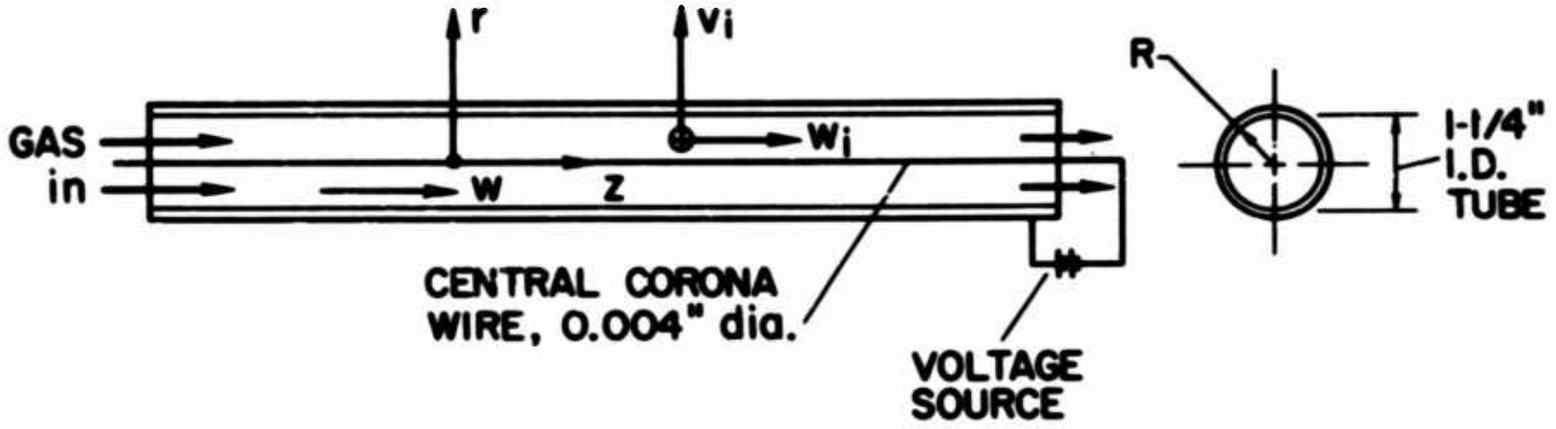

Fig. 10 - Coordinate system for round tube

Substituting Eq. (4) into Eq. (5) results in

$$\int_A (\rho_c w + \rho_c K E_z)\, dA = 0 \tag{9}$$

or

$$\frac{1}{A}\int_A \rho_c E_z\, dA = -\frac{1}{A}\int_A \rho_c \frac{w}{K}\, dA \tag{10}$$

It can be recognized that each integral in Eq. (10) represents the mean value of a function. Hence we can write

$$(\rho_c E_z)_m = -\frac{(\rho_c w)_m}{K} \tag{11}$$

and noting that the electrostatic body force along the axis of the channel is

$$F_z = \rho_c E_z \tag{12}$$

Then the mean value of $\rho_c E_z$ is equal to the mean value of the body force. Substituting into the fluid flow equation for channel flow with a body force one obtains

$$\mu \nabla^2 w - \frac{1}{K}(\rho_c w)_m = \frac{\partial p}{\partial z} \tag{13}$$

Non-dimensionlizing this equation for a round tube,

$$\frac{d^2 w}{d\eta^2} + \frac{1}{\eta}\frac{dw}{d\eta} - \frac{(\rho_c w)_m}{\rho_{c_m} w_m} N_{\rho_c} = N_{Re} \frac{\partial p^*}{\partial \zeta} \tag{14}$$

where

$$N_{\rho_c} = \rho_{c_m} L^2/\mu K,\ \rho_c^* = \frac{\rho_c}{\rho_{c_m}},\quad \eta = r/R,\ \zeta = z/R,\ W = \frac{w}{w_m}$$

The charge number, N_{ρ_c}, is a new dimensionless parameter which characterizes flow with ionization. It represents the ratio of the charge

forces to the viscous force in the flow. Assuming the charge density is constant one can solve the equation to get

$$w_m = - \frac{\frac{R^2}{8\mu} \frac{\partial p}{\partial z}}{\left(1 + \frac{N_{\rho c}}{8}\right)} \tag{15}$$

and the friction factor becomes

$$f_D = \frac{64}{N_{Re}} \left(1 + \frac{N_{\rho c}}{8}\right) \tag{16}$$

As a typical case consider the following values, $K = 2 \times 10^{-4}$ m^2/volt-sec, $R = 0.01587$ m, $i = 10^{-3}$ amp, channel length, $\ell = 1.7$ meters, $\mu = 1.783 \times 10^{-5}$ kg/m-sec, then $\rho_{c_m} = 2.5 \times 10^9$ charges/c.c. The charge number becomes

$$N_{\rho c} = \frac{R^2}{\mu K} \rho_{c_o} = 12.$$

This is a surprisingly large value. Substituting this value of the charge number into Eq. (16) it is found that

$$f_D = \frac{64}{N_{Re}} (2.5)$$

Comparison with the data of Fig. 1 reveals that this value of f_D is similar in magnitude to that actually observed during test. Test data for $i = 1000$ μa, indicate $f_D = 2.1\ (64/N_{Re})$. From Eq. (16) for the mean velocity it is possible to define an effective friction factor.

$$\mu_e = \mu \left(1 + \frac{N_{\rho c}}{8}\right) \tag{17}$$

for the round tube.

Through the use of an expression for viscosity obtained from the kinetic theory it is possible to express the charge number in terms of the Knudsen number. From kinetic theory viscosity can be expressed as

$$\mu = a_1 N m \bar{c} \lambda \tag{18}$$

where a_1 is a constant equal to 1/3 for the elementary derivation of viscocity. Mobility of an ion can be expressed as

$$K = \frac{a_2 \, q \, \lambda_1}{m_1 \, c} \tag{19}$$

where a_2 is a constant depending upon the theory used. Substituting for μ and K in the charge number, one obtains

$$\frac{\rho_{c_m} L^2}{\mu K} = a_3 \frac{1}{N_{K_n}^2} \frac{(N_i)}{N} \tag{20}$$

where N_i/N is the charge density ratio. The constant a_3 is a function of a_1 and a_2 and has a value of the order of unity. It can be seen that the Knudsen number acts to amplify the amount of charge that is present. Since N_{K_n} for the case under consideration is of the order of 10^{-5}, a very large amplification can result. The foregoing expression for the mean velocity is analogous to an expression derived by Steutzer.[9]

An extension of the "induced mean body force" concept is very appealing and analyses were conducted using the idea.[10] Such analyses provided results which compared well with the test data, and showed the flattening of the velocity profiles actually observed. If the analyses were indeed valid it raised the possibility that simular actions could be observed in flat channels and in external boundary layers as well.

5. Evaluation of Channel Flow Action

Studies were then initiated in two separate directions, flat plate channel flow and external boundary layers on flat plates. The flat channel consisted of a long duct 5/8" high by 5" wide by 10 feet long. Corona wires (0.004" dia.) were stretched lengthwise and were spaced 1/2" apart. Static pressure taps were located along the length of the channel to measure the pressure drop. Figure 11 illustrates the arrangement. Data obtained on the pressure drop are shown in Fig. 12 where it can be seen that the pressure drop is linear along the channel. Thus it does not appear that the ion-flow action in the channel is an end effect. Figure 13 shows typical friction factor vs. N_{Re} data for the flat channel. It is similar to that found for the round pipe earlier.

In an attempt to prove or disprove the hypothesized existence of an induced body force, a series of tests were run to determine the current distribution along the length of the flat channel. The need

PARALLEL PLATE FLOW CHANNEL

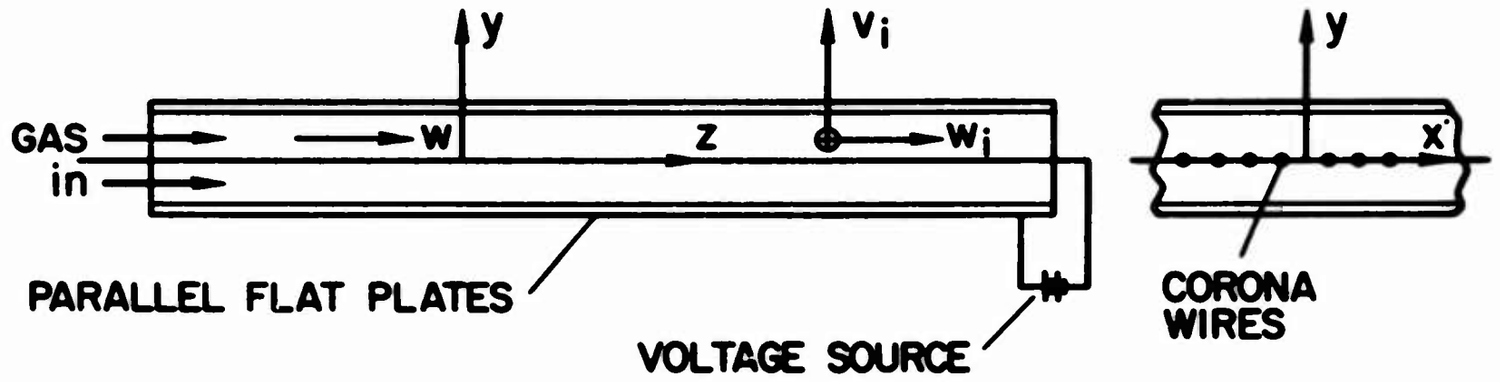

Fig. 11 - Coordinate system for flat channel

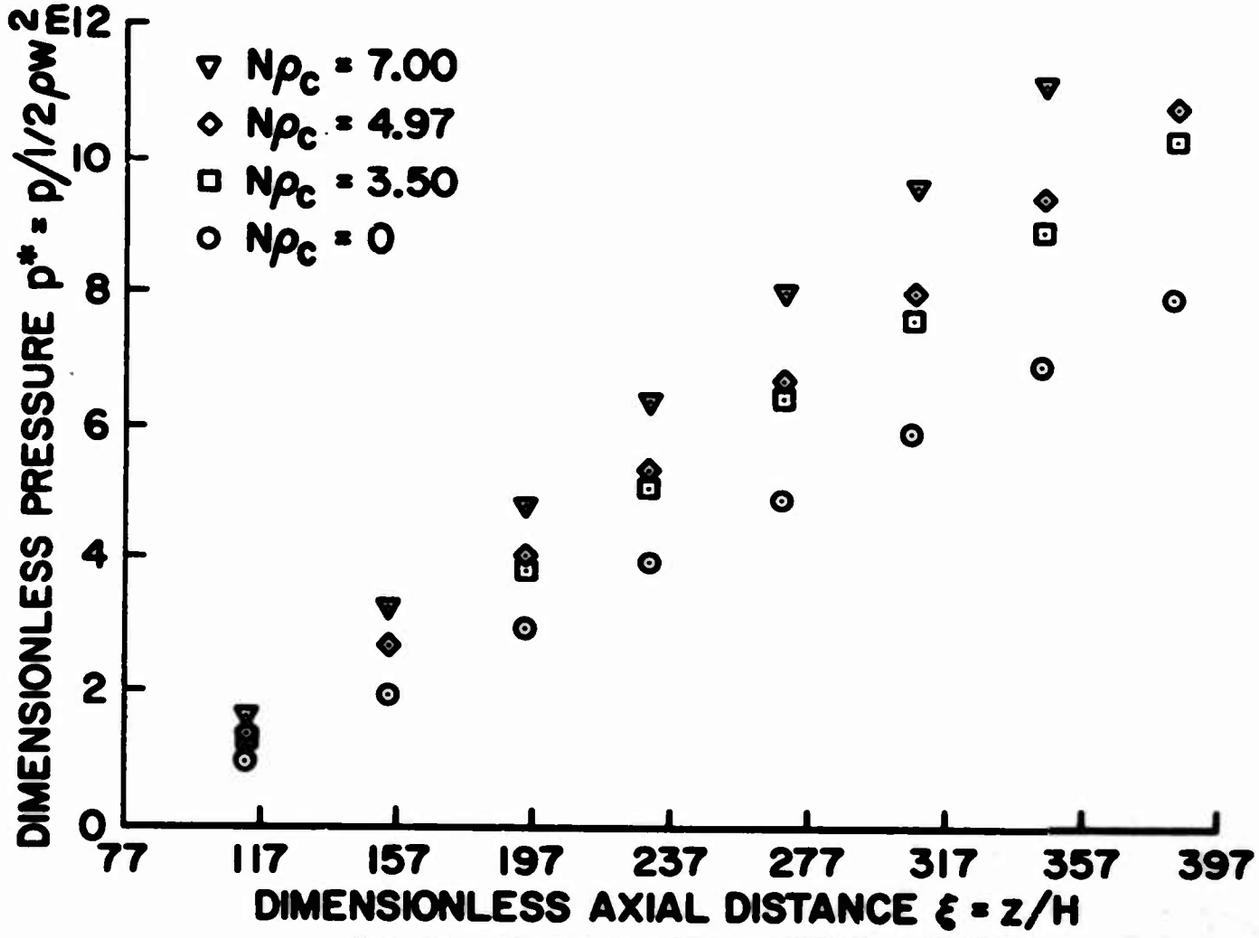

Fig. 12 - Static pressure along the flat duct

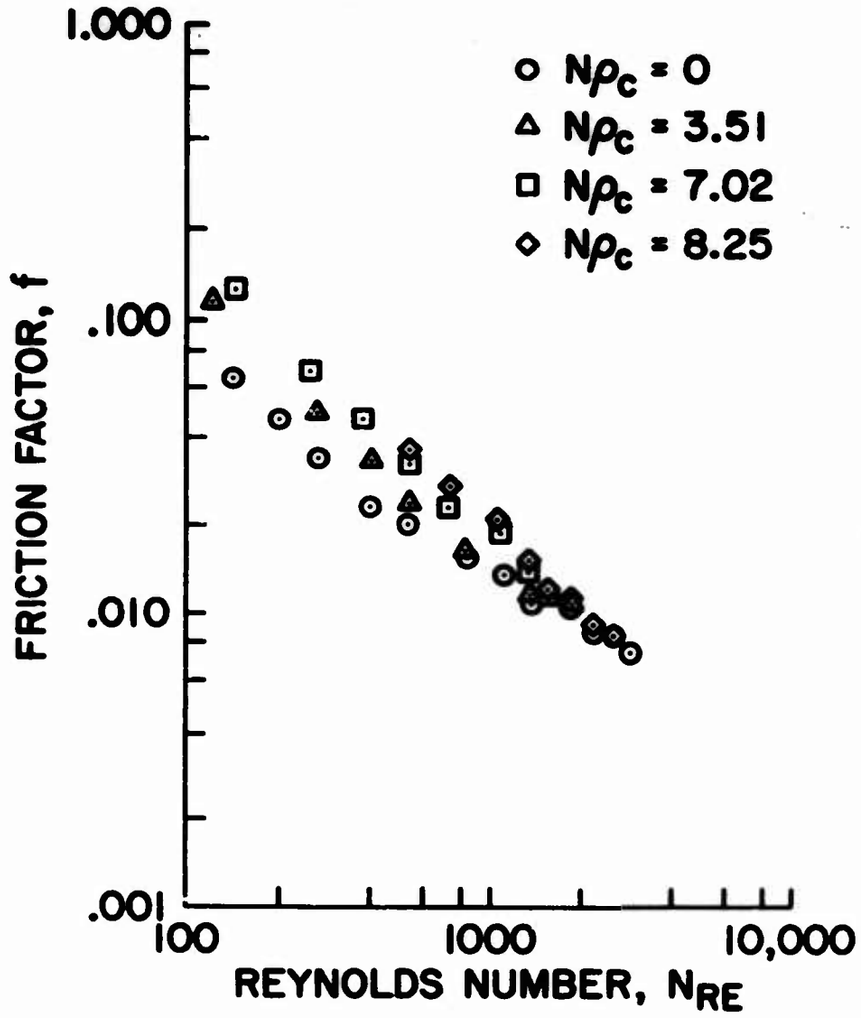

Fig. 13 - Friction factor vs. N_{Re} for flat duct

for such current measurements arises from a consideration of the electrical field equations. The current involved in a corona discharge is a nonlinear function of the applied voltage. During the discharge phase a small voltage or electric field change can lead to a very significant change in the corona current. Thus, if the radial or transverse E field is varied in the channel locally for any reason, then one would anticipate a change in the local current. Next if one considers the Maxwell equation

$$\nabla X \bar{E} = - \frac{\partial \bar{B}}{\partial t} \tag{21}$$

for the case with $\bar{B}$ small,

$$\nabla X \bar{E} = 0 \tag{22}$$

and the following equation is significant.

$$\frac{\partial Ey}{\partial z} = \frac{\partial Ez}{\partial y} \tag{23}$$

where z is along the channel and y is transverse as shown in Fig. 11. If a body force exists in the channel which is a function of the stream velocity along the channel, that is $F_z = f(w/k)$, and since $F_z = \rho_c E_z$, then E_z would be a function of y, and $\partial Ev/\partial z$ could be non-zero. This would imply that the transverse field, Ey, could vary along the channel.

To study the possible variations in current, the flat channel was modified so that the current along one surface could be monitored along its entire length. Figure 14 illustrates the modified channel with the individual conducting silver electrodes painted on a plastic sheet. These electrodes can be seen exposed on the right hand side of the figure. Two traversing pressure probes can be seen on the left. In conducting the tests the current to each segment was measured and the local current density determined. The results are plotted in Fig. 15. The data points are very scattered. If a significant variation in E_y occurs with flow, one would expect to see a distinct change in current density as the flow velocity is increased from zero. Study of the data does not reveal any truly marked difference in current density. The data do indicate however, that the phenomena are not solely "end effects" at either end of the channel. Thus because no clear-cut change in current density was found, the possiblity of the induced body force was seriously called into question. At the same time, data on external flow testing, which will be described subsequently,

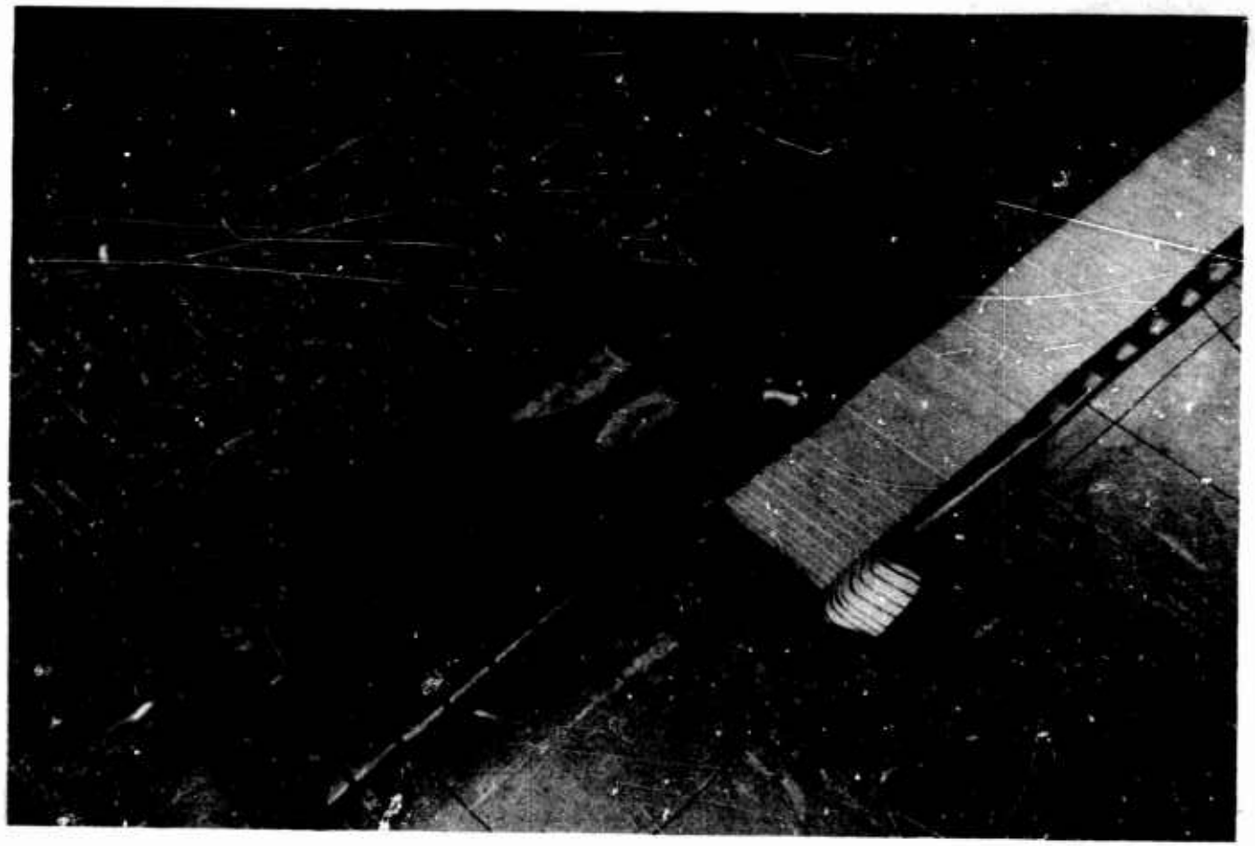

Fig. 14 - Flow channel showing transverse electrodes

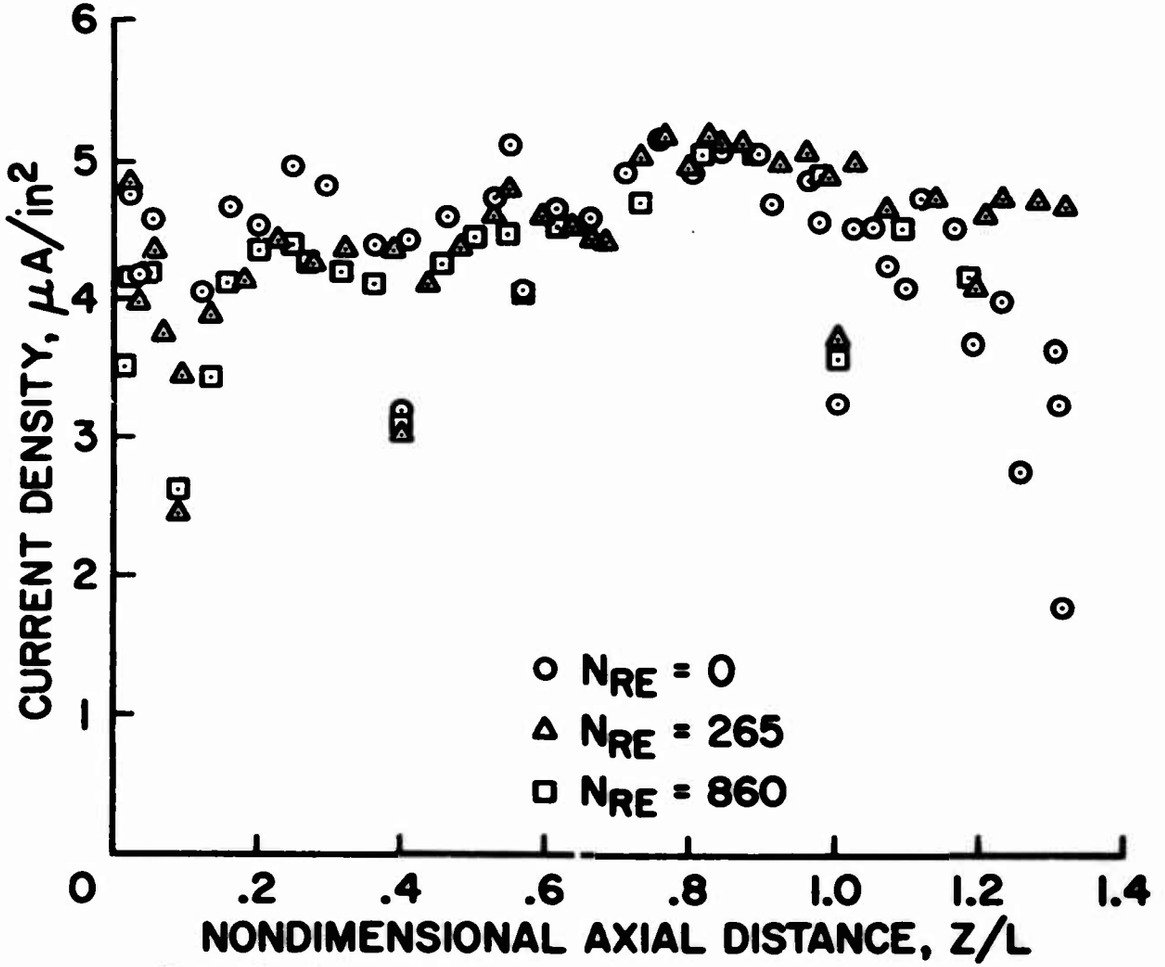

Fig. 15 - Current density along length of flat channel

also indicated that a significant induced streamwise body force probably did not occur.

A reconsideration of the ion-flow interaction led to the consideration that the changes to friction factor and velocity profiles in the channels could be the result of secondary flows. Accordingly a two-pronged effort was initiated, involving an analytical and an experimental study.

The analytical approach was based upon flow of a fluid between concentric cylinders with ions moving under the influence of an applied field in a radial direction. Because of the collisions between the charges and the fluid an electrical body force in a radial direction results. Such a radial force may be considered analogous to the centrifugal force in Taylor's problem with rotating concentric cylinders and hence it was hypothesized that a pattern of internal vortices could possibly be induced.[11,12] The coordinates used in the analysis are shown in Fig. 16. The analysis started with the Navier Stokes and included the radial body force term and ion diffusion term. The fluid was assumed incompressible, field distortions due to ion perturbations small, constant conductivity in the fluid, fluid properties unchanged by ionization, and that the perturbations were axisymmetric. After a perturbation analysis, the applicable equations in a nondimensional form become

$$\frac{\partial u}{\partial r} + \frac{u}{r} + \frac{\partial w}{\partial z} = 0 \tag{24}$$

$$\frac{\partial}{\partial t}\left[\frac{\partial w}{\partial r} - \frac{\partial u}{\partial z}\right] = \left[\nabla^2 - \frac{1}{r^2}\right]\left[\frac{\partial w}{\partial r} - \frac{\partial u}{\partial z}\right] - E\,\frac{\partial n}{\partial z} \tag{25}$$

$$\frac{\partial n}{\partial t} + u\,\frac{\partial \bar{n}}{\partial r} - \frac{D_i}{\nu}\,\nabla^2 n = 0 \tag{26}$$

Following Taylor, it was assumed that

$$u = u_1 (r) \cos \lambda z\, e^{\sigma t} \tag{27}$$

$$w = w_1 (r) \sin \lambda z\, e^{\sigma t} \tag{28}$$

$$n = n_1 (r) \cos \lambda z\, e^{\sigma t} \tag{29}$$

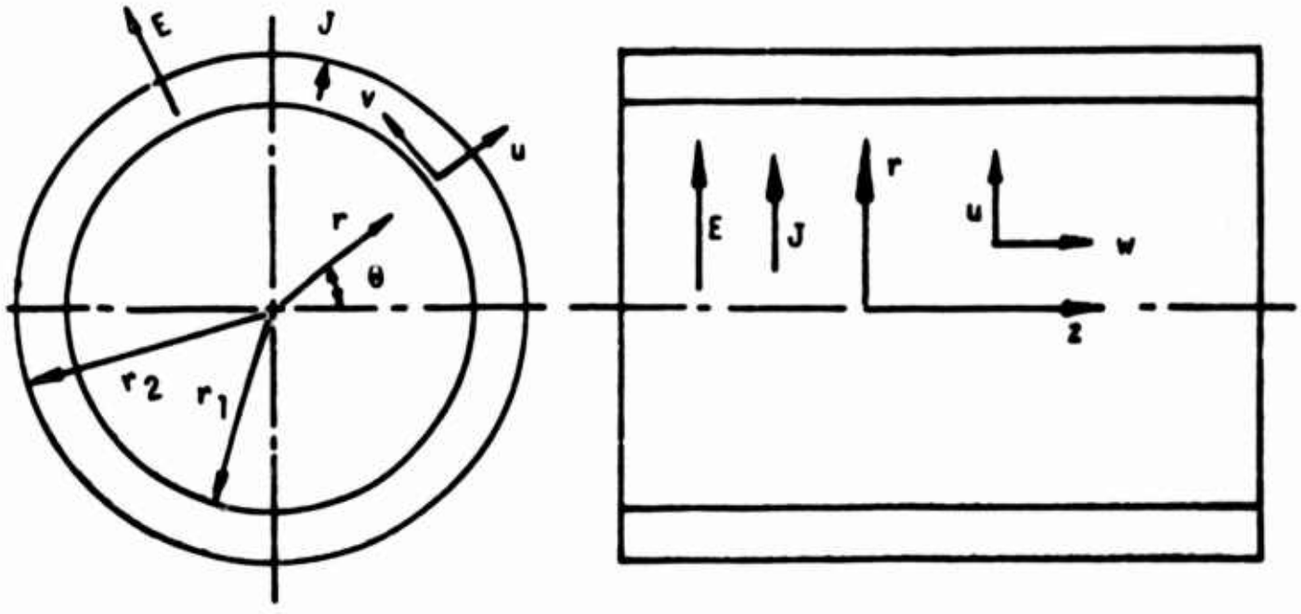

Fig. 16 - Coordinate system for concentric cylinders

where λ and σ are the nondimensional wave number and amplification factor, respectively. With substitution of these assumed forms for the perturbed quantities Eqs. (24), (25), (26) reduce to

$$\left(\frac{d^2}{dr^2} + \frac{d}{dr}\frac{1}{r} - \lambda^2 - \sigma\right)\left(\frac{d^2}{dr^2} + \frac{d}{dr}\frac{1}{r} - \lambda^2\right) u_1 = \lambda^2 E n_1 \qquad (30)$$

$$\left(\frac{d^2}{dr^2} + \frac{1}{r}\frac{d}{dr} - \lambda^2 - \sigma\right)\ n_1 = \frac{\nu}{D_1}\frac{d\bar{n}}{dr}\, u_1 \qquad (31)$$

The boundary conditions of the Eqs. (30) and (31) are that the perturbation quantities, u, v, n, induced by convection, are to vanish at each of the bounding cylinders. Furthermore, the situation of limiting or neutral stability is given by $\sigma = 0$. The problem was next restricted to a limiting case where the distance between cylinders is small compared to inner cylinder radius, and an analogy with Taylor problem results. In this case the terms $1/r$ are small compared to d/dr and the above equations become

$$\left(\frac{d^2}{dr^2} - \lambda^2\right)^2 u_1 = \lambda^2 E n_1 \qquad (32)$$

$$\left(\frac{d^2}{dr^2} - \lambda^2\right) n_1 = \frac{\nu}{D_1}\frac{d\bar{n}}{dr}\, u_1 \qquad (33)$$

The nondimensional independent variable r was changed to $\eta = (r-r_0)/\delta$ (r dimensional) and Eqs. (32) and (33) were combined, for the case where E can be approximated as constant, to give

$$(D^2-a^2)^3\, u_1 = -\, a^2 T u_1 \qquad (34)$$

where

$$D = \frac{d}{d\eta} \quad \text{and} \quad T = -\,\frac{\nu}{D_1}\frac{\delta^3 E}{r_1^3}\frac{d\bar{n}}{d\eta}$$

is the electric Taylor number. The boundary conditions to be satisified by u_1 are

$$u_1 = DU_1 = (D^2-a^2)^2 u_1 = 0 \quad \text{at} \quad \eta = \pm \tfrac{1}{2} \tag{35}$$

In terms of dimensional variables, T takes the form

$$T = - \frac{\ell^4 E}{\mu D_i} \frac{d\pi}{dr} \tag{36}$$

It can be shown that the electric Taylor number, T, in the form of Eq. (36) represents the ratio of the destabilizing electric force to the stabilizing viscous force. The solution of Eq. (34) subject to Eq. (35) is an eigenvalue problem leading to a relation between a and T. The minimum value of T is the critical Taylor number and was found to be 1707.8 at a = 3.13.[13]

Thus, since as a limiting case the electrical problem reduced to the same form as Taylor's problem, it appeared logical to expect some type of internal secondary flows to form within the channel.

An experimental investigation was initiated to determine if secondary flows were present in the channel. Because the basic flow velocities were of the order of a few feet per second, measurement of the very small secondary flows was a significant problem. Because of the intense electrical fields, involved use of hot wire anemometry was ruled out, and pitot probes were insensitive to the small disturbances. Consequently, recourse was made to a technique which used electrical probes placed in the fluid stream. The arrangement is shown in Fig. 17 where the secondary flow as hypothesized is shown. The two probes shown were insulated and were connected to ground potential through a resistor. The induced secondary flow could assist the ion motion to the end surface of one probe and oppose ion motion to the second probe. A slight difference between the current and potential of the two probes should result if some type of vortex pattern exists in the channel. This potential difference was applied to an oscilloscope. Typical results are shown in Figs. 18 and 19. It can be seen that fairly regularly spaced oscillations do occur with a spacing of the order of one diameter. Thus, it appears likely that some secondary motion does exist within the channel. It can also be seen that as the Reynolds number increases the regular large waves disappear as indicated in the previous friction factor tests, Fig. 8.

It was concluded therefore, that the ion-flow interactions within the channel were probably the result of the creation of secondary flows by the electric wind pressure and not the result of an induced axial body force.

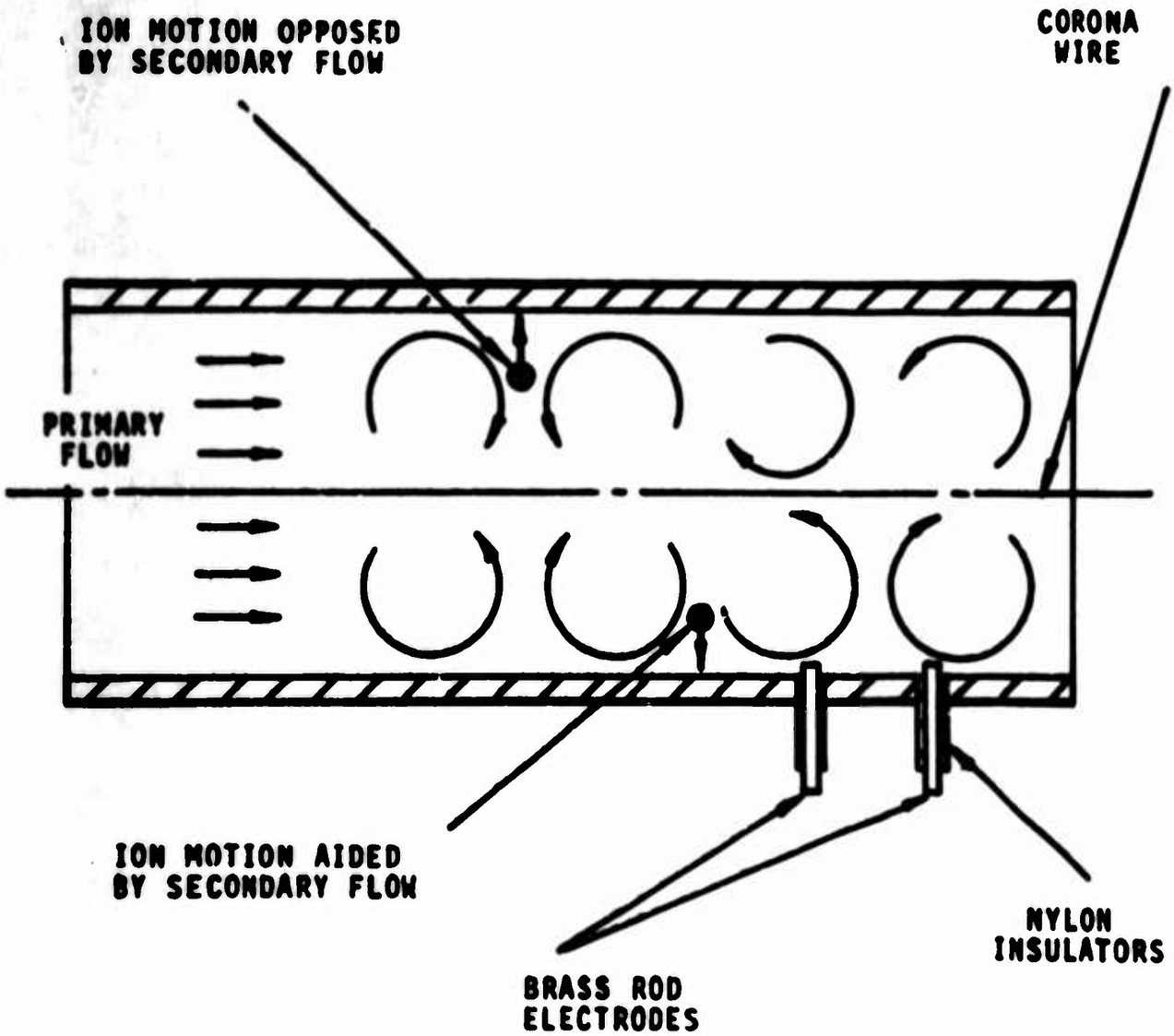

Fig. 17 - Detection of induced velocities with electrostatic probes

Re = 0
N = 0
SWEEP = 0.1 SEC/CM
AMPLITUDE = 0.5 MV/CM

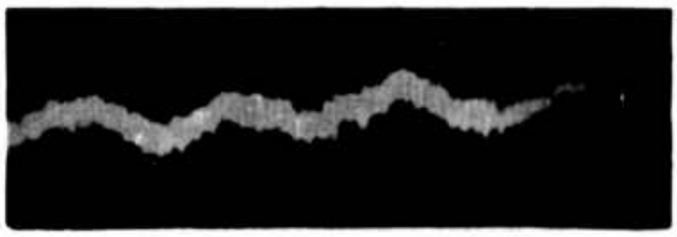

Re = 0
N = 12.75
SWEEP = 0.1 SEC/CM
AMPLITUDE = 1 MV/CM

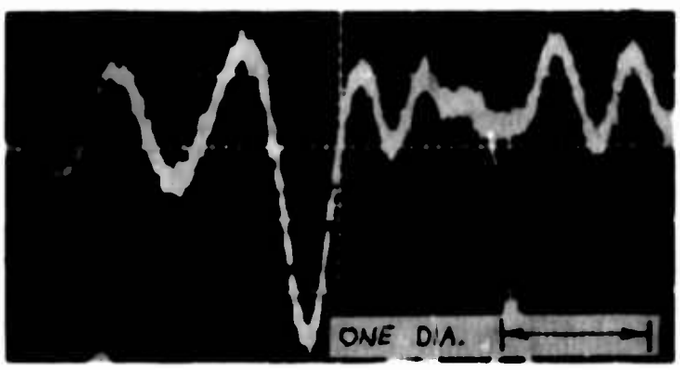

Re = 435
N = 12.75
SWEEP = 0.1 SEC/CM
AMPLITUDE = 1 MV/CM

Fig. 18 - Probe voltage oscillations indicating possible secondary flow

Re = 715
N = 12.75
SWEEP = 0.1 SEC/CM
AMPLITUDE = 2 MV/CM

Re = 1330
N = 12.75
SWEEP = 0.1 SEC/CM
AMPLITUDE = 1 MV/CM

Re = 1780
N = 12.75
SWEEP = 0.05 SEC/CM
AMPLITUDE = 1 MV/CM

Fig. 19 - Probe voltage oscillations indicating possible secondary flow

6. External Flows

Concurrent with the internal flow study of the nature of the ion-flow interaction in the channel, a program was initiated to study the possible existence of the hypothesized body force in external boundary layer flow. Analytical and experimental investigations were initiated. The analysis was based upon using the Prandtl boundary layer equation for a flat plate including a stream wise body force of a form similar to Eqs. (11) and (12).[11] The equation then became

$$v \frac{\partial w}{\partial y} + w \frac{\partial w}{\partial z} = \nu \frac{\partial^2 w}{\partial y^2} - \frac{\rho_c w}{\rho K} \tag{37}$$

If the charge density is assumed constant through the boundary layer the equation takes the form

$$v \frac{\partial w}{\partial y} + w \frac{\partial w}{\partial z} + \alpha w = \nu \frac{\partial^2 w}{\partial y^2} \tag{38}$$

where

$$\alpha = \frac{\rho_c}{\rho K}$$

This equation is of the same form as Rossow's equation for flow of a conducting fluid over a flat plate in the presence of a transverse magnetic field.[14] Rossow's solutions indicate that the boundary layer is distorted by the magnetic field and that a condition of incipient separation can be reached.

To determine the possible effects experimentally, a heated flat plate was mounted in a flow channel and the effects of ionization and a transverse field were studied.[15] The plate assembly was mounted in a Mach Zehnder interferometer. Corona wires were stretched above the surface of the plate in a streamwise direction and a high voltage applied between the wires and the plate. The plate was heated electrically and the plate surface temperature was monitored by the use of thermocouples imbedded in the plate material. The physical basis for the tests was that at significant stream velocity if a streamwise body force existed, it should have increasing influence on the boundary layer as the ionization was increased. Since the thermal boundary layer is a good measure of the velocity boundary layer, a study of the fringe patterns obtained should provide a means of determining the effects of the ionization on the external boundary layer. The experimental arrangement is shown in Fig. 20.

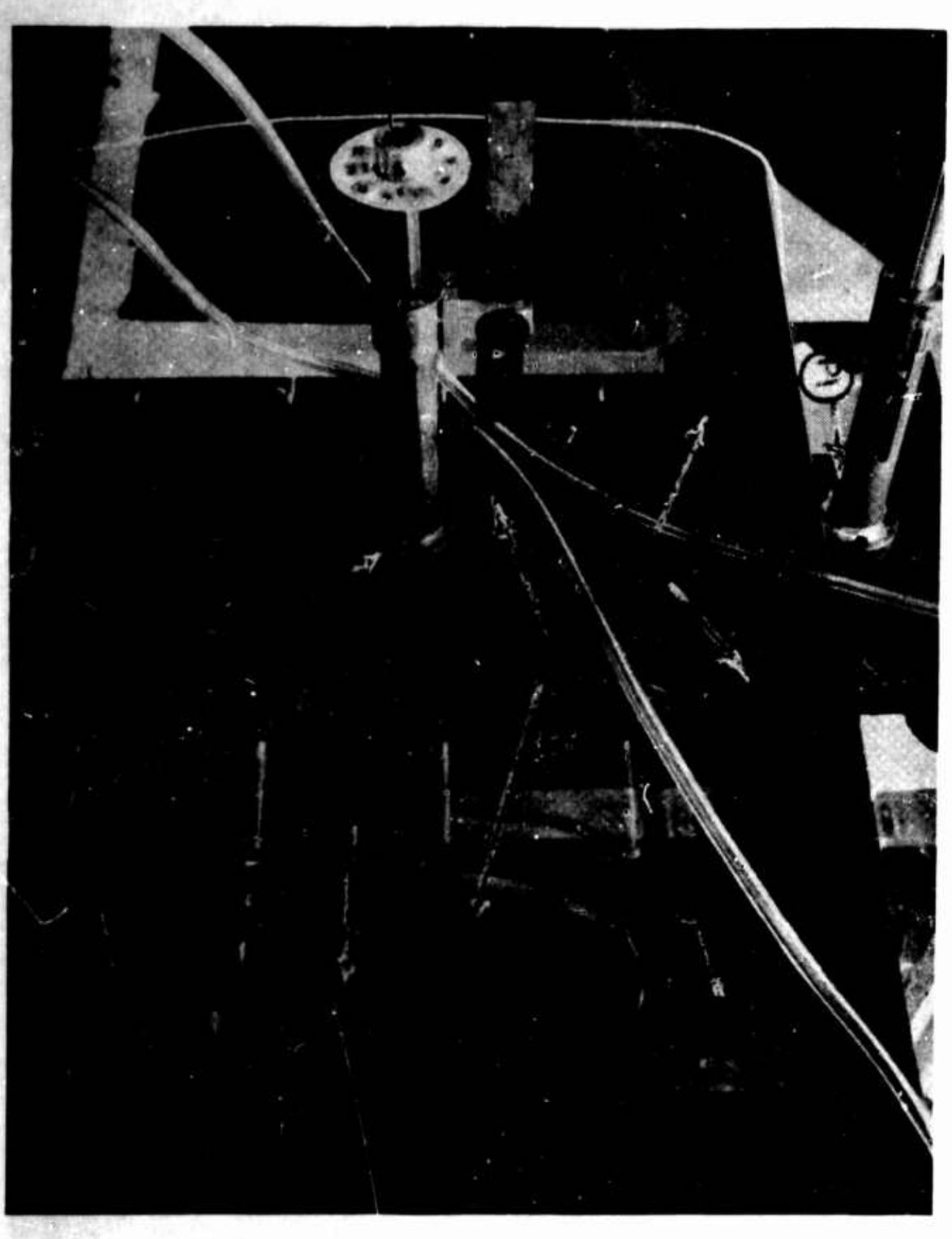

Fig. 20 - Test section of interferometer test of external boundary layer flow with applied field
(A) optical flats (B) plate supports (C) vertical axis adjustment
(D) reference length "T" (P1, P2, P3) pressure tap locations

The most significant result is shown in Fig. 21 wherein the ratio of the Nusselt number with ion current to the Nusselt number without current is plotted against a nondimensional velocity. This figure shows that at the higher stream velocities there is no significant influence of the ion currents. At low velocities the effects on heat transfer are large, but this can be expected since at the very low velocities the electric wind actions can predominate as was found from the previous free convection tests with electrostatic fields. These tests strongly supported the conclusion found from the channel studies than an induced axial body force does not seem to exist.

7. External Flows - Transition

A separate effort was initiated to study the possible influence of an electrostatic field (ions) on boundary layer transition.[16] A flat plate, 3' x 6', was mounted in a low turbulence tunnel and corona wires were suspended above the plate surface as shown in Fig. 22. Electric fields were impressed between the wires and the metal surface of the plate. The purpose of the study was to use electrically induced perturbations to couple with the natural (Tollmein-Schlichting) oscillations in the laminar boundary layer. Corona wire spacing and the impressed A-C electric field component were selected to match the predominant wave length and frequency of the boundary layer oscillations. Boundary layer transition was located by means of a near surface impact pressure probe that was traversed slowly from the rear of the plate towards the leading edge. The most significant results are shown in Fig. 23. It is shown that transition from laminar to turbulent flow as indicated by the low point in the curves has been shifted backwards along the plate by the corona discharge. This delayed transition was found to be repeatable. The actual mechanism for this transition delay is still the subject for study. It is interesting, but no effect of frequency was found during the tests.

8. Flow Attachment

Because the energy involved in electrostatic actions is usually small, it is necessary to consider those fluid processes where changes to the flow require only a small amount of energy or force. A typical situation of this kind occurs in the fluid attachment as found in a flip-flop fluid amplifier element. An experimental program was initiated to determine what effects electrostatic actions might have on attachment and the flipping action of a flip-flop unit.[17] The experimental equipment for a large exploratory unit is shown in Fig. 24. Air passes from the left-hand side through a plenum chamber, out a nozzle and into the splitter plate region to the right. Two side port control channels are shown above and below the nozzle exit region. The unit was five inches wide with a nozzle slot height of 0.1 inch. Several electrostatic arrangements were tried but the most interesting results were obtained with corona wires and ground electrodes located in each control channel. In operation, a voltage was applied between

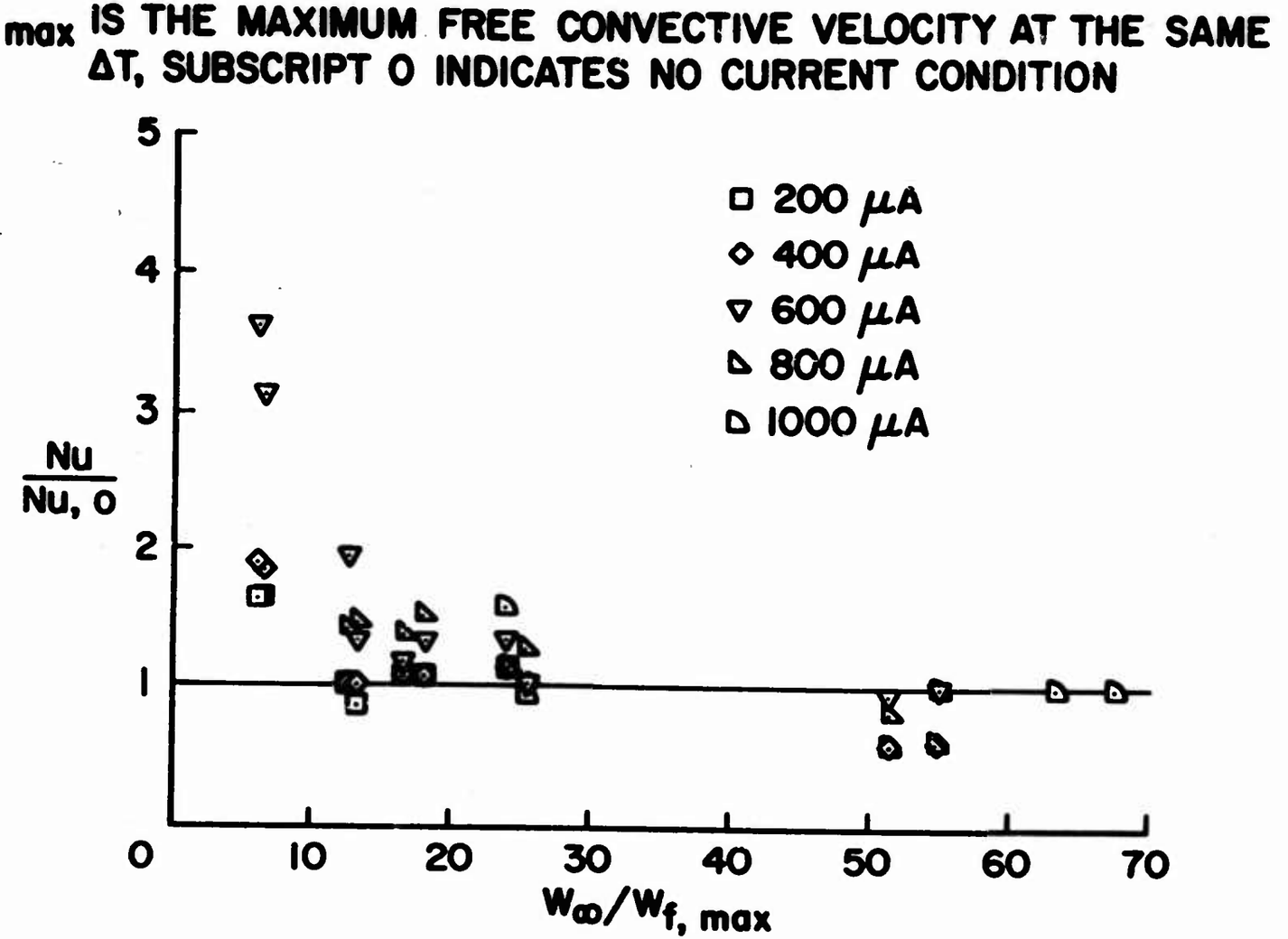

Fig. 21 - Effect of increasing channel velocity on heat transfer with applied field

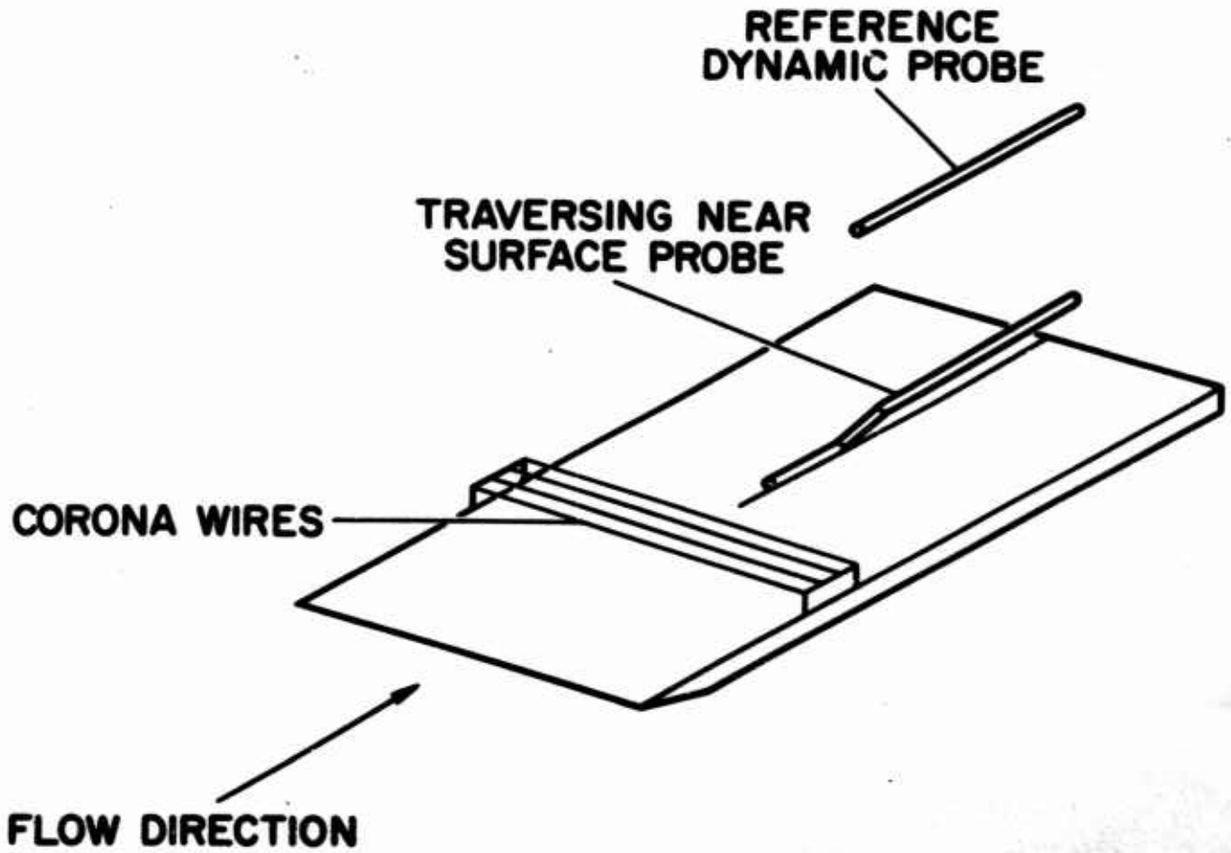

Fig. 22 - Boundary layer transition test - flat plate with corona wires

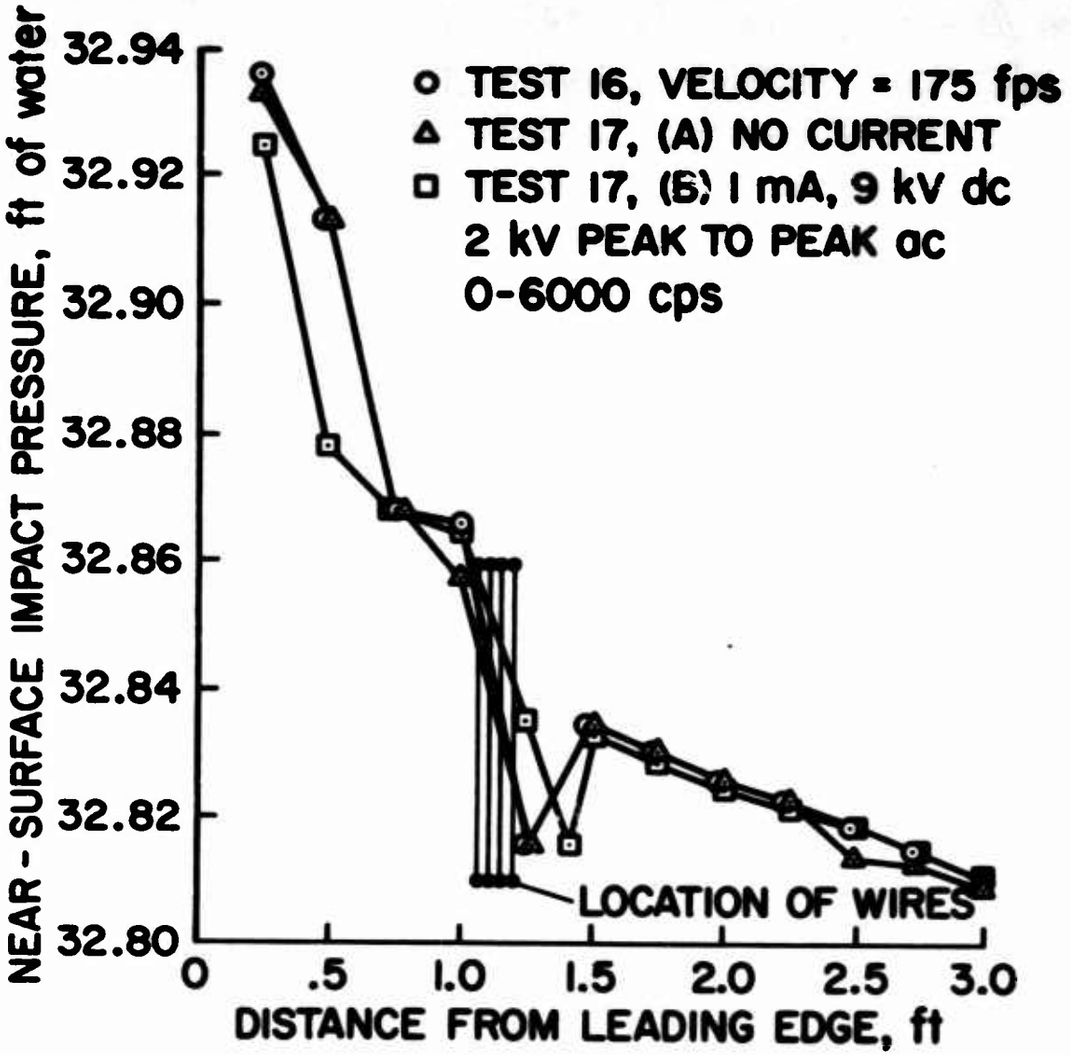

Fig. 23 - Shift of transition with corona discharge

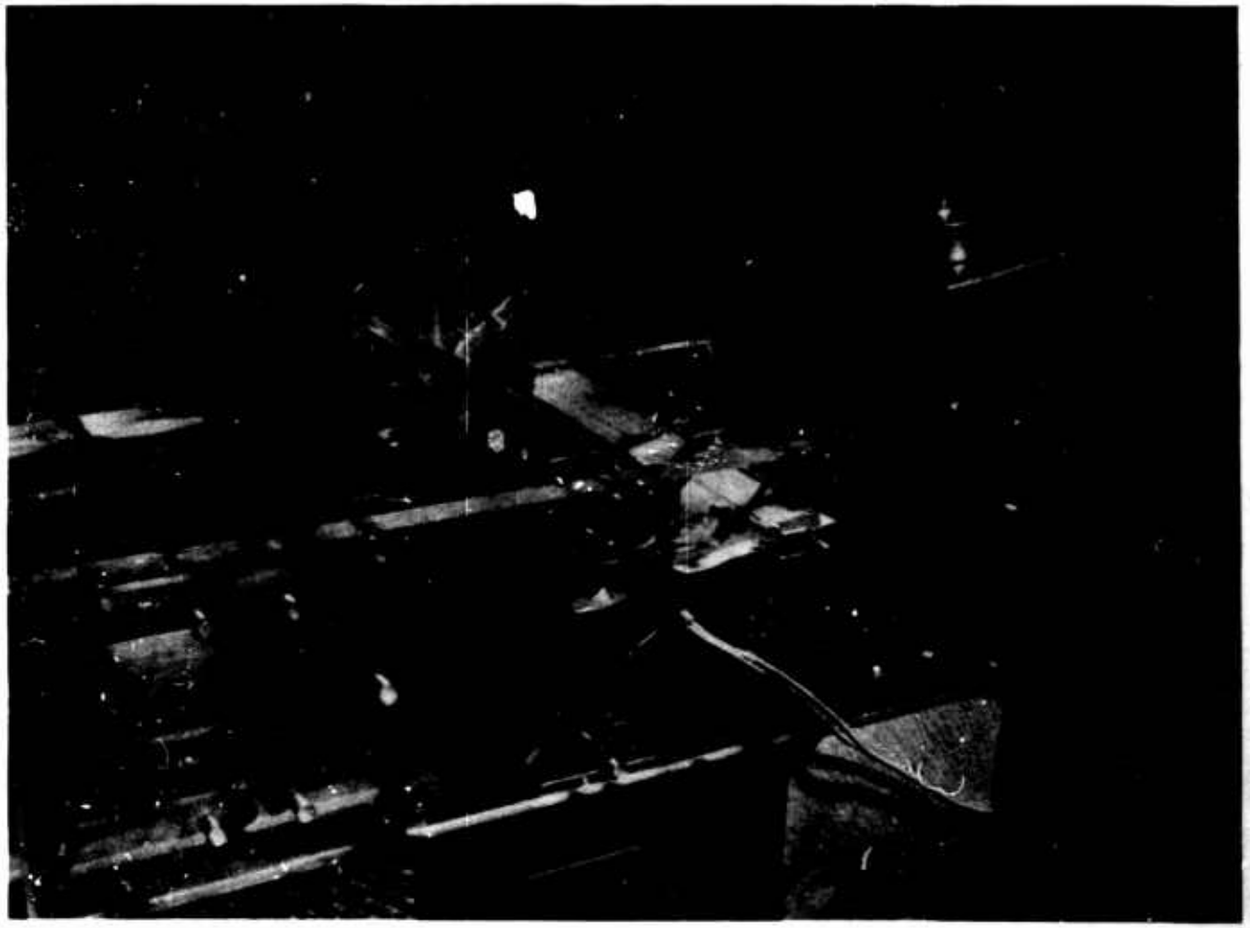

Fig. 24 - Corona wind flip-flop amplifier unit

the corona wire and ground electrode in one control channel. The electric wind then issued from the side port and would cause the main stream jet to move to the opposite side. When the corona voltage was switched to the other electrode the reverse action would take place. Thus the electric wind acted similarly to the side port air input for ordinary flip-flop fluid elements. The power required to flip the main stream is presented in Fig. 25. Typical downstream velocity profiles outward from each side wall are shown in Fig. 26.

Because of the success in achieving flipping action with the electric wind, a brief study of a smaller unit was accomplished.[18] This unit had a main nozzle width of 0.20 inch and a height of 1/4 inch. The configuration is shown in Fig. 27. The study included several different configurations of electrodes, side port plenum chamber arrangements, and a wide range of flows. In general, the unit operated satisfactorily with typical data shown in Figs. 28 and 29. Figure 28 illustrates that powers of the order of 0.02 watt are necessary to flip the mainstream and Fig. 29 indicates a flow ratio between control flow, Q_c, and primary flow, Q, of the order of 0.125. Attempts were made to determine the maximum frequency at which the unit would follow the input electrical pulses. A hot wire anemometer was used to determine the output flow position, but unfortunately considerable difficulty was experienced with the unit and little useful data were obtained. It was estimated that the upper limit of the device based upon very limited testing of the order 10-20 cps.

B. CHANGE OF PHASE

The possibility of using electrostatic fields to influence the change of phase of a fluid is particularly intriguing. During change of phase, definite surfaces are usually present where surface forces due to fields can be induced. There is also the large difference in the number of molecules per unit volume between the phases and thus body force terms could also be active. One would anticipate, therefore, that suitable application of electrical fields could alter the normal processes during the change of phase of a fluid. Three general cases are considered, boiling of a liquid, condensation of a vapor, and frost formation upon a cold surface.

In the case of boiling, very interesting work has been done by Bonjour et al., Markels, and Choi.[19,20,21] Their work indicates very large increases in boiling heat transfer rates due to applied electrostatic fields, particularly in the "burn-out" region of the boiling heat transfer curve. Increases in heat transfer of up to several hundred precent have been recorded by these investigators. They have also noted a complete change in the character of the boiling that takes place.

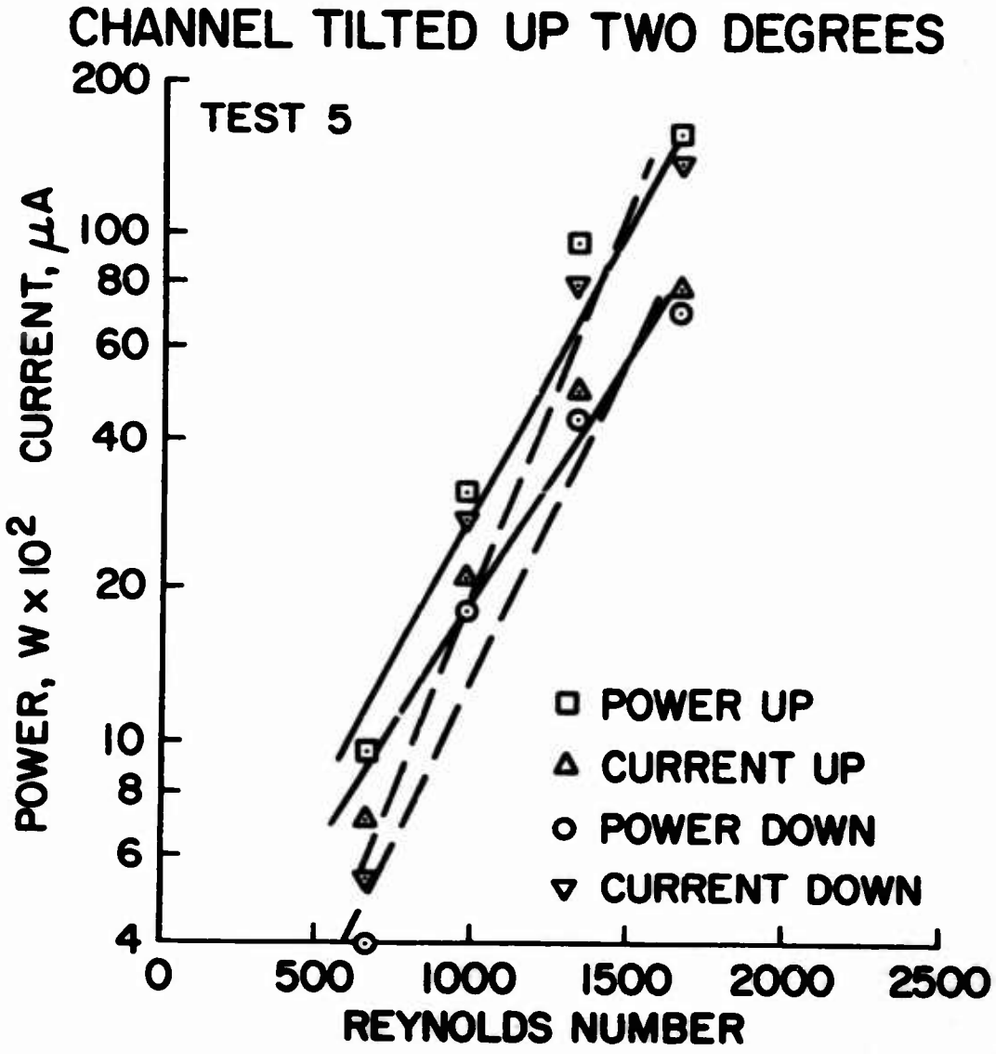

Fig. 25 - Power and current required to flip the flow in large flip-flop unit

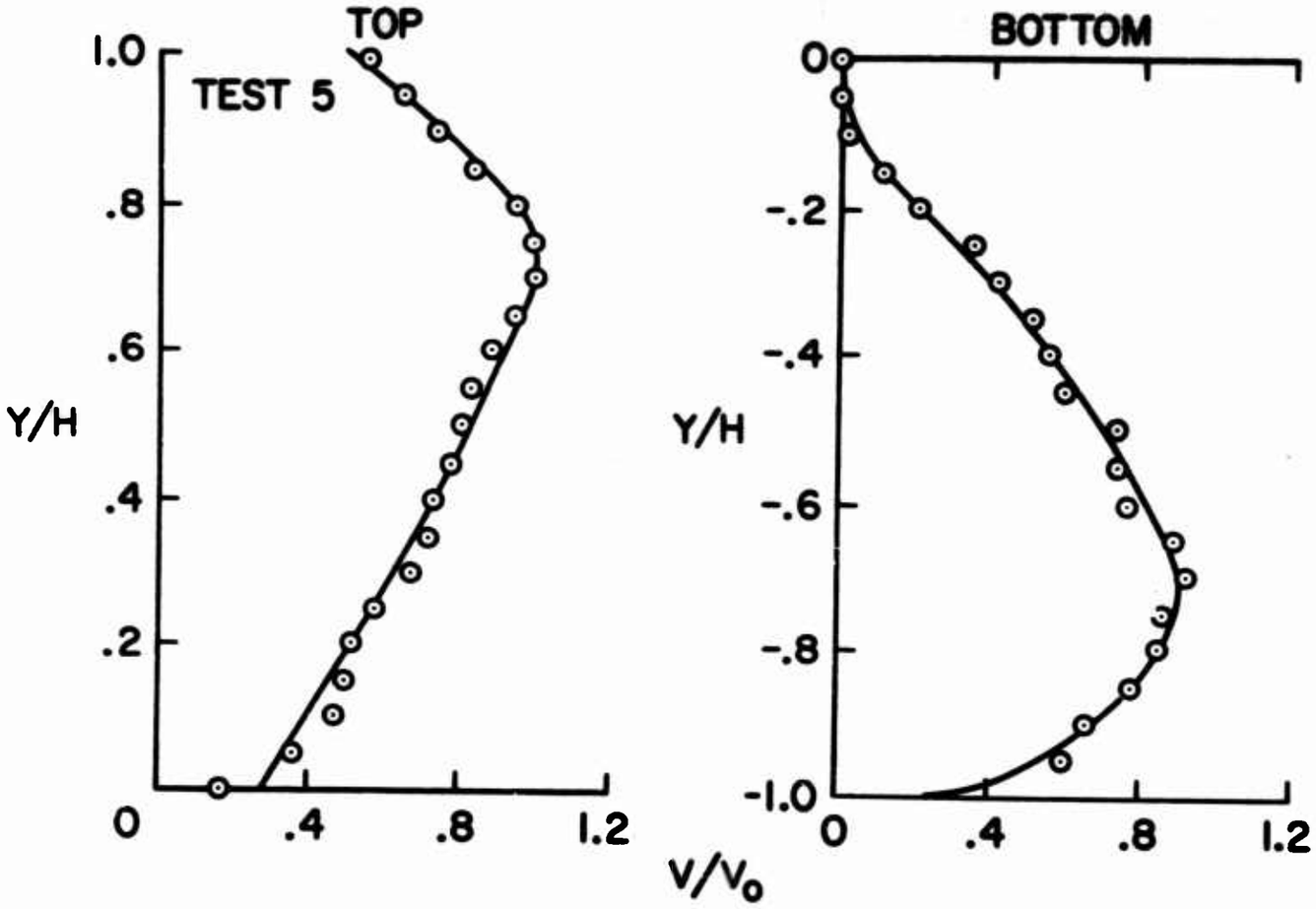

Fig. 26 - Velocity profiles downstream of the jet

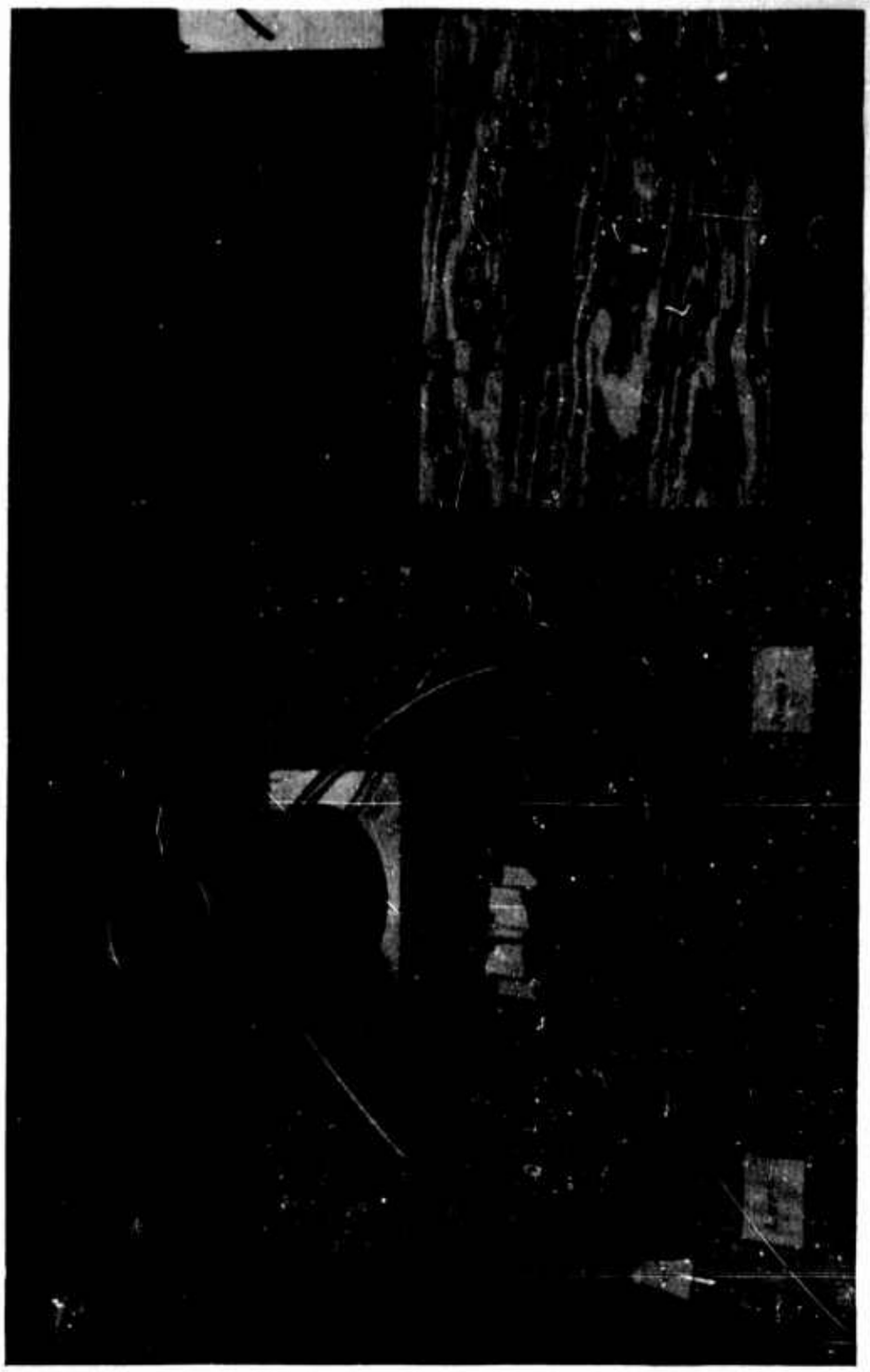

Fig. 27 - Smaller flip-flop unit with plenum chamber

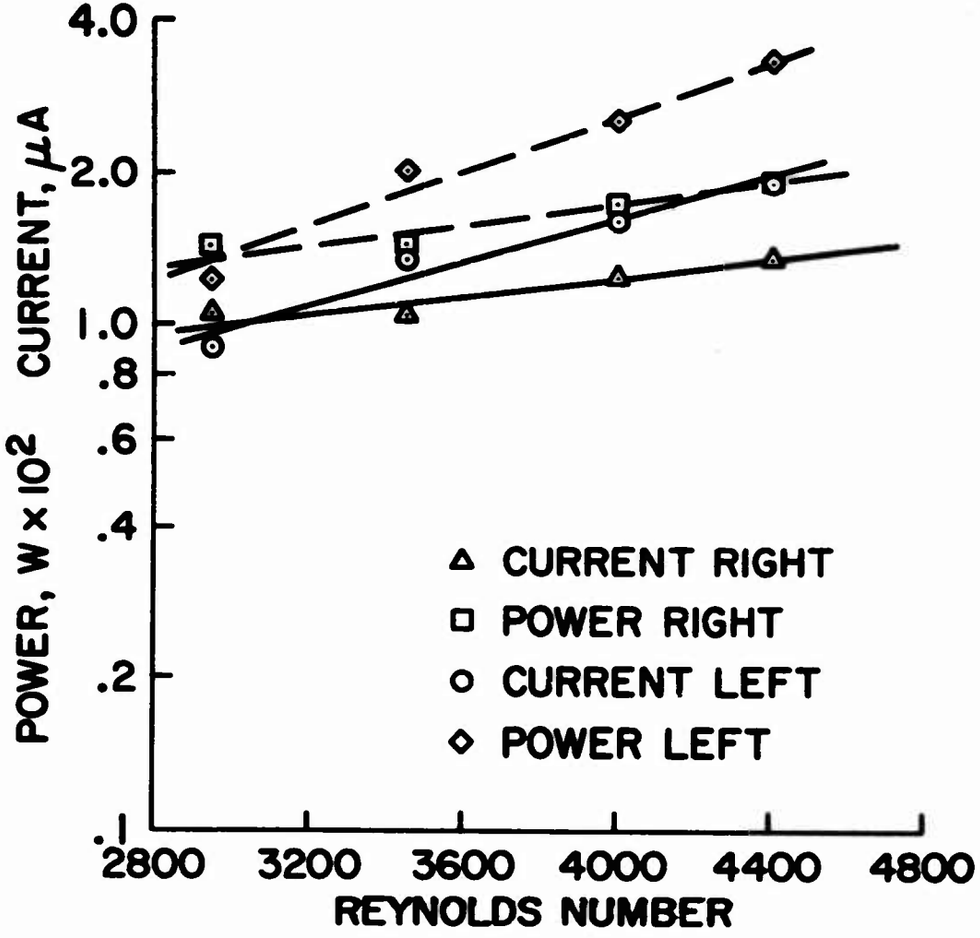

Fig. 28 - Power and current for the small unit
A = 1 inch

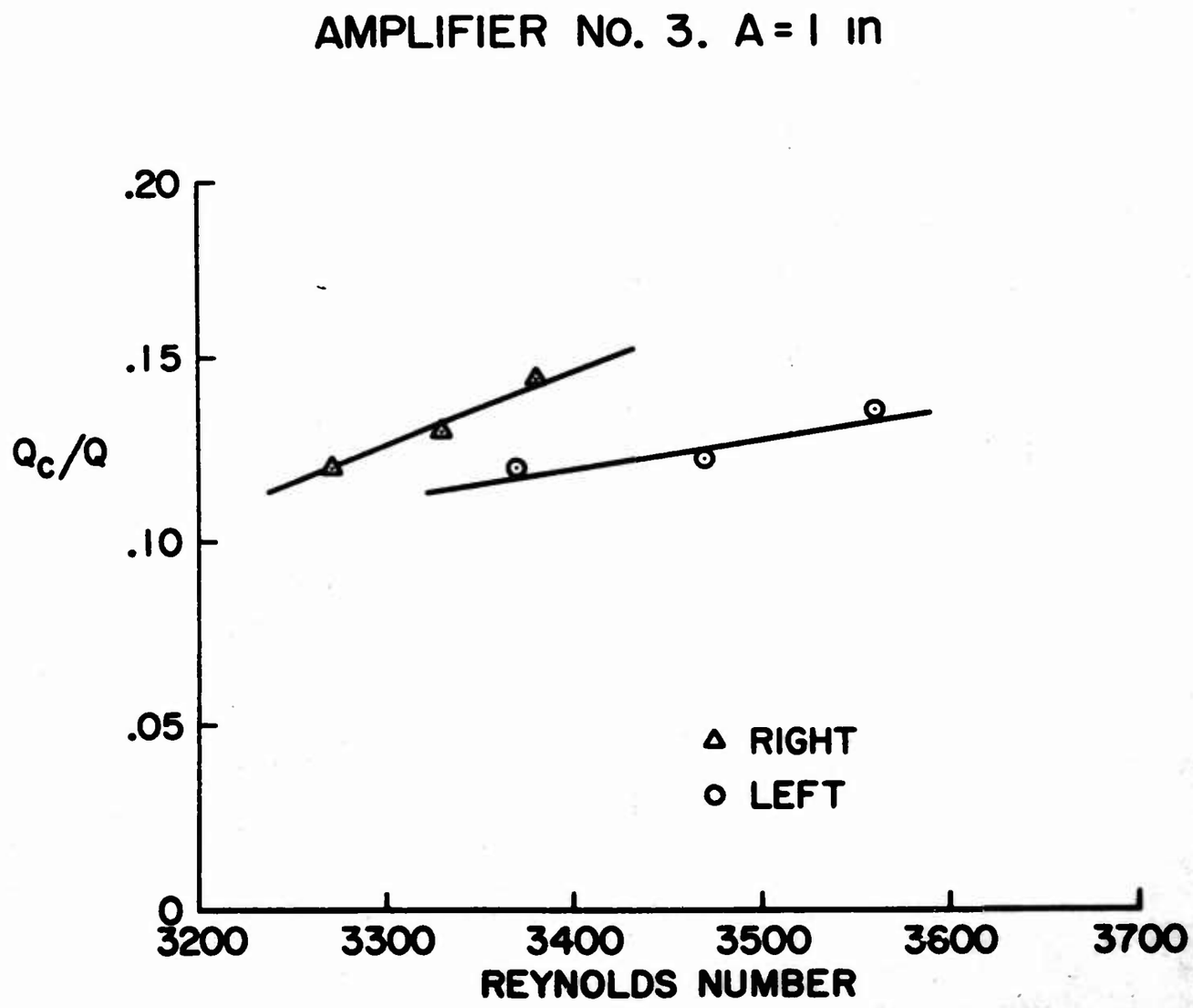

Fig. 29 - Ratio of control flow to primary flow for smaller unit

1. Condensation of Vapor

The condensation of vapors in the presence of a field was studied concurrently and independently by Choi and by this author.[22, 23] The study of condensation of vapors utilized an experimental arrangement shown in Fig. 30. Freon 113 was boiled by means of the electrical heaters in the bottom of the container. The cooled copper plate acting as the condenser surface is seen on the side of the container. The electrical fields were achieved by placing various electrodes directly in front of the copper plate. Shown in the sketch is a single wire electrode. In operation, the Freon boiled, and then the Freon vapor condensed on the cooled plate and ran down the plate back into the pool of Freon at the bottom. The heat balance was achieved by very carefully monitoring the mass flow rate of the coolant and the change in its temperature. The most significant results were achieved using a five-mesh screen grid located approximately 1/4 inch ahead of the copper plate. The results are shown in Fig. 31. It can be seen that an almost threefold increase in heat transfer occurs with the application of the electrostatic field. The line drawn represents the Nusselt theory for laminar condensation. The power required to accomplish the increased heat transfer is indicated in Fig. 32 and it can be seen that only a very low amount of energy is involved in obtaining the increased heat transfer. The actual condensation process with the field imposed is very interesting to observe. The condensation test rig is brought up to an equilibrium condition and the voltage is slowly increased between the screen grid and the cooled copper plate. No observable effect of the field is noted up to a critical value of the voltage. Above this value the condensate surface first becomes wavy then becomes very rough in appearance. During the increased condensation process, approximately as much condensate is observed to run off the screen grid as runs off the cooled plate, yet no observable spray is seen between the plate and the grid. Since the grid remains at vapor temperature it is obvious the condensation process does not occur on the grid.

It is believed that the mechanism involved is similar to that of colloid electric propulsion.[24] Very fine charged droplets of freon liquid are ejected from the condensate surface and are accelerated by the electrical field across the gap to the grid electrode where they collect and run off. No mist is seen simply because the droplets are very small.

2. Frost Formation and Heat Transfer with Fields

A simple experimental setup was used to investigate the behavior of frost formation in electric fields. The setup consisted of three parts: the test plate, made of a 1/2-inch thick sheet of copper and having a frosting surface of 6 x 9 inches; the refrigerating system, which was used to cool the test plate by circulating precooled refrigerant through the back of the plate; and the high voltage

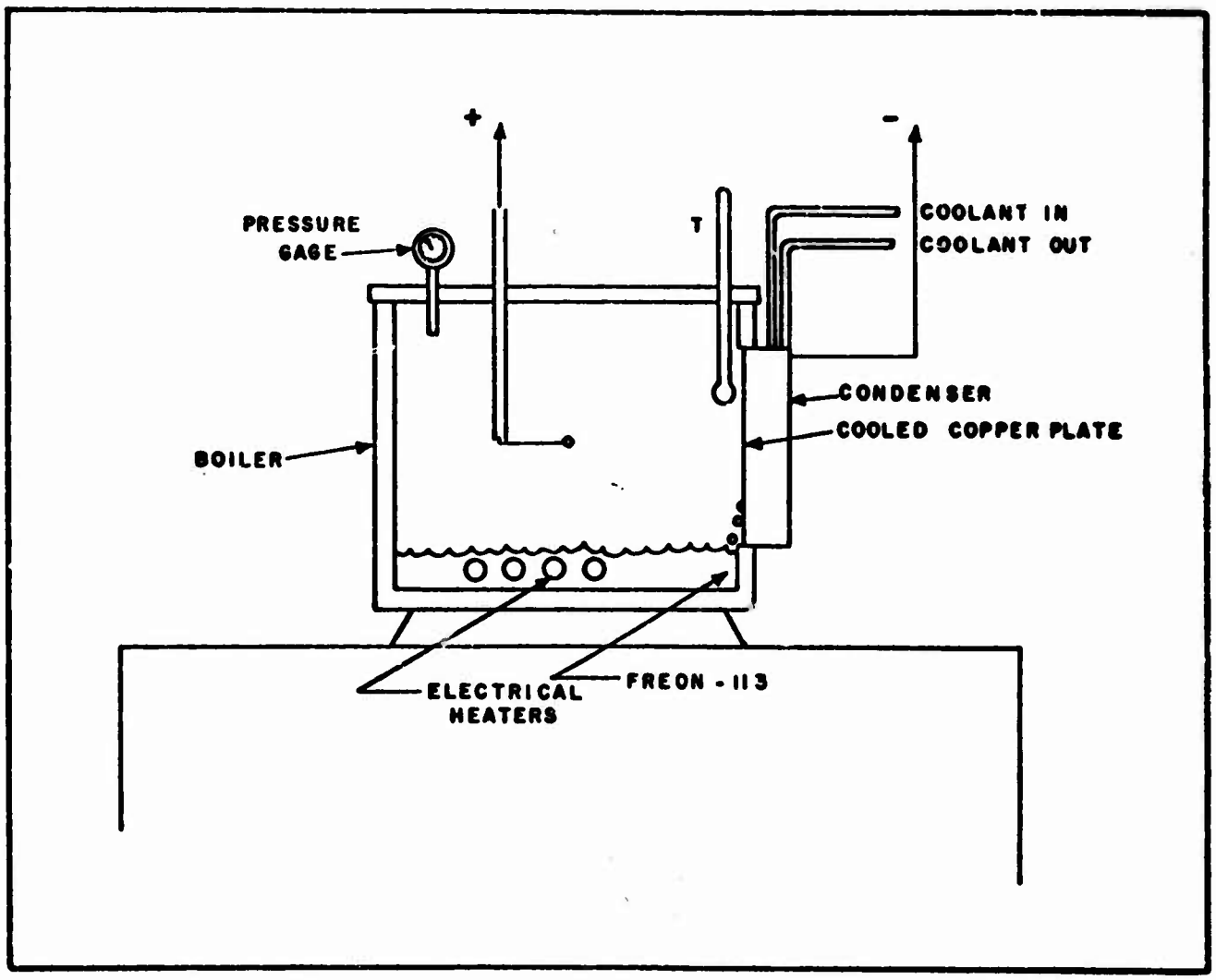

Fig. 30 - Schematic arrangement of experiments of condensation with fields

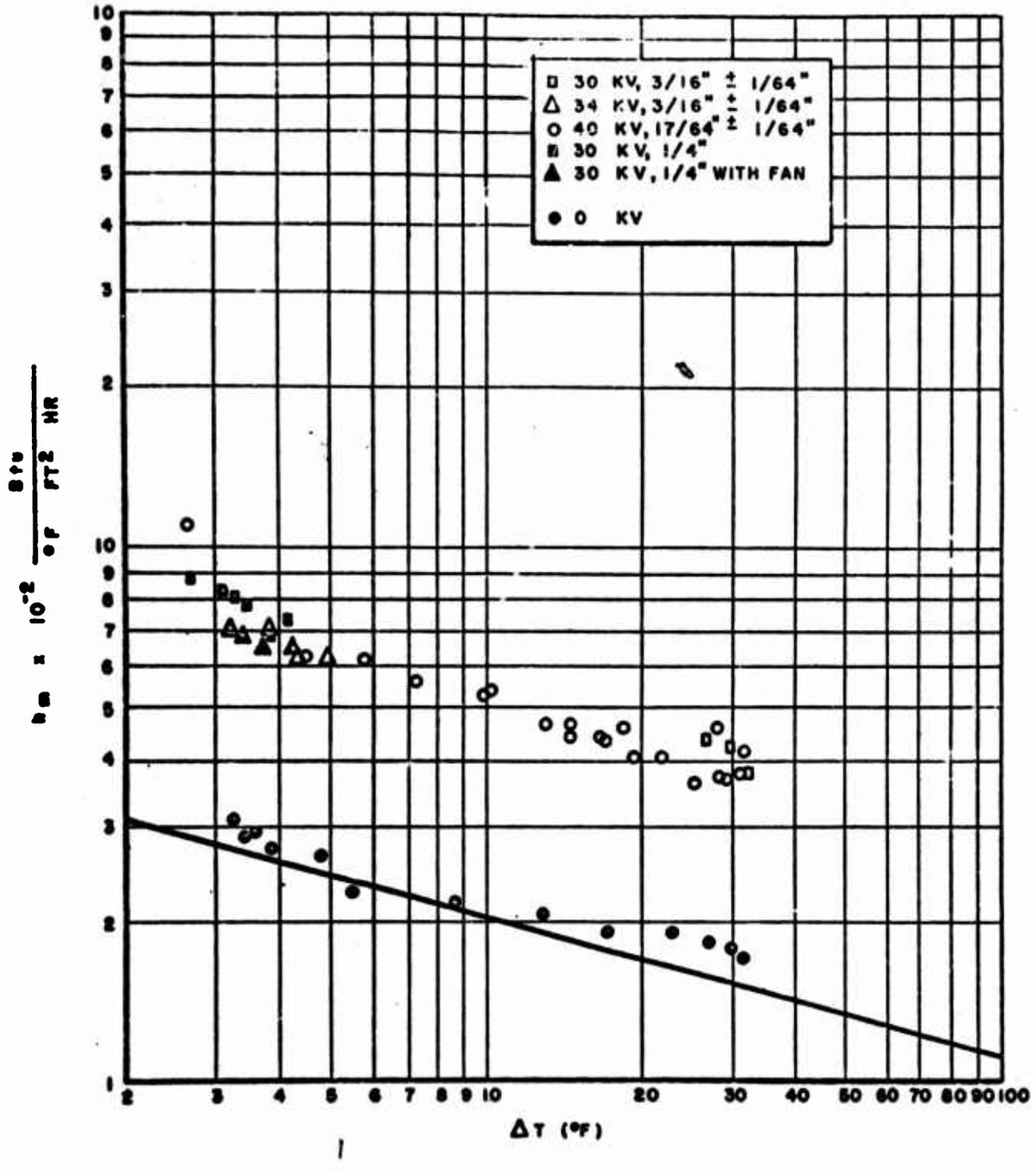

Fig. 31 - Effect of applied field to condensation heat transfer

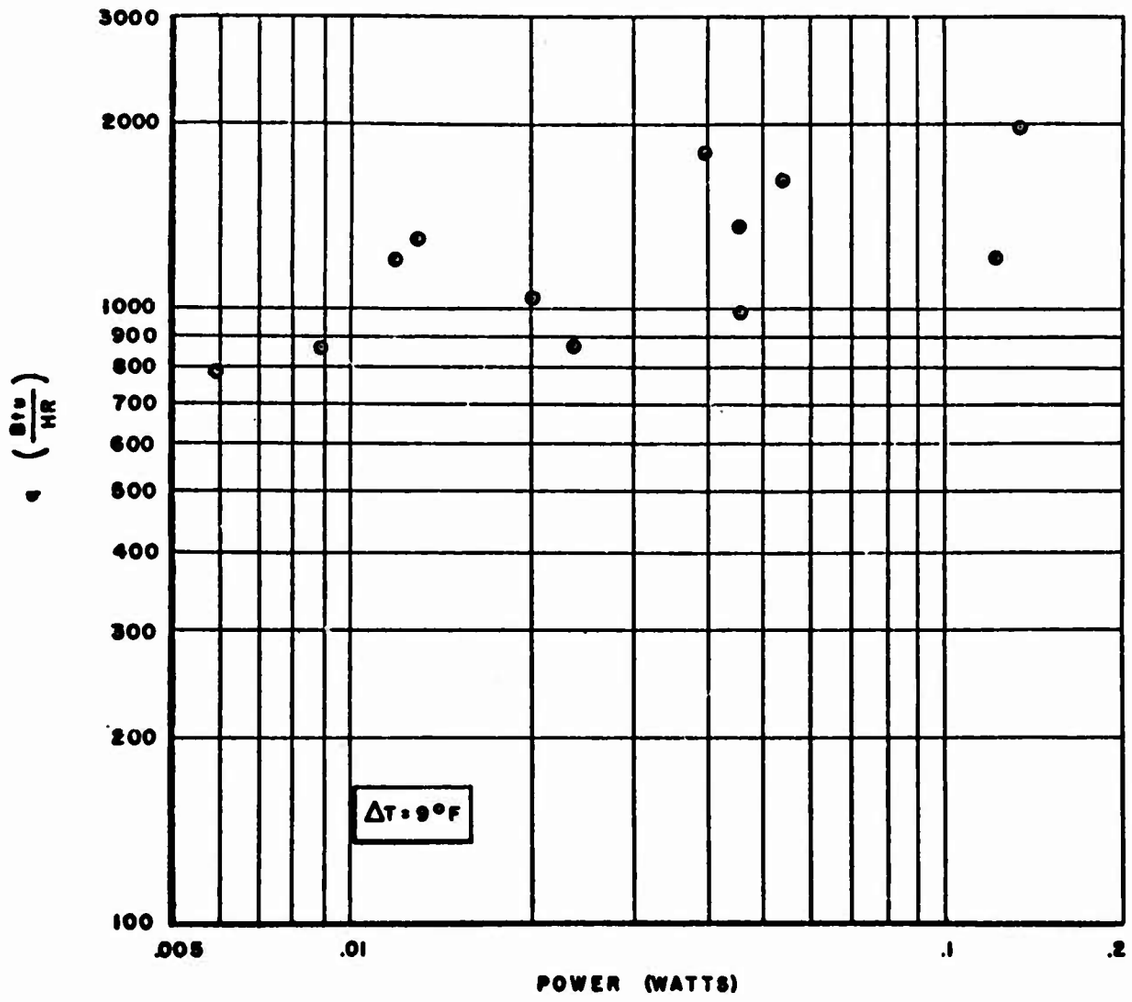

Fig. 32 - Variation of condensation heat transfer with electrical power input

power supply, which provided the strong electric fields. The test plate was installed vertically and the experiments were carried out under ambient air conditions.

Preliminary tests were conducted using uniform and nonuniform fields to determine the possible effects of electric fields on frosting. The uniform field was achieved by applying high voltage across the test plate and a parallel wire screen. A nonuniform field was established by using a horizontal corona wire parallel to the centerline of the plate with the wire positive. In both cases, the test plate was grounded. The results of the preliminary tests can be summarized as follow :

1. A uniform field does not seem to have any observable effects on frosting at the initial stages of the process. But it remains to be determined whether a uniform field will affect the growth of frost at a later stage when loose frost begins to form.

2. A nonuniform field characterized by a corona discharge has significant effects on frost formation.

3. For the case of wire-plane electrode configuration, the frost formed a strip centered along the line of normal projection of the wire on the plate. In the direction transverse to the strip, the frost layer achieved a maximum thickness at the center and thinned out in both directions with increasing distances from the center. Along the frost strip transverse ridges were observed to appear. These may be due either to the inherent non-uniformity of the corona or to an electrohydrodynamic instability induced by the field. Figures 33 and 34 show effects on frost.

4. The effects of corona discharges on frosting can be attributed to the impingement of electric wind induced by the corona, which changes the flow field from free convection to forced convection.

A second experimental sequence using single wire-plane electrode configuration was undertaken to study the flow field created by the impinging electric wind and to provide further information on electric field effects on heat and mass transfer processes in connection with frost formation. The mass transfer data indicated that for a test period of five minutes an increase of 200% in the total frost accumulated could be obtained at a total current of 100μa, as compared to the case of no field. The rate of increase of frost deposition decreased with current, suggesting the existence of an upper limit on the total frost versus total current curves. The heat transfer data

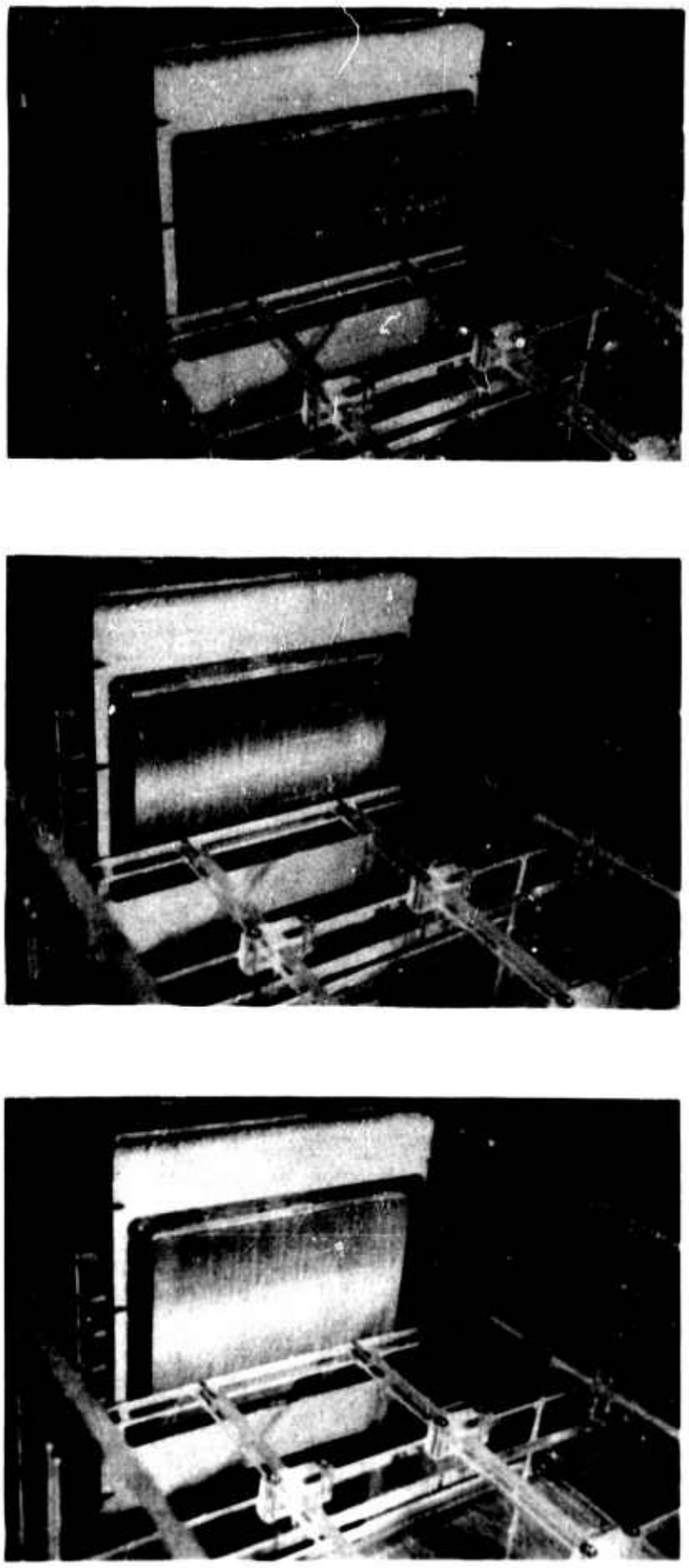

Fig. 33 - Initial frost build-up with electric field

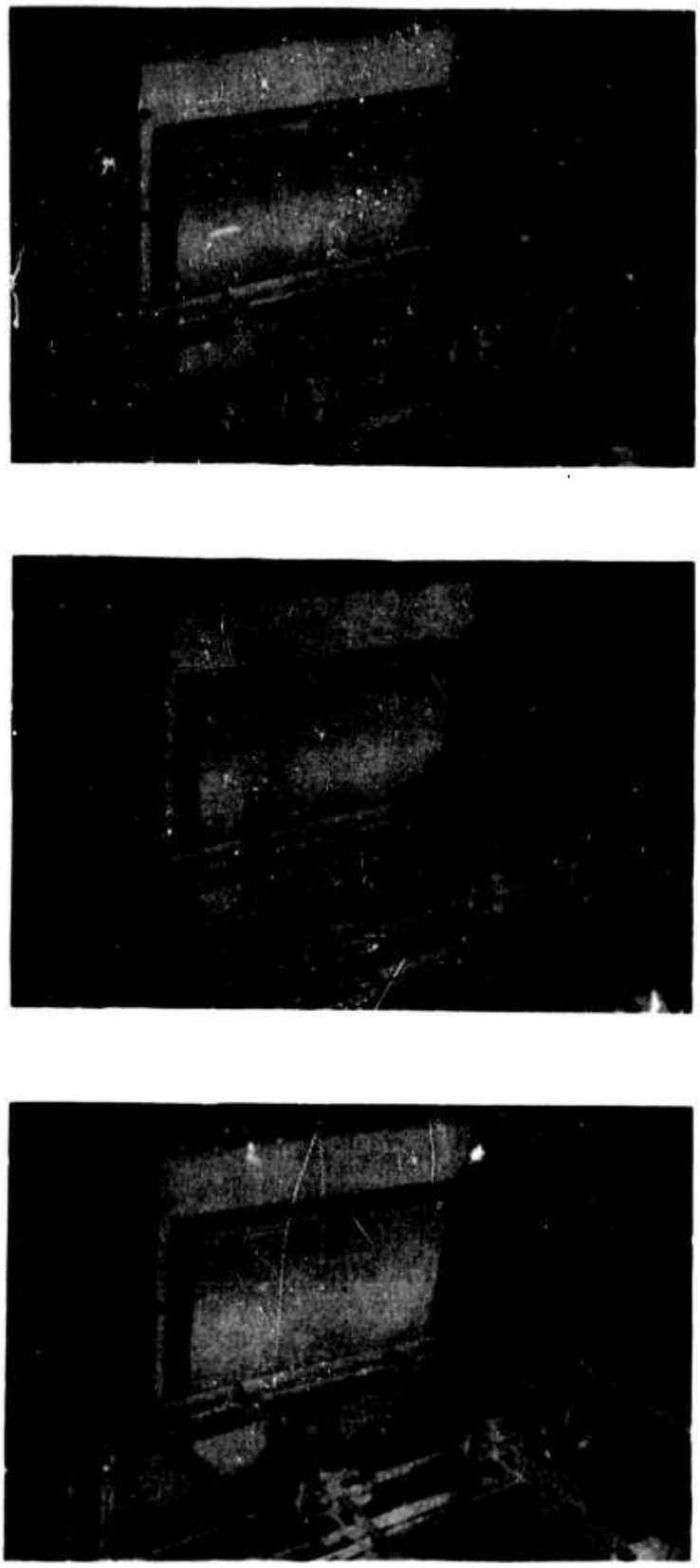

Fig. 34 - Frost build-up at later time

also showed a significant increase in total heat transfer rate in the presence of corona discharge with an increase of up to 100% at 150μa.

The velocity distribution of the electric wind was measured by means of a total head pitot traverse. It was found that the wind was confined to a narrow region within one inch from the stagnation point and the velocity assumed a bell-shaped distribution, Fig. 35. Current distribution was also measured underneath the corona wire by using a segmented electrode on the cooled plate. The result is shown In Fig. 36 for various values of applied voltage. Because of the similarity of the two curves, velocity and current, each curve was nondimensionalized and compared assuming a centerline value of unity. The remarkable agreement is shown in Fig. 37. With the test plate acting as a cathode, the boundary layer velocity profile on the plate surface was measured at a distance two inches from the stagnation point and was found to be similar to that of a wall jet. Because of the presence of the strong electric field, it was not possible to measure the velocity distributions in the stagnation region and the transition zone.

The flow field produced by an impinging electric wind and the associated heat and mass transfer processes were theoretically analyzed. Comparisons were made between theoretical predictions and experimental data. Figures 38 and 39 show that the correlation was quite good for the case of frost formation with applied electrical fields while only a fair degree of agreement was achieved between the heat transfer theory and data with fields present. In summary, it appears that significant changes in frost formation are induced by the forced convection produced by the electric wind.

C. FLAME HEAT TRANSFER WITH FIELDS

Another possible area of investigation of the effects of electric fields fall in the area of the effect of fields on flame or combustion heat transfer. During combustion of relatively high degree of ionization takes place. It is of interest to determine whether this nautral ionization can be utilized to affect the heat transfer characteristics of flames. To study this, flat parallel diffusion flames of propane and air were formed in a flat combustion chamber; the wall on the fuel side served as an anode and the wall on the air side was the cathode across which a D.C. voltage of 3200 volts was impressed.[25] Four flames were investigated; three flames at equal velocities with various proportions of propane and one flame at a higher velocity. The leanest mixture was nonluminous and the richest mixture very luminous. The combustion chamber had segmented anode and cathode walls and was instrumented to measure local current density, local heat transfer rate, electric pressure, exhaust composition, and exhaust temperature as a function of applied voltage. The flames could be viewed through a window in the edge wall of the combustion chamber.

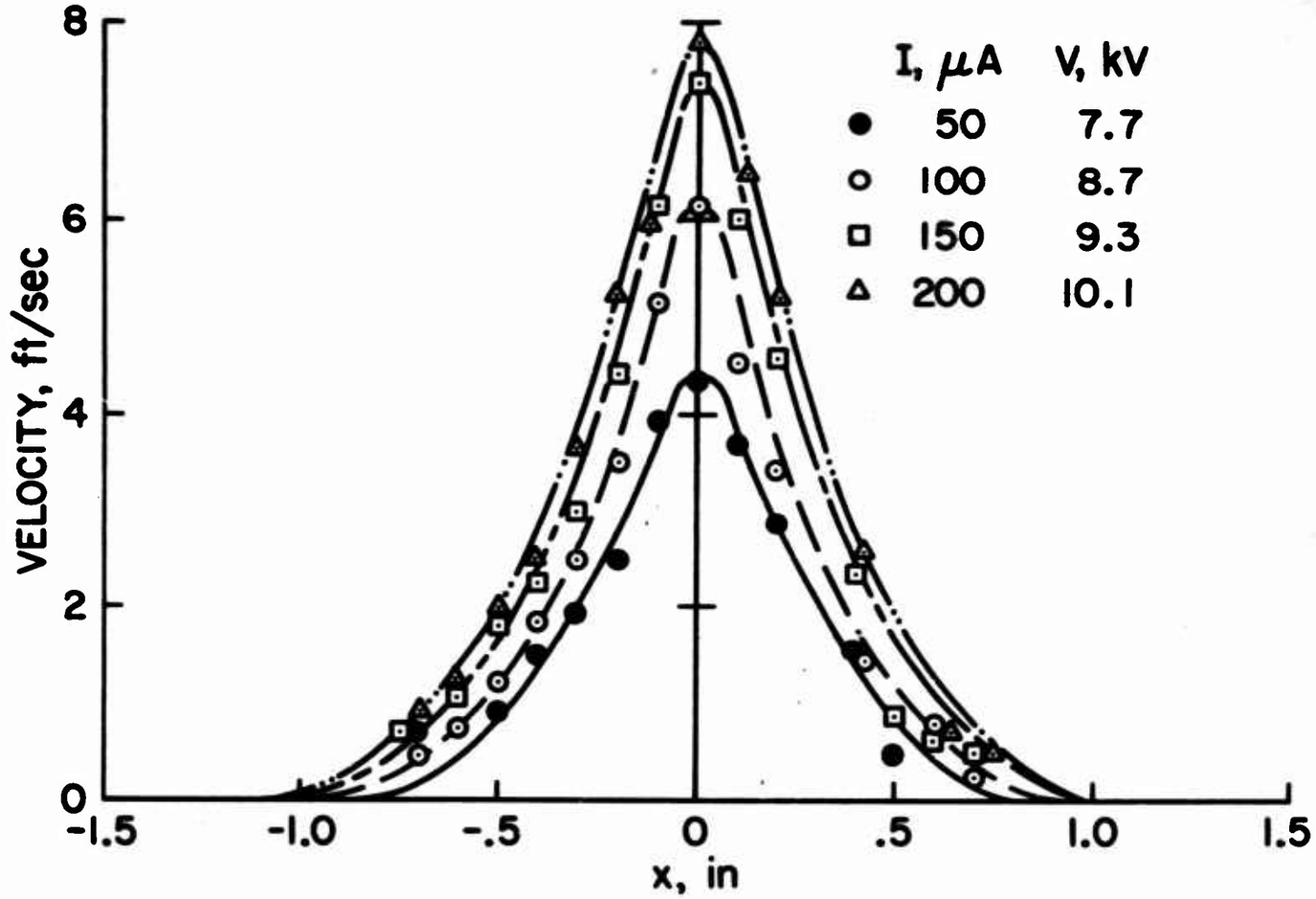

Fig. 35 - Velocity distribution of the electric wind behind a fine wire

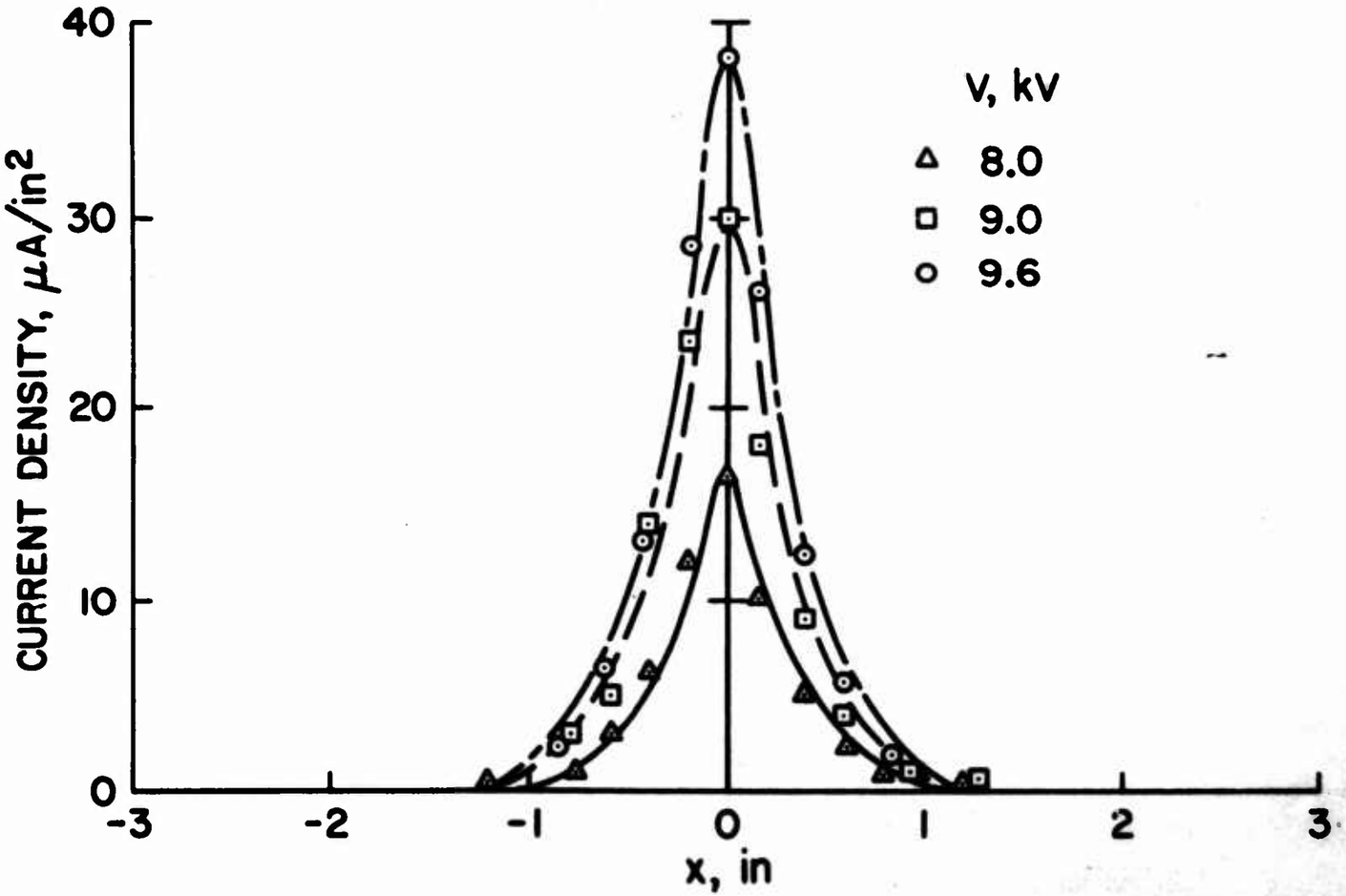

Fig. 36 - Current density distribution along the frosting plate surface

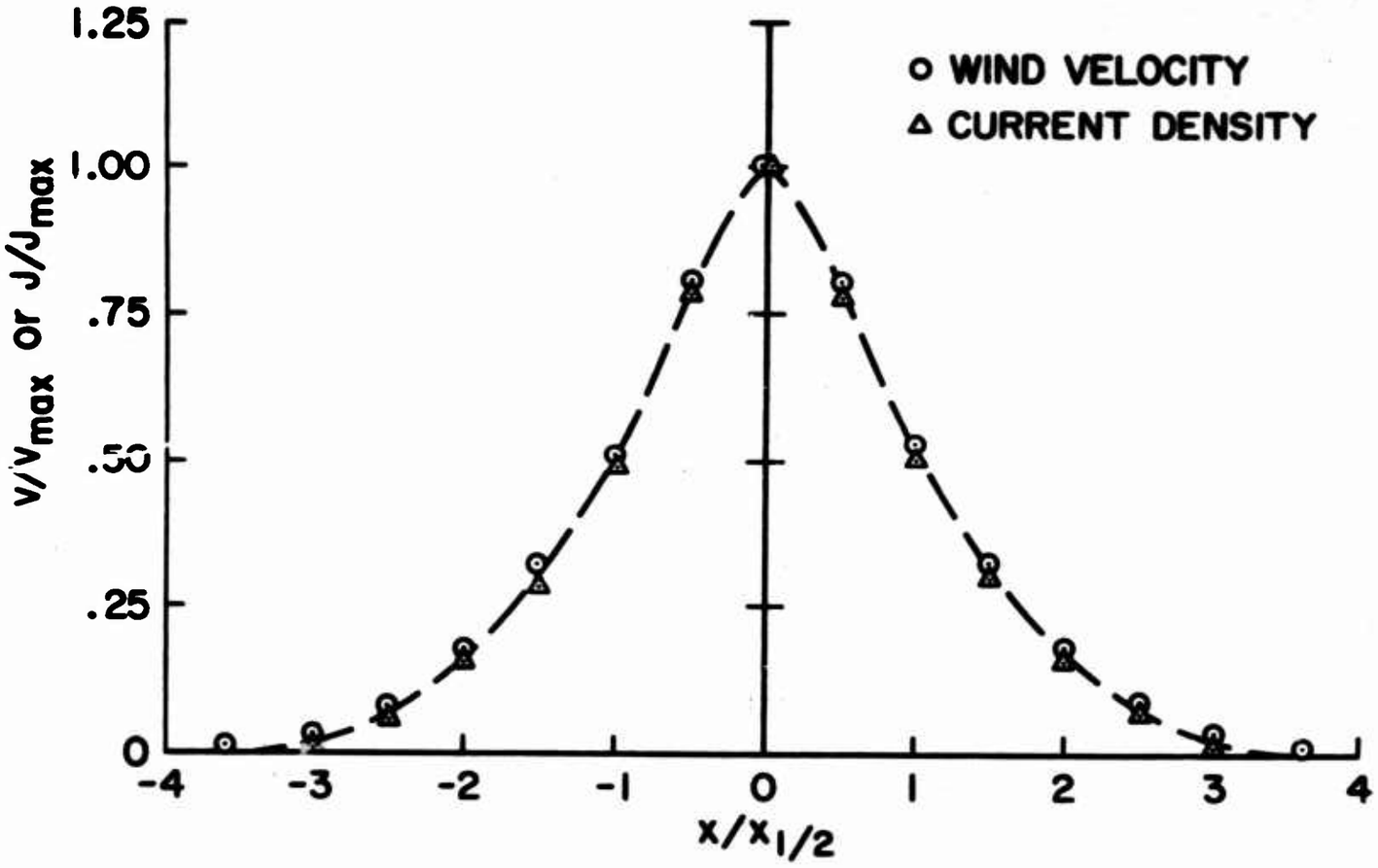

Fig. 37 - Comparison between dimensionless current density and electric wind velocity distribution

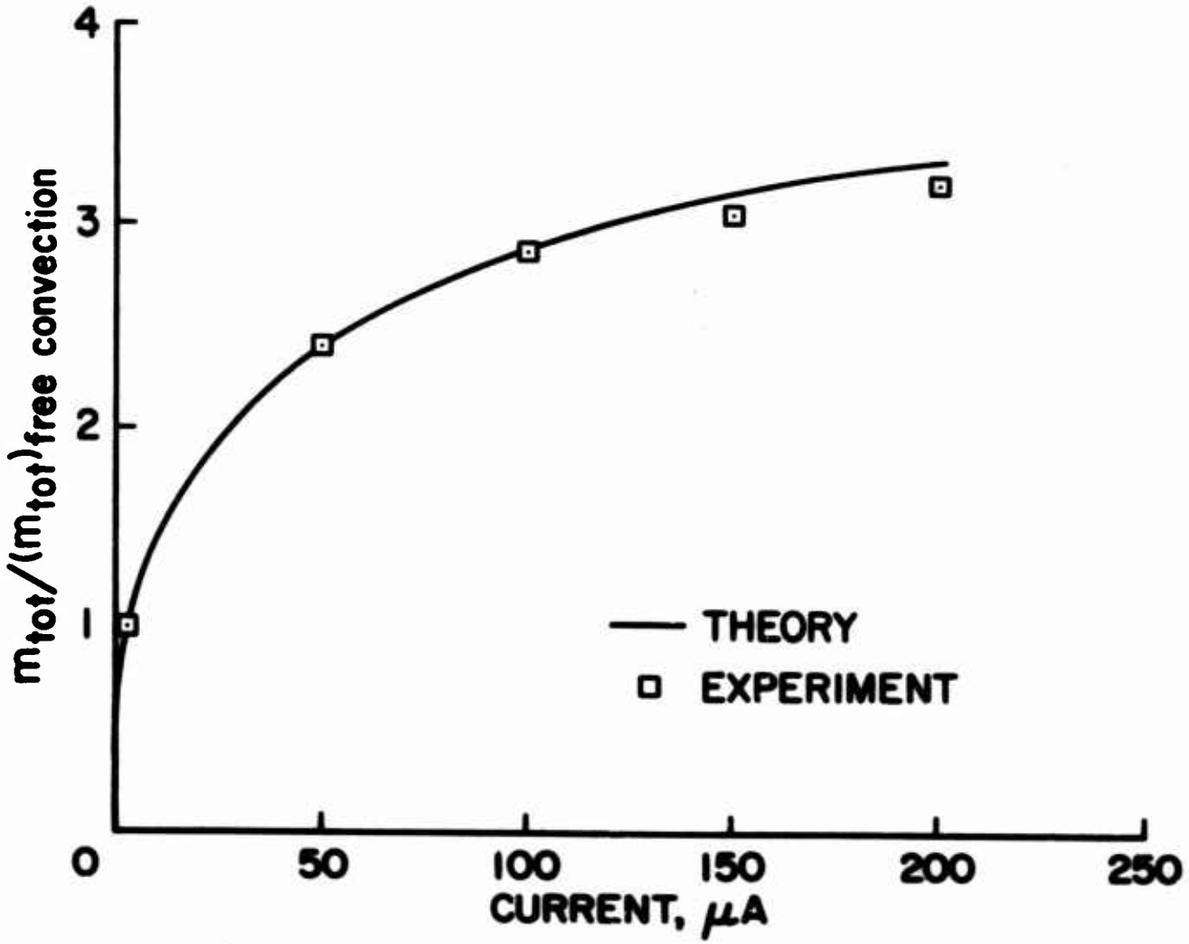

Fig. 38 - Comparison between theory and experiment for mass transfer

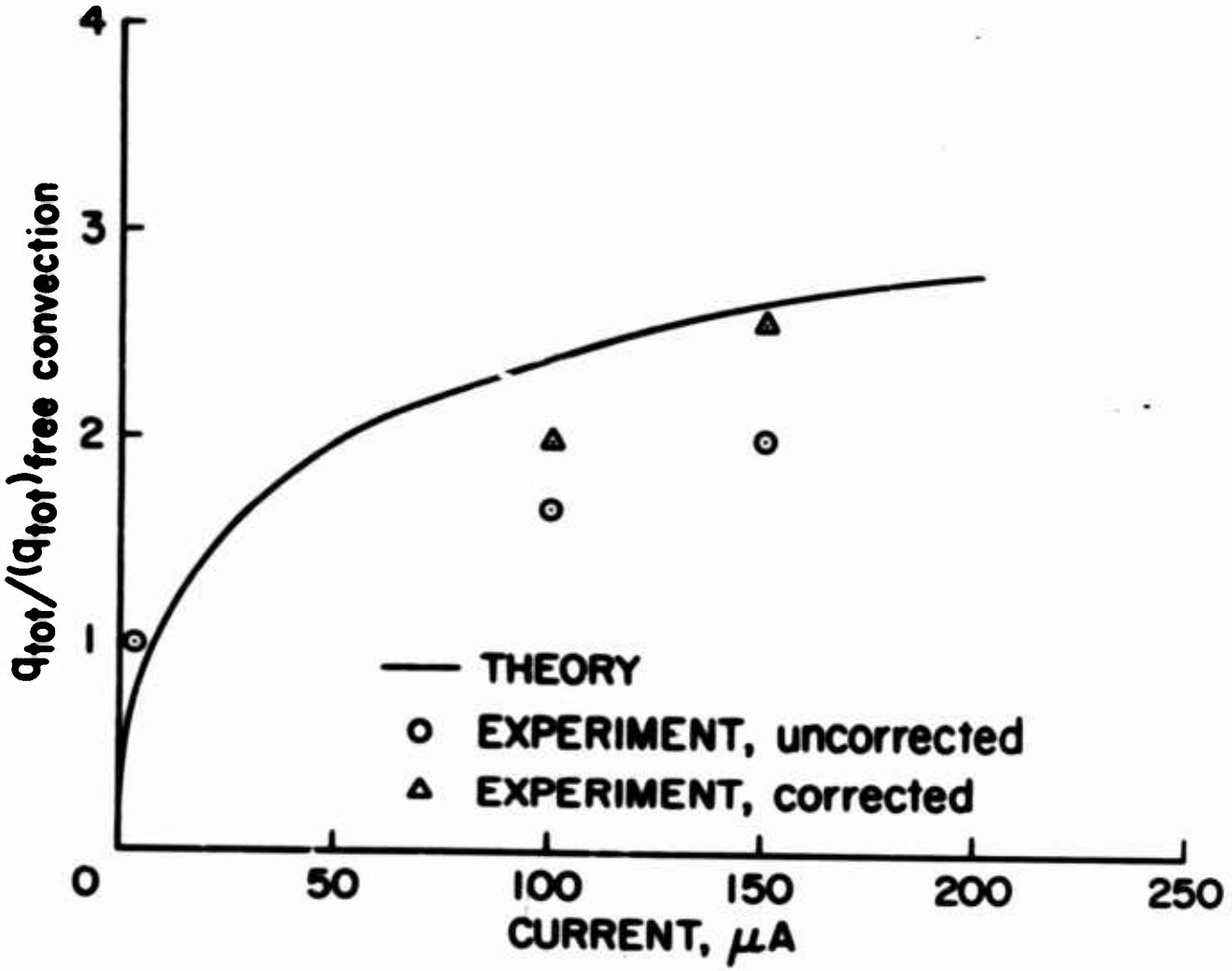

Fig. 39 - Comparison between theory and experiment for heat transfer

Figure 40 shows the experimental setup used. The upper picture shows the parallel sided combustion rig with the many heat transfer coolant loops and thermocouple wires. The lower picture shows the gas analyzer equipment and the coolant pump. Figure 41 shows a typical flame under various levels of applied electrical field. The severe distortion of the flame is clearly evident.

The applied electric field was found to affect the flame through three different mechanisms. It was shown that a gradient in current density along the flame was responsible for an induced gas motion away from the flame in the zone containing positive ions. Such an induced motion affected the concentrations of fuel and air in the chamber to cause the flame to move toward the cathode.

Another interaction between the field and the flame was the onset of a flickering condition which, with increasing voltage, appeared at upper parts of the flame first. A parameter for describing flame instability was set up which indicated that conditions near the saturation voltage of the flame favored instability. A stabilizing parameter proportional to the concentration gradients in the combustion chamber was defined which indicated that the flame gets less stable in the regions further downstream. Onset of stability was detected by an unsteadiness in the flame current observed on an oscilloscope.

A third mechanism was the attachment of electrons to carbon particles or molecules in upper parts of the flame. The resulting electrically induced drift of the negative ions tended to reverse the trend of induced motion toward the cathode at lower parts of the flame.

The electric interactions with the flame were found to affect greatly the heat transfer rates, especially near the base of the flame. At the highest voltages applied, the flame was observed to impinge directly on the cathode with increase in local heat transfer over the no voltage case of up to a factor of 6. The anode heat transfer rate near the base of the flame was found to be reduced up to 85%. At progressively higher parts of the flame, the electric effect decreased. Typical data are shown in Fig. 42. It is, therefore, concluded that heat transfer rates can be either increased or decreased in a controlled manner by the application of fields.

The maximum current density from the flames were only of the order of either microamperes per square inch of flame surface and, therefore, direct effects of current such as recombination were extremely small compared to the heat transfer rates.

Appreciable decreases in the amount of carbon monoxide and unburnt hydrocarbon were found to be obtained by the application of voltage; solid carbon formation was found to increase. A possible explanation for the increase in solid carbon is the electron attachment to carbon particles in the pyrolysis zone with a subsequent movement away from the flame, favoring escape of the particles from combustion.

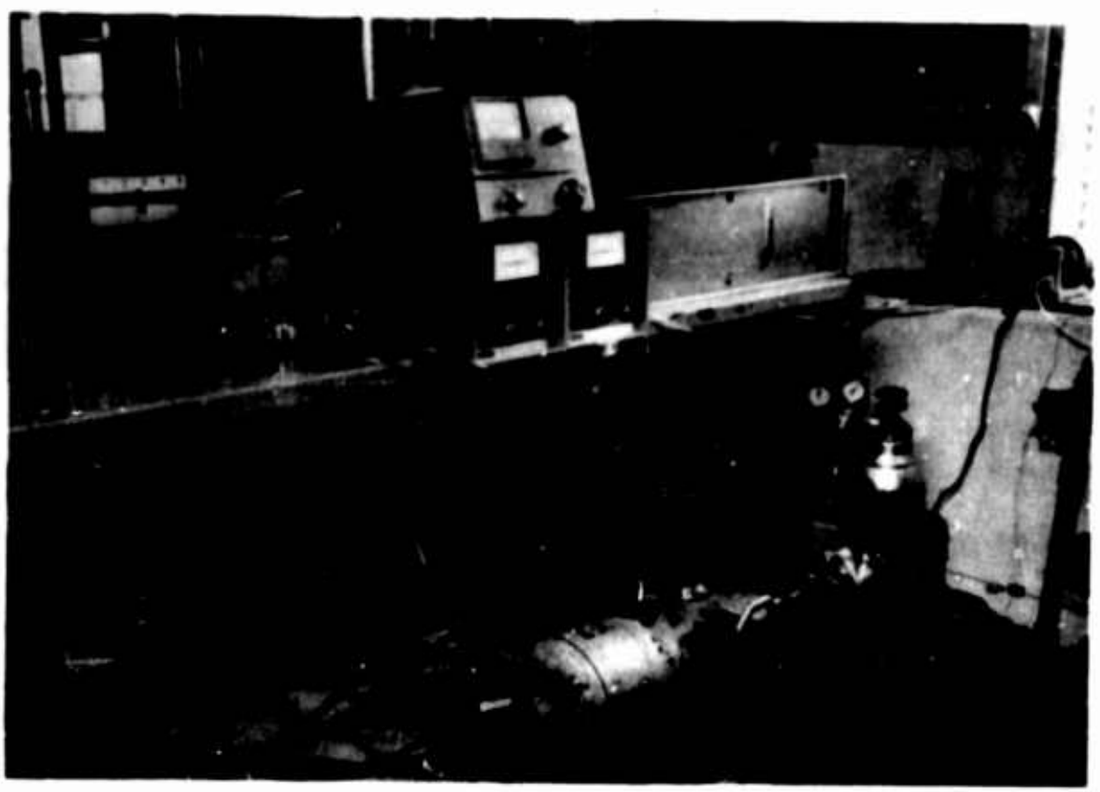

Fig. 40 - Experimental apparatus for flame heat transfer with electric field. Upper figure shows combustion chamber. Lower figure shows gas analyzer and pumping equipment

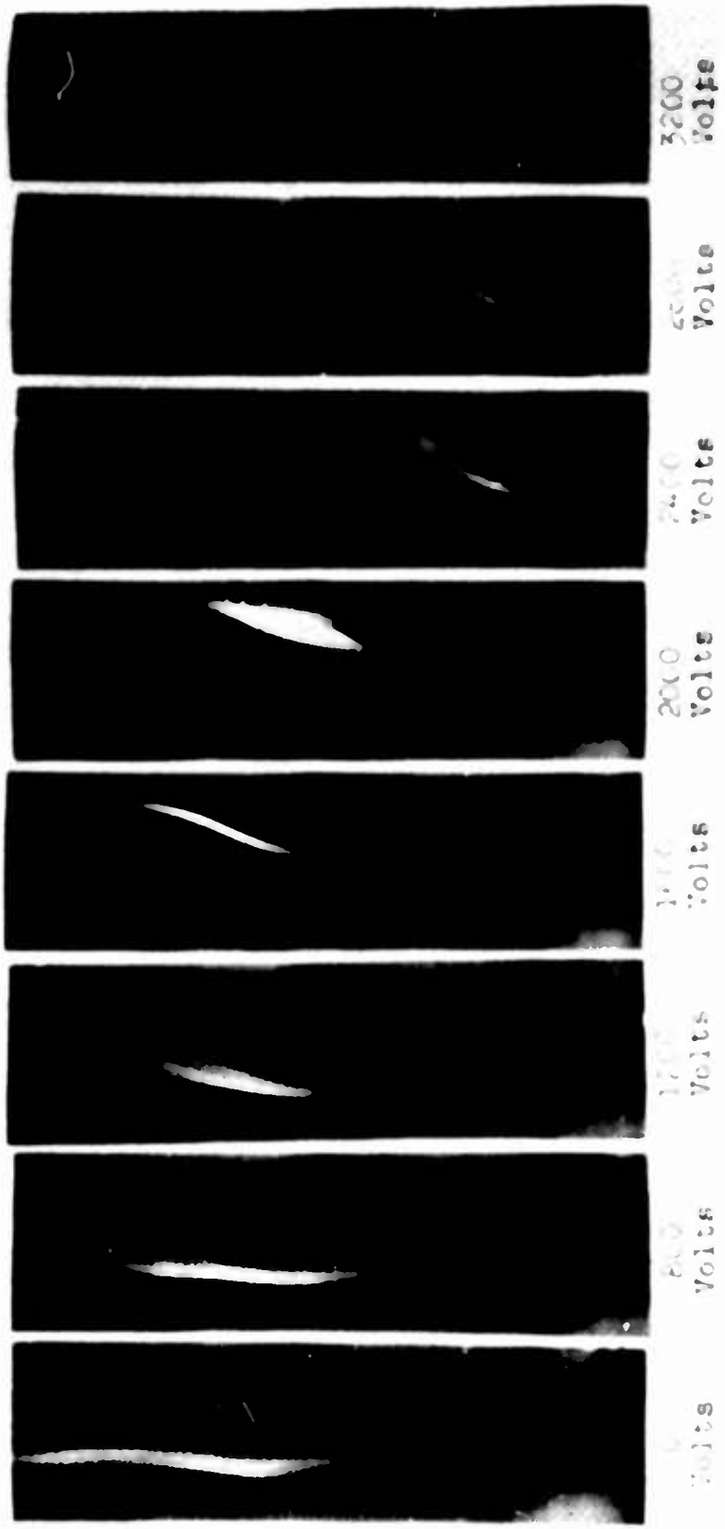

Fig. 41 - Distortion of a flame due to applied field

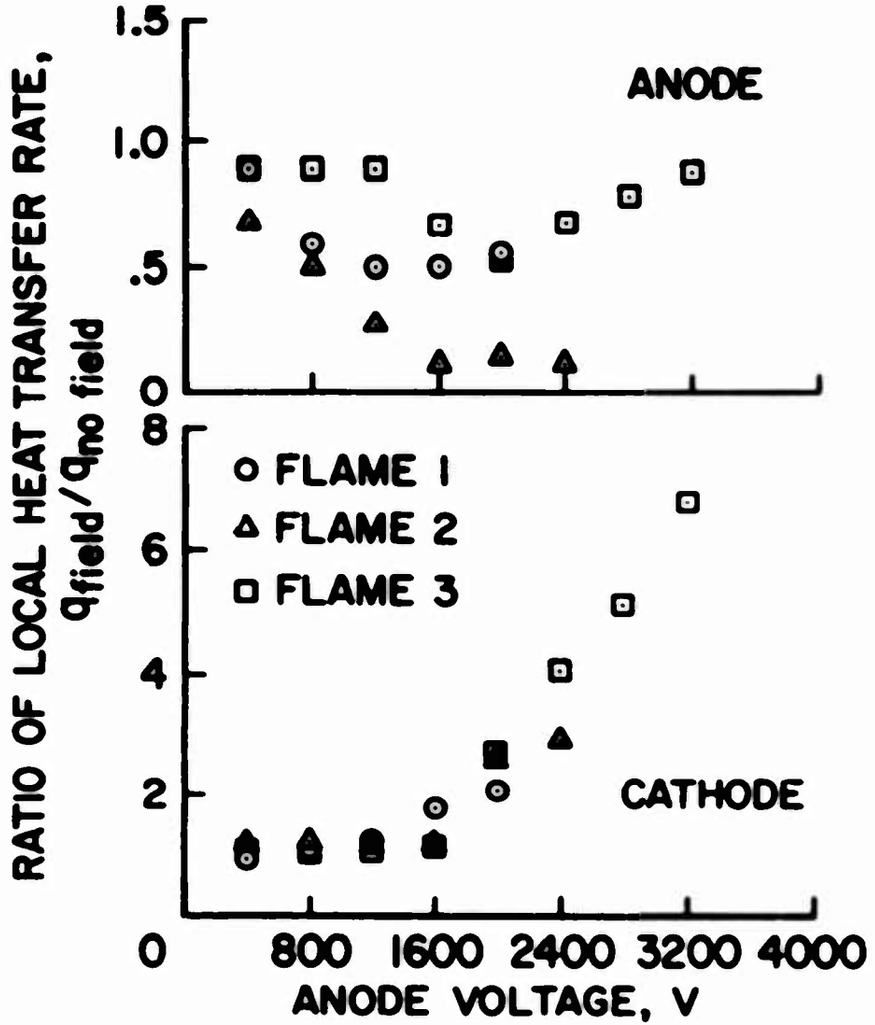

Fig. 42 - Effect of the electric field on heat transfer rate

There were indications that the heat transfer was convection controlled, but a possible strong mechanism for an electric effect on luminous flames was outlined. It may be possible to control the emissivity of flames through the influence of the electric field on the formation, growth, or combustion of charged particles in the flame.

D. ION FLOW DIAGNOSTICS

It is considered possible to utilize ions injected into a gas stream as a means to study the basic nature of the fluid flow. Since in the case of air, the ions would be either O_2 or N_2 ions, they would tend to travel with the fluid readily and follow the particles paths with little delay. In the case of steady flow they would indicate the actual streamline pattern. As an illustration of their use in this manner one has only to look at the study of the secondary flows in the channel using electrostatic probes, or to the work of Donnelly on secondary flows.[26] It is apparent that the ion currents are responsive to the fluid flow situation and that further investigation in this direction is warranted.

1. Velocity Meter

One of the most intriguing applications of the use of electrostatic effects in flow diagnostics is the air velocity meter being studied by Professor Durbin of Princeton.[27] In this device the air flow to be measured passes through a cylinder. At the axis of the cylinder a coaxial electrode is placed in which a central thin disk is placed as a corona discharge electrode. In the inner wall of the cylinder an outer electrode is located which has a finite well controlled internal resistance. A corona discharge is initiated between the corona electrode and the cylinder wall. The ions created tend to move radially across the gap towards the cylinder wall. The air flow moving through the cylinder carries the ions downstream and they impinge on the outer wall slightly downstream of the discharge electrode. When this happens, the potential drop along the wall resistor is now different for the forward part of the resistor as contrasted to the aft portion. By means of a suitable external bridge and an electrical balancing circuit, the device will indicate the velocity of flow which caused the axial drift of the ions. The device is quite sensitive and it is believed that it can easily measure velocities down to a few feet per second. An early calibration curve is shown in Fig. 43.

2. External Flow Ion-Diagnostic Studies

In an attempt to extend the ion-diagnostic techniques to large scale flows, a series of tests were run in the Army Aeronautical Research Laboratory's 7 x 10-Foot Wind Tunnel at Ames Research Center.

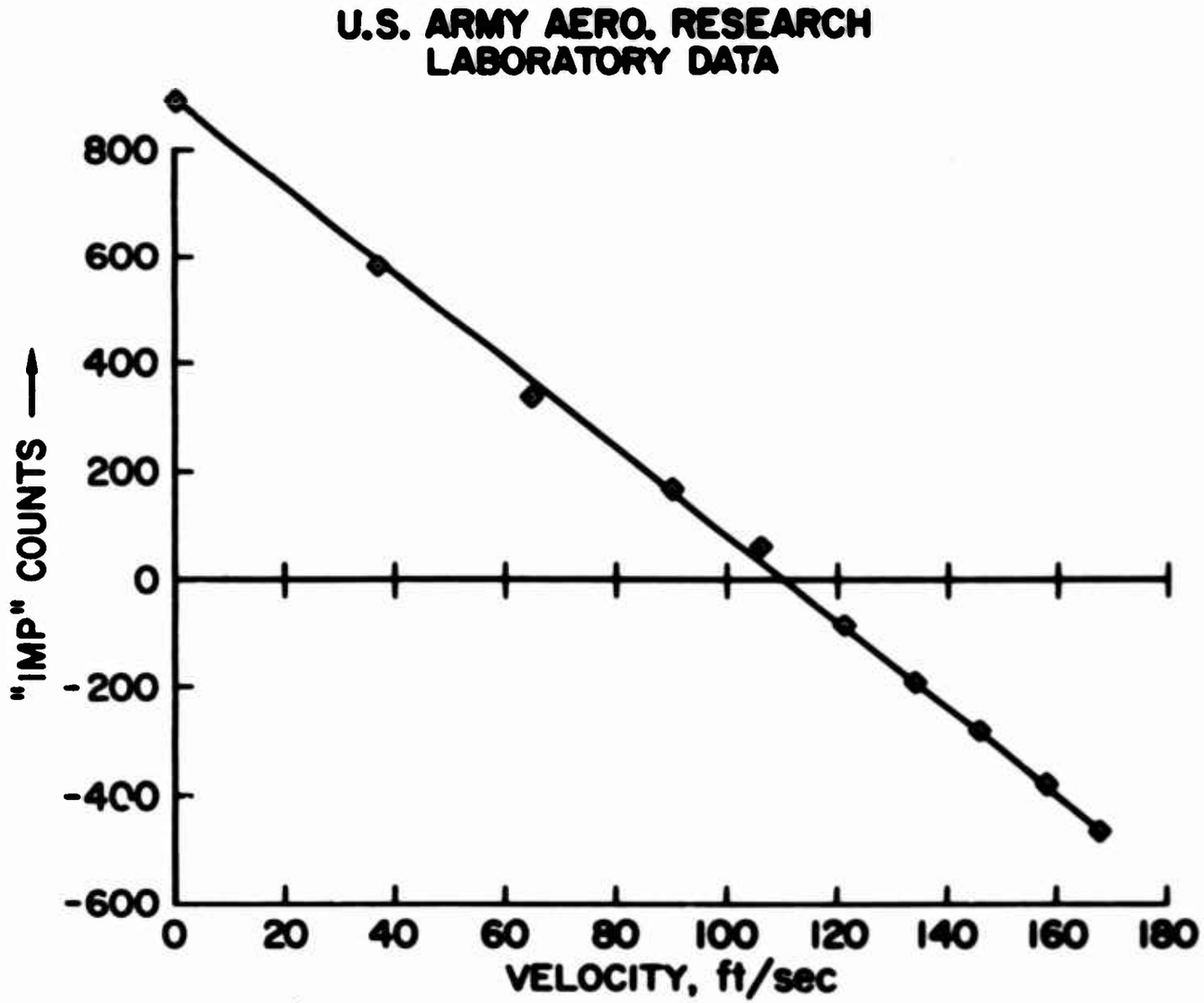

Fig. 43 - Calibration curve for velocity meter

Initial tests were conducted on a six-inch diameter cylinder three feet in length mounted crosswise to the airstream. Ions were created by a fine wire (0.0015" dia.) electrode located ahead of the cylinder. Field shaping electrodes were placed at the same forward location as the corona wire but above and below the wire. Several conducting electrode strips were mounted on the cylinder and each strip was grounded through a common resistor (12 megohms). The arrangement is shown in Fig. 44. The electrical output of ea · strip was monitored by filtering the signal developed across the grounding resistor through a Krohn-Hite filter, and observing the wave motion on an oscilloscope. The first oscilloscope picture, Fig. 45, shows the voltage trace at a forward position on the cylinder as well as one on the aft part of the cylinder. The velocity is at a tunnel q of one (30'/sec). The regular oscillations of the upper traces is indicative of the basic flow about the cylinder. These oscillations are believed to be caused by potential flow oscillations which accompany the periodic vortex shedding associated with the Von Karman vortex street. The lower trace illustrates the flow condition in the aft "dead water" region of the cylinder and it is very clear that a significant difference exists in the two regions. The upper traces of Fig. 46 illustrate the flow at a position on the cylinder just forward of the maximum height of the cylinder, and the lower traces show the flow at a position somewhat aft of the maximum position. It is believed that the upper trace still follows the overall gross oscillations of the flow. The lower trace showing somewhat erratic motion appear to indicate a separated region of flow aft of the maximum height of the cylinder. Thus, the ion technique seems to be giving proper information from a qualitative standpoint.

Next a splitter plate was mounted directly aft of the cylinder at the centerline. It was 18 inches long and fitted with an aluminum plate at the rear to provide strength. The splitter plate was used in an attempt to reduce the periodic shedding from the cylinder. Ion-diagnostic tests were run with this configuration, and typical results are shown in Fig. 47. The upper trace represents the flow near the front of the cylinder and the lower trace, the flow in the aft position near the juncture of the splitter plate and the cylinder. This figure can be compared with Fig. 45 and it can be seen that the oscillations are no longer as cleanly periodic as seen previously without the splitter.

Current measurements were also taken at the aft edge of the splitter plate in an attempt to determine if the ion measurement technique could be effective at a point over two feet away from the corona wire. In Fig. 48 a comparison is made between a current trace from an electrode at the most forward side of the cylinder, and a trace from the rear plate. The top "wide trace" is from the front of the cylinder and the lower widely oscillating trace is from the aft plate. It is clearly evident that the ion technique is effective at significant distances from the source. It should be noted that the vertical scale of this trace is reduced by one-half from previous pictures.

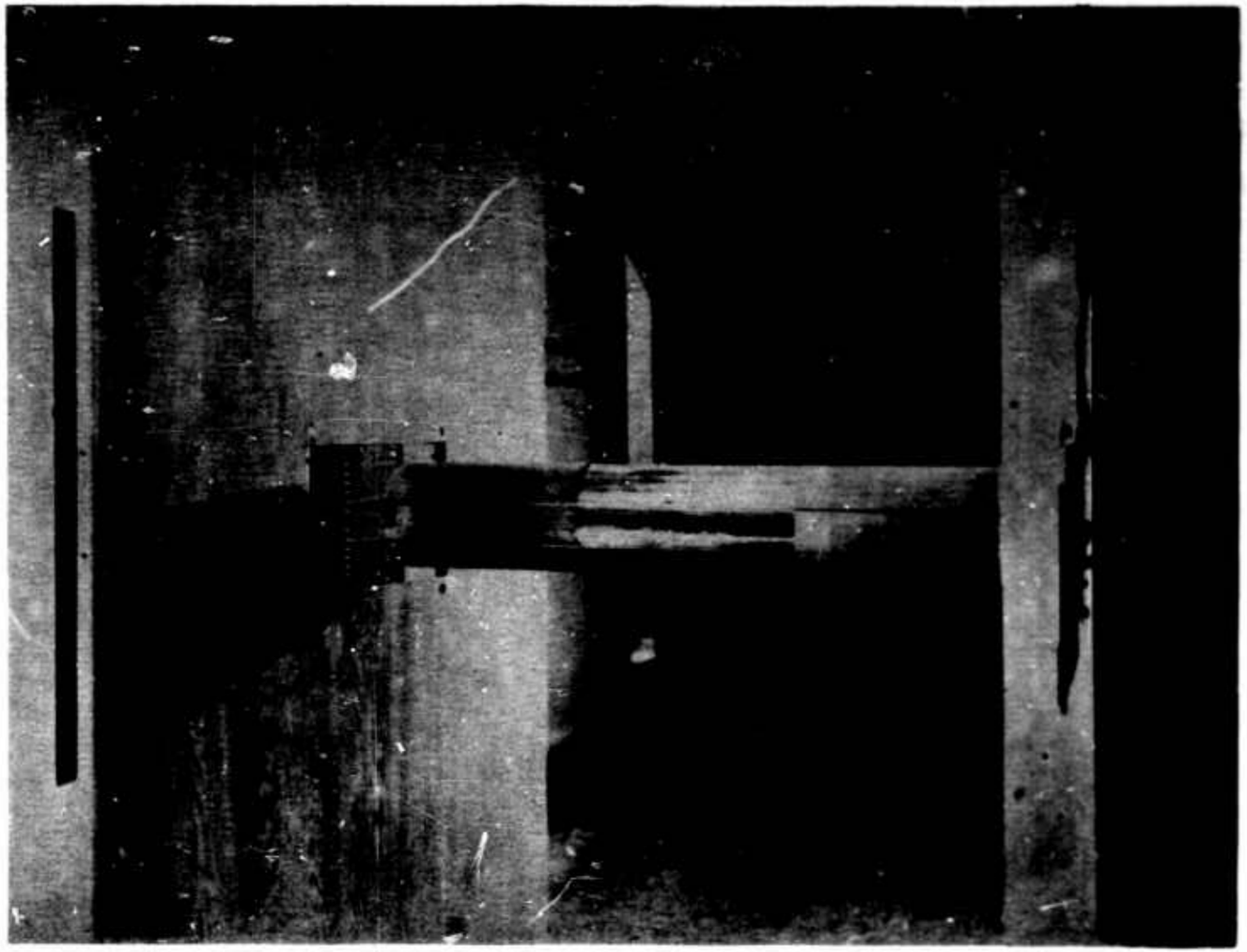

Fig. 44 - Six-inch diameter cylinder showing electrodes. U. S. Army Aero Research Laboratory, 7 x 10 tunnel

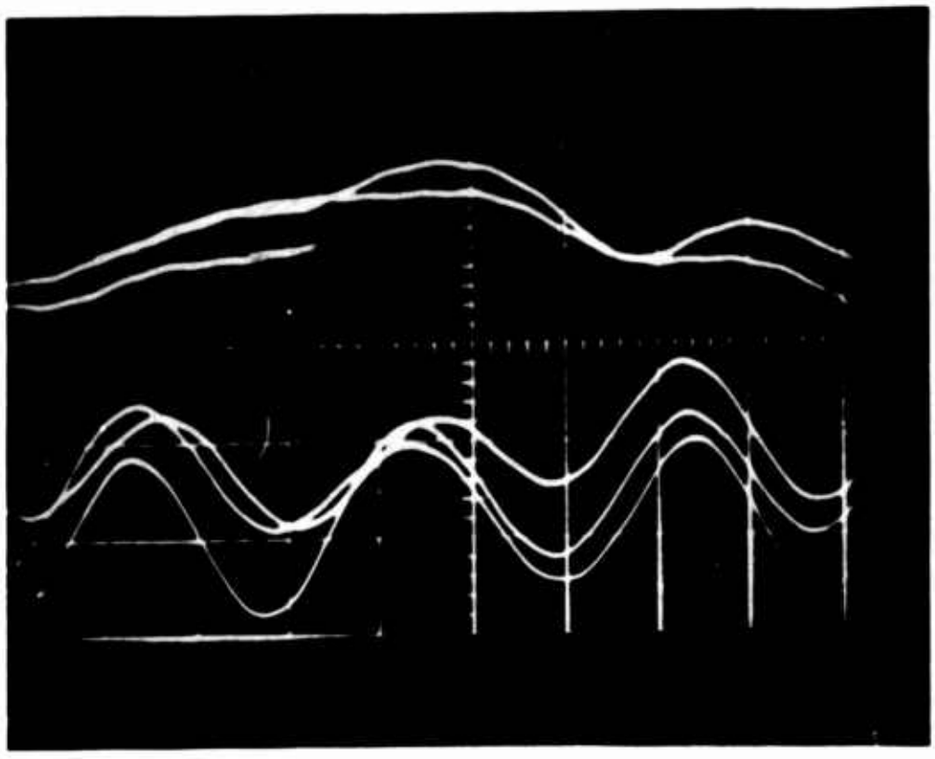

Fig. 45 - Oscilloscope traces. Current 3μa, q = 1. Upper trace from forward side of cylinder. Lower trace from rear of cylinder. Vertical scale 2mv/cm

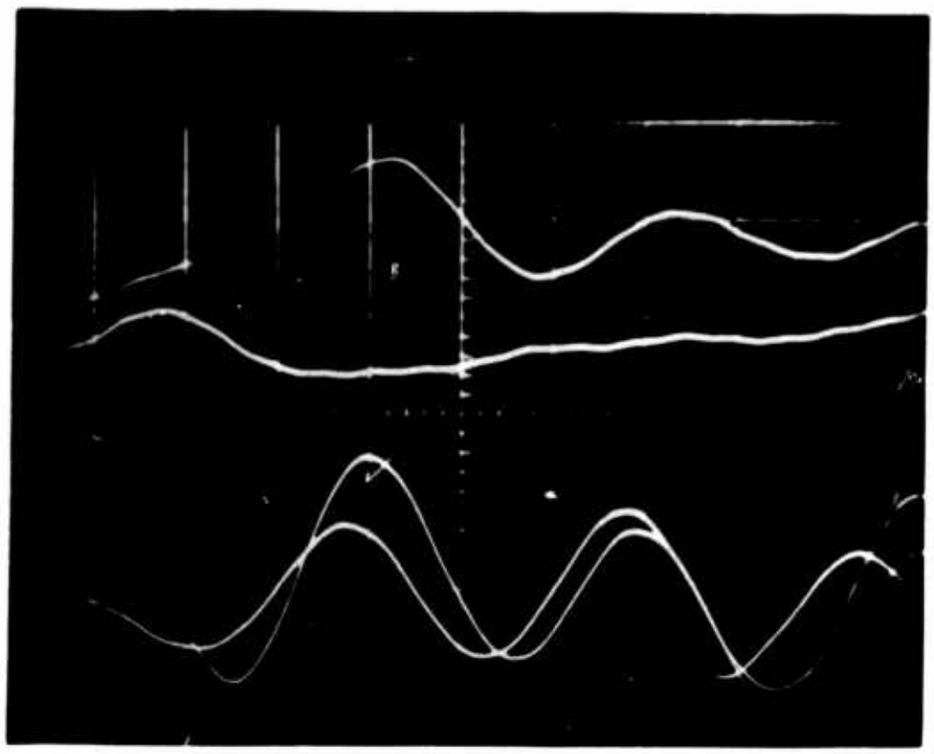

Fig. 46 - Oscilloscope traces. Current 3μa, q = 1. Upper trace just ahead of maximum cylinder width and lower trace just aft. Vertical scale 2mv/cm

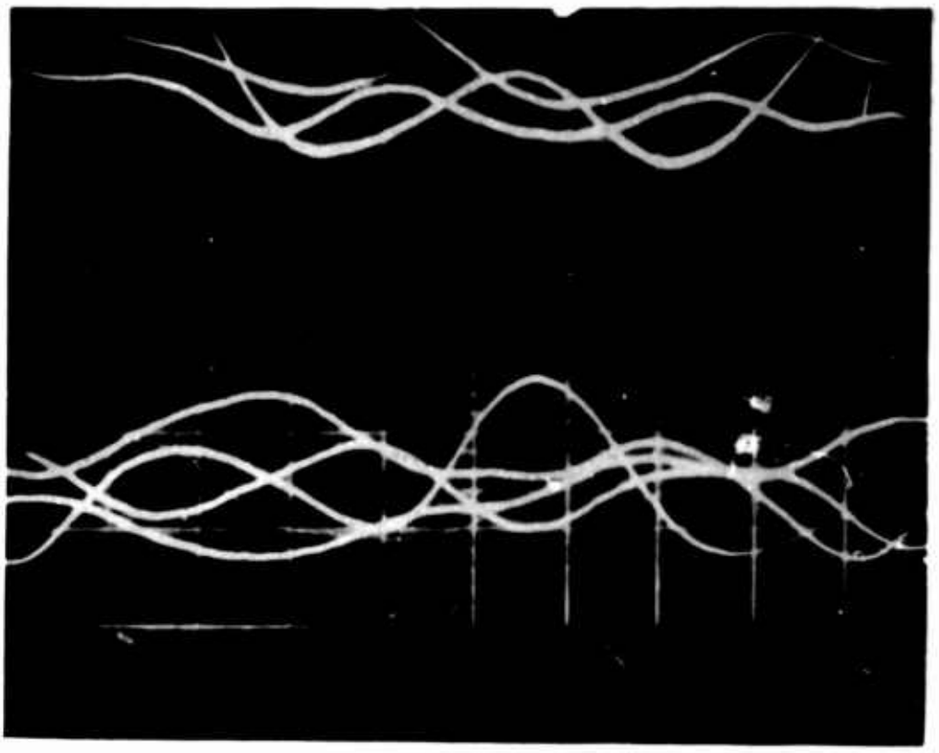

Fig. 47 - Cylinder with splitter plate. Current 10μa. Upper trace from forward position on cylinder. Lower trace from rear of cylinder. 5mv/cm scale. q = 1.0

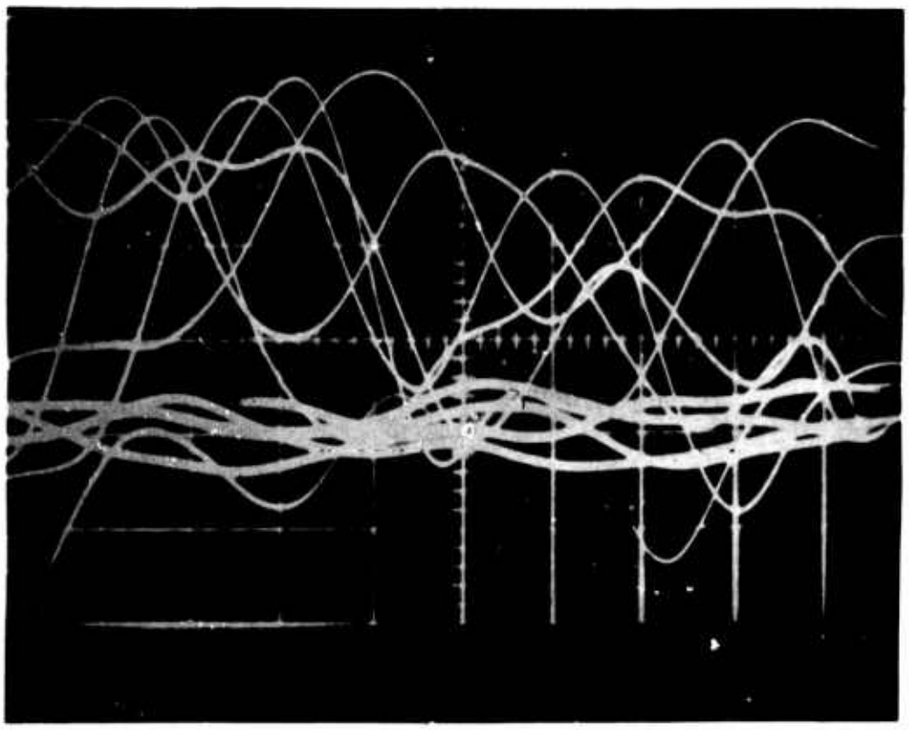

Fig. 48 - Cylinder with splitter plate. Current 10μa. Upper trace from nose cylinder. Lower trace from aft edge of splitter plate. 10mv/cm scale. q = 2.0

Next, tests were run with a flat plate mounted in the 7 x 10 wind tunnel using the same corona wire and field shaping electrodes. The arrangement can be seen in Fig. 49. Collecting electrodes were provided on the surface of the plate by using conducting silver paint as described previously. The electrodes were strips 1/2 inch wide, 1/3 inch apart and twelve inches long. Each was grounded through a 12-megohm resistor. The plate was aligned parallel to the stream and for a tunnel q of one the following pictures of flow oscillation were obtained, as shown in Fig. 50. The top trace in Fig. 50 illustrates the oscillation in flow four inches aft of the leading edge. The oscillations may indicate the possible presence of a separation bubble near the leading edge. The next trace from a strip 1-1/2 inches aft of the first trace, although it shows excursions, does not show significant oscillations. The remaining traces located along the plate to a position approximately 30 inches aft of the leading edge are relatively smooth in appearance.

All the foregoing traces were made with an electrical filter which filtered out all frequencies above 15 cps. Several attempts were made to locate boundary layer characteristic oscillations of the Tollmein-Schlichting type or the turbulence after transition. Unfortunately, the high frequency noise in the electrical measuring equipment was too great and no useable data were obtained on high frequency oscillations in the flow.

Initial tests were also conducted on an NACA 0012 airfoil in the Army Aeronautical Research Laboratory wind tunnel. A corona wire and field shaping electrode similar to that used previously were mounted in front of the airfoil. Collecting electrodes were located on the surface of the blade and consisted of painted silver on a plastic sheet in a manner similar to that used on the flat plate. The airfoil used was a 8-3/8 inch chord helicopter tail rotor blade and was mounted vertically from the floor of the wind tunnel. The angle-of-attack of the airfoil could be varied and the corona wire installation moved with the airfoil. Initial tests at a tunnel q of one, and an angle of attack of zero degrees indicated erratic electric trace behavior for traces near the nose of the airfoil, while the traces along the upper and lower surface were generally smooth. The erratic trace behavior near the nose is a logical subject for further study. When the airfoil angle of attack was raised to values where stall should occur, the traces over the "upper surface" leading edge showed some irregularity, but aft of the 50% chord the upper surface trace oscillated very widely and erratically indicated the presence of a fully separated flow, that is, "stall" (Fig. 51).

From the limited work accomplished to data on the ion-flow diagnostic technique, it appears that it holds great promise as a velocity or mass flow measuring method, it holds promise in indicating the gross nature of flow disturbances such as potential flow or separation regions, and it holds promise in providing the integrated history

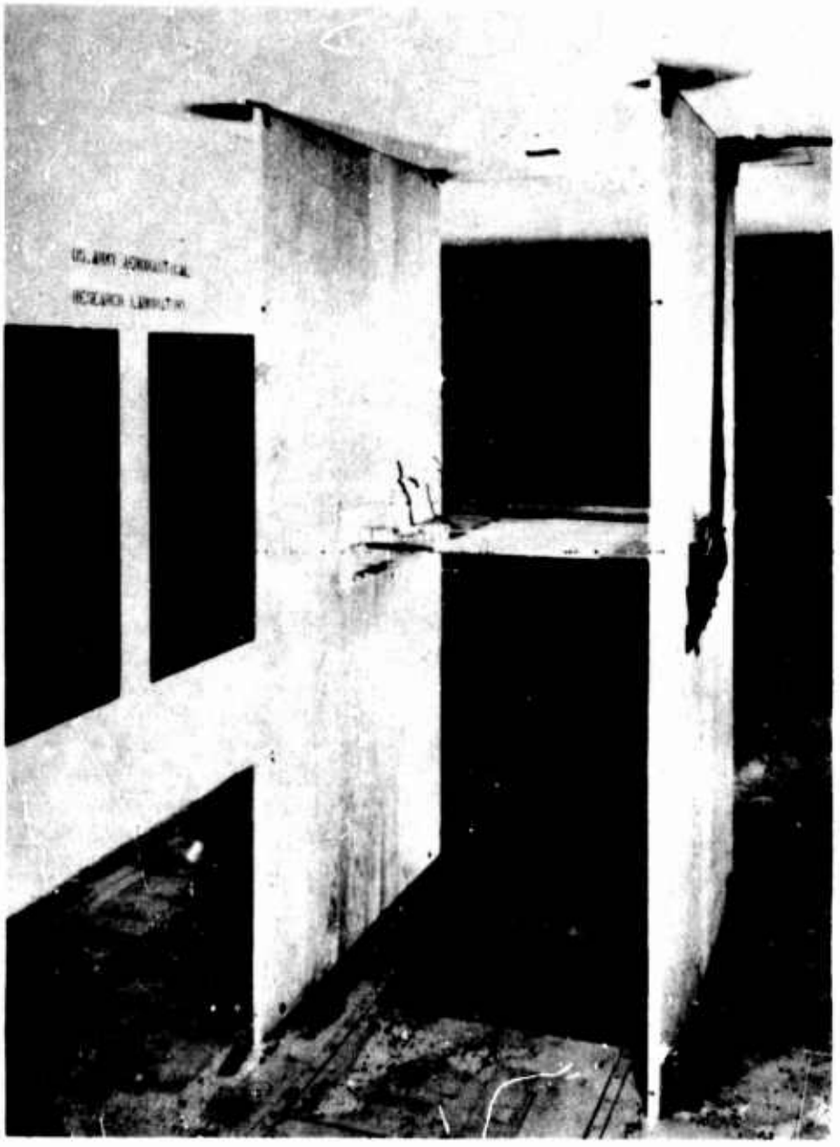

Fig. 49 - Flat plate mounted in 7 x 10 wind tunnel

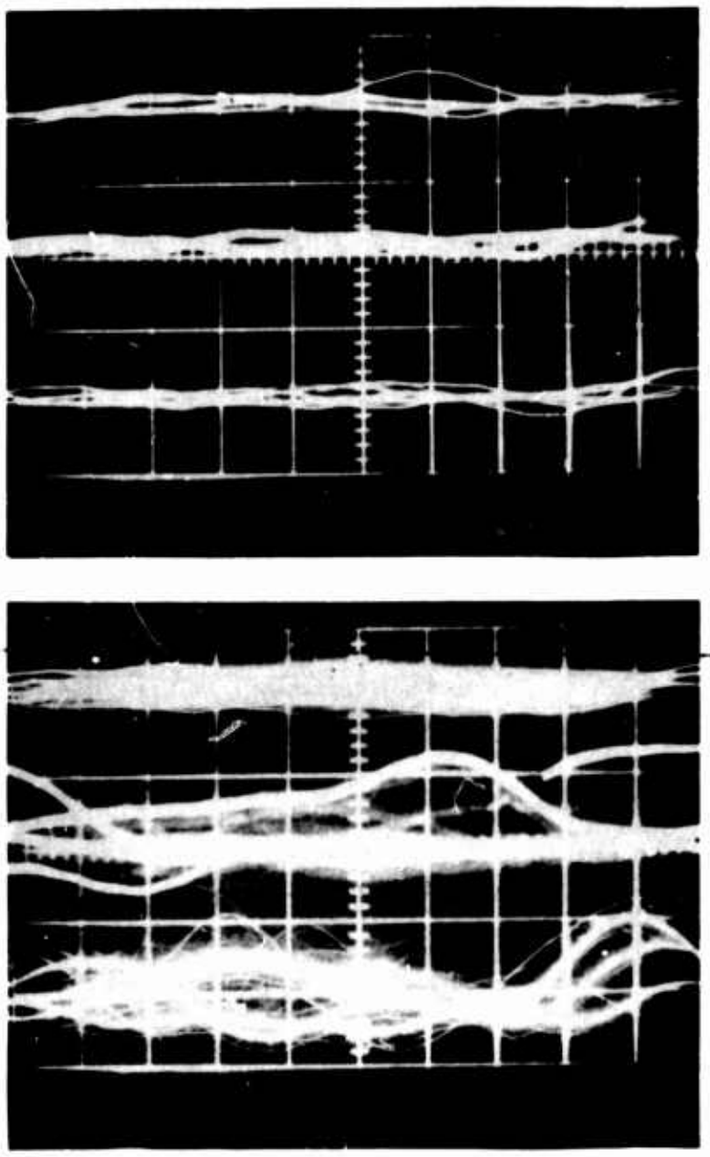

Fig. 50 - Oscilloscope traces from various positions along the surface of the flat plate. q = 1, i = 5μa. Upper trace is four inches back of leading edges. Remaining trace electrodes spaced rearward approximately to 20 inches aft of first trace electrode

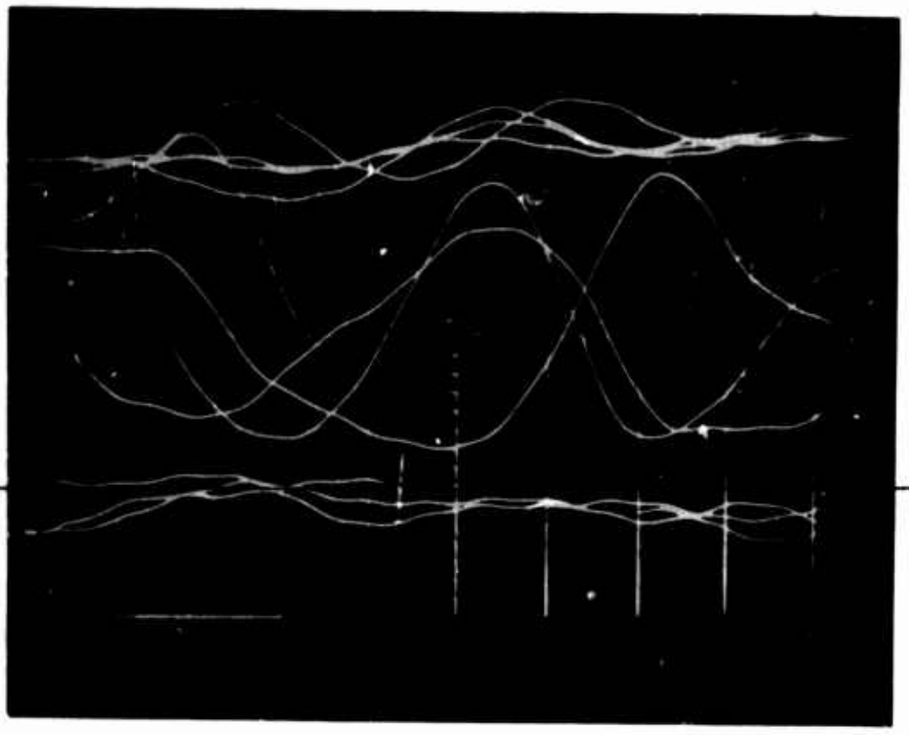

Fig. 51 - Ion-diagnostic traces at rear surface of 0015 airfoil.
Adjacent electrode locations - 5/8 inches apart on surface

of flow along a streamline. With instrumentation available to date, however, it has not been possible to study the details of the boundary layer flow with regard to frequency oscillations above approximately 25 cps.

E. POWER GENERATION

One area of very active interest in electrofluidmechanics is that of electrical power generation. Although this investigator has not personally conducted studies in this area, a brief discussion will be presented for completeness. Power generation with electrostatic is accomplished in a manner similar to the familiar Van De Graff electrostatic high voltage generator. Usually a closed circuit fluid flow is established in a channel. At the high velocity portion of the channel ions are created by a corona discharge. These ions are carried downstream by the high velocity flow against an electrical field. The flow thus does work against (upon) the charges and an electrostatic potential (work per unit charge) is created. Such devices usually develop very high voltages, low currents, and are D.C. in nature. Their primary advantage over the MHD power generators lies in lower temperature requirements in the system. The group under von Ohain at the Air Force Aerospace Research Laboratories has been very active in this area of endeavor.

IV. SUMMARY

The entire area of electrofluidmechanics offers a tremendous challenge to those working in both research as well as applied fluid mechanics. The range of possible interactions is very broad, and seems to be limited only by the limits of the individual investigator. A stringent word of caution is suggested, however, to those who may wish to pursue research in this field of endeavor. The energy density that can be created by an electrostatic field is very small, and co-commitantly the forces that can be developed are very small. If one attempts to obtain high forces with a field, full electrical breakdown will invariable occur. Secondly, the various electrostatic actions tend to occur simultaneously. For example, it is difficult to achieve pure dielectrophoretic action without some pure charge phenomena interacting at the same time, and under such circumstances it is only too easy to misinterpret the results.

It is believed, however, that the foregoing summary of the research that has been conducted does indicate that real opportunity exists for further research and application in the area of electrostatic-fluid interactions.

REFERENCES

1. Landaw, L. D., and Lifshitz, E. M., "Electrodynamics of Continuous Media," Addison-Wesley Publishing Co, Reading, Mass., 1960.

2. Melcher, James, "Field Coupled Surface Waves," Massachusetts Institute of Technology Press, Cambridge, Massachusetts, 1963.

3. Velkoff, H. R., "Electrofluidmechanics, Investigation of the Effects of Electrostatic Fields on Heat Transfer and Boundary Layers," ASD TDR-62-650, Aeronautical Systems Division, Air Force Systems Command, WPAFB, Ohio 1962.

4. O'Brien, R. J., and Shine, A. J., "Some Effects of an Electric Field on Heat Transfer from a Vertical Plate in Pree Convection," Journal of Heat Transfer, Vol. 84, Series C, Nr. 1, Feb., 1967.

5. Franke, Milton, "Effects of Electrostatic Fields on Free-Convection from Plates in Air," Dissertation, Dept. of Mechanical Engineering, The Ohio State University, Columbus, Ohio, 1967.

6. Velkoff, H. R., "The Effects of Ionization on the Flow and Heat Transfer of a Dense Gas in a Transverse Electrical Field," Heat Transfer and Fluid Mechanics Institute Proceedings, Stanford University Press, Palo Alto, California, 1964.

7. Andrade, E. N., and Dodd, C., "The Effect of an Electric Field on the Viscosity of Liquids," Proceedings of the Royal Society of London, Vol. 187 (1949), Vol. 204 A (1951), and Vol. 225 A (1954).

8. Elton, G. A. H., and Hirschler, F. G., "Electroviscosity," Proceedings of the Royal Society of London, Series A, Vol. 194, (1948), Vol. 198 (1949).

9. Stuetzer, O. M., "Apparent Viscosity of a Charged Fluid," The Physics of Fluids, Vol. 4, No. 10, Oct., 1961.

10. Velkoff, H. R., "An Analysis of the Effect of Ionization on the Laminar flow of a Dense Gas in a Channel," Air Force Aero Propulsion Laboratory, Report RTD-TDR-63-4099, Wright-Patterson Air Force Base, Ohio, October, 1963.

11. T. Chuang and H. Velkoff, "Analytical Studies of the Effects of Ionization on Fluid Flows," The Ohio State University Research Foundation Report RF-1864-6, Columbus, Ohio, June 1967.

12. Velkoff, H., Chuang, T., and Pejack, E., "The Electrically Induced Instability of a Fluid Contained between Two Concentric Cylinders," Submitted to Journal of Fluid Mechanics, July 1968.

13. Chandrasekhar, S., "Hydrodynamic and Hydromagnetic Stability," Oxford University Press, London, 1961.

14. Rossow, V. J., "On Flow of Electrically Conducting Fluids over a Flat Plate in the Presence of a Transverse Magnetic Field," NACA Report TN 3971, May, 1957.

15. Godfrey, R, and Velkoff, H. R., "An Interferometric Study of the Effects of Corona Discharge on the Temperature Profiles on a Flat, Uniform Temperature Plate in Forced Convection," The Ohio State University Research Foundation Report RF-1864-4, Columbus, Ohio, June, 1967.

16. Ketcham, J, and Velkoff, H. R., "The Effect of an Electrostatic Field on Boundary Layer Transaction," Technical Note AIAA Journal, June 1968.

17. Eiler, G. P., "An Experimental Investigation of the Influence of Electrostatic Fields on Flow Attachment," The Ohio State University Research Foundation Report RF-1864-1, Columbus, Ohio, Aug., 1966.

18. Velkoff, H. R., and Bishop, J., "A Study of a Corona Wind Digital Fluid Amplifier Element," The Ohio State University Research Foundation Report RF-1864-3, Columbus, Ohio, March, 1967.

19. Bonjour, E., Verdier, R. L., and Weil, L., "Electroconvection Effects on Heat Transfer," Chemical Engineering Progress, Vol. 58, No. 7, 1962.

20. Markel, M., and Durfee, R. L., "The Effect of Applied Voltage on Boiling Heat Transfer," Atlantic Research Corporation Technical R eport, Alexandria, Virginia, 1962.

21. Choi, H. Y., "Electrohydrodynamic Boiling Heat Transfer," T.U.M.E.R. 62-3, Tufts University, Boston, Mass., 1962.

22. Velkoff, H. R., and Miller, J., "The Effect of an Electrostatic Field on the Condensation of Vapor," Air Force Aero Propulsion Laboratory, Report RTD-TDR-63-4008, WPAFB, Ohio, Feb, 1964.

23. Choi, H. Y., "Electrohydrodynamic Condensation Heat Transfer," Journal of Heat Transfer, Vol. 90, Series C, Feb., 1968.

24. Velkoff, H. R., and Miller, J., "Condensation of Vapor on a Vertical Plate with a Transverse Electrostatic Field," Journal of Heat Transfer, Vol. 87, Series C, May, 1965.

25. Pejack, E., and Velkoff, H. R., "Effects of a Transverse Electric Field on the Characteristics and Heat Transfer of a Diffusion Flame," The Ohio State University Research Foundation Report RF-1864-8, Columbus, Ohio, Nov., 1967.

26. Donnelly, R. J., "Experiments on the Stability of Viscous Flow Between Rotating Cylinders, V. The Theory of the Ion Technique," Proceedings of the Royal Society of London, A, Vol. 283, p. 520, 1965.

27. Durbin, E. J., and Vause, C. R., Unpublished Studies at the U.S. Army Aeronautical Research Laboratory, Ames Research Center, Moffett Field, California, 1968.

28. Chuang, T. H., and Velkoff, H. R., "Effect of Fields on Heat and Mass Transfer to a Subfreezing Surface," The Ohio State University Research Foundation Report RF-1864-9, Columbus, Ohio, September, 1968.

Unclassified

Security Classification

DOCUMENT CONTROL DATA - R & D

(Security classification of title, body of abstract and indexing annotation must be entered when the overall report is classified)

1. ORIGINATING ACTIVITY (Corporate author)
The Ohio State University Research Foundation
Columbus, Ohio

2a. REPORT SECURITY CLASSIFICATION
Unclassified

2b. GROUP
N/A

3. REPORT TITLE
STUDIES OF THE EFFECTS OF ELECTROSTATIC FIELDS ON FLUID FLOWS

4. DESCRIPTIVE NOTES (Type of report and inclusive dates)
Interim Summary Report - October 1, 1964 - January 31, 1969

5. AUTHOR(S) (First name, middle initial, last name)
Velkoff, Henry R.

6. REPORT DATE	7a. TOTAL NO. OF PAGES	7b. NO. OF REFS
January 1969	90	28

8a. CONTRACT OR GRANT NO.
DA-31-124-ARO-D-246

b. PROJECT NO
2001050B700, 1D12, 40A142

c.

d.

9a. ORIGINATOR'S REPORT NUMBER(S)
Technical Report # 10

9b. OTHER REPORT NO(S) (Any other numbers that may be assigned this report)

10. DISTRIBUTION STATEMENT
Distribution of this document is unlimited.

11. SUPPLEMENTARY NOTES

12. SPONSORING MILITARY ACTIVITY
US Army Research Office - Durham
Durham, North Carolina

13. ABSTRACT

An overall review of studies of electrostatic interactions with fluid flows is presented. Review of prior studies involving ions with free convection, and channel flows is presented along with prior studies of field effects on condensation. The cause of large changes in laminar channel flow with ionization was studied both analytically and experimentally. The changes were determined to result from an electrically induced destabilization of the flow. External ion-flow boundary layer actions were studied and some influence on transition was found. Significant changes to frost formation and flame heat transfer under the action of an impressed E field were found. The possible use of ions injected into a gas stream as a flow diagnostic technique was explored and is considered a very logical area for future exploration.

DD FORM 1 NOV 68 1473

Unclassified

Security Classification

14 KEY WORDS	LINK A		LINK B		LINK C	
	ROLE	WT	ROLE	WT	ROLE	WT
Electrostatic Ion-flow interactions Electric field heat transfer Frost formation Frost formation with fields Electric-flow instability Electrohydrodynamics Electrofluidmechanics Ion-flow diagnostics						

and flow equations is attempted, it leads to a complex nonlinear equation. Another approach based upon the actual experimental problem is possible. It can be assumed that the low velocity flow does not affect the mechanism of the corona discharge materially and consequently the corona charge density can be treated independently from the flow. In addition, because of the length of the channel used in the tests, it can also be assumed that the transverse charge density distribution is essentially constant along the axis of the channel. Figure 10 illustrates the coordinates used.

The current equation along the axis of the channel can be written as:

$$J_z = \rho_c w + \rho_c K E_z \tag{4}$$

The boundary conditions on the problem require that the current path must close in the system and that all charge that leaves the wire must reach the channel wall. This condition requires that no net current flows out of the channel, $i_z = 0$ at the end of the channel. Hence

$$\int_A J_z \, dA = 0 \tag{5}$$

For the cylindrical case the radial current density is given by

$$J_r = i_r / 2 \pi r l \tag{6}$$

Using div $\overline{J} = 0$, for cylindrical coordinates,

$$\frac{1}{r} \frac{\partial r J_r}{\partial r} + \frac{\partial J_z}{\partial z} = 0 \tag{7}$$

and substituting J_r from Eq. (6)

$$\frac{\partial J_z}{\partial z} = 0 \tag{8}$$

since i_r must be a constant.

CORRECTED

4

ROUND TUBE CHANNEL WITH CENTRAL WIRE

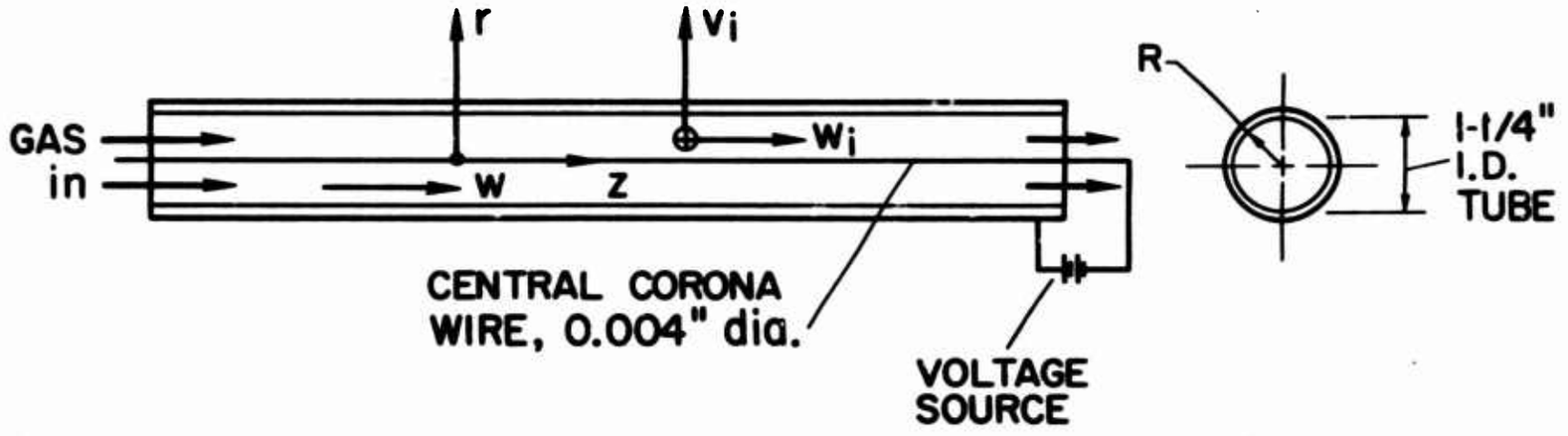

Fig. 10 - Coordinate system for round tube

Substituting Eq. (4) into Eq. (5) results in

$$\int_A (\rho_c w + \rho_c K E_z)\, dA = 0 \tag{9}$$

or

$$\frac{1}{A}\int_A \rho_c E_z\, dA = -\frac{1}{A}\int_A \rho_c \frac{w}{K}\, dA \tag{10}$$

It can be recognized that each integral in Eq. (10) represents the mean value of a function. Hence we can write

$$(\rho_c E_z)_m = -\frac{(\rho_c w)_m}{K} \tag{11}$$

and noting that the electrostatic body force along the axis of the channel is

$$F_z = \rho_c E_z \tag{12}$$

Then the mean value of $\rho_c E_z$ is equal to the mean value of the body force. Substituting into the fluid flow equation for channel flow with a body force one obtains

$$\mu \nabla^2 w - \frac{1}{K}(\rho_c w)_m = \frac{\partial p}{\partial z} \tag{13}$$

Non-dimensionalizing this equation for a round tube,

$$\frac{d^2 w}{d\eta^2} + \frac{1}{\eta}\frac{dw}{d\eta} - \frac{(\rho_c w)_m}{\rho_{c_m} w_m} N_{\rho_c} = N_{Re}\frac{\partial p}{\partial \zeta} \tag{14}$$

where

$$N_{\rho_c} = \rho_{c_m} L^2/\mu K,\ \rho_c^* = \frac{\rho_c}{\rho_{c_m}},\quad \eta = r/R,\ \zeta = z/R,\ W = \frac{w}{w_m}$$

The charge number, N_{ρ_c}, is a new dimensionless parameter which characterizes flow with ionization. It represents the ratio of the charge

CORRECTED

forces to the viscous force in the flow. Assuming the charge density is constant one can solve the equation to get

$$w_m = - \frac{\frac{R^2}{8\mu} \frac{\partial p}{\partial z}}{\left(1 + \frac{N_{\rho c}}{8}\right)} \tag{15}$$

and the friction factor becomes

$$f_D = \frac{64}{N_{Re}} \left(1 + \frac{N_{\rho c}}{8}\right) \tag{16}$$

As a typical case consider the following values, $K = 2 \times 10^{-4}$ m^2/volt-sec, $R = 0.01587$ m, $i = 10^{-3}$ amp, channel length, $\ell = 1.7$ meters, $\mu = 1.783 \times 10^{-5}$ kg/m-sec, then $\rho_{c_m} = 2.5 \times 10^9$ charges/c.c. The charge number becomes

$$N_{\rho c} = \frac{R^2}{\mu K} \rho_{c_o} = 12.$$

This is a surprisingly large value. Substituting this value of the charge number into Eq. (16) it is found that

$$f_D = \frac{64}{N_{Re}} (2.5)$$

Comparison with the data of Fig. 1 reveals that this value of f_D is similar in magnitude to that actually observed during test. Test data for i = 1000 μa, indicate $f_D = 2.1\ (64/N_{Re})$. From Eq. (16) for the mean velocity it is possible to define an effective friction factor.

$$\mu_e = \mu \left(1 + \frac{N_{\rho c}}{8}\right) \tag{17}$$

for the round tube.

Through the use of an expression for viscosity obtained from the kinetic theory it is possible to express the charge number in terms of the Knudsen number. From kinetic theory viscosity can be expressed as

$$\mu = a_1 N m \bar{c} \lambda \tag{18}$$

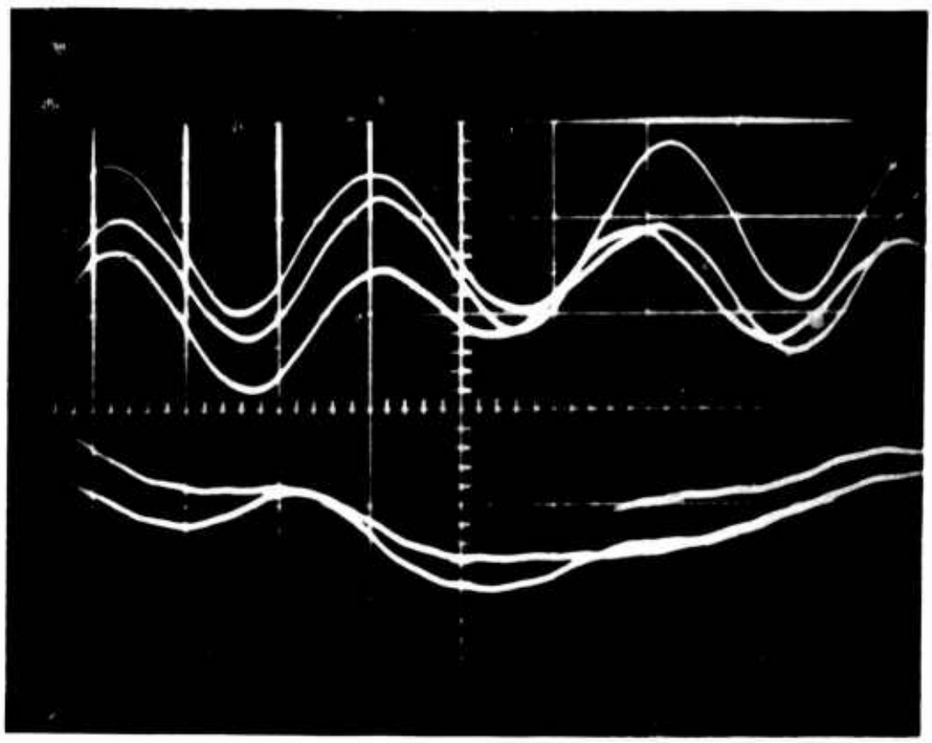

Fig. 45 - Oscilloscope traces. Current 3μa, q = 1. Upper trace from forward side of cylinder. Lower trace from rear of cylinder. Vertical scale 2mv/cm

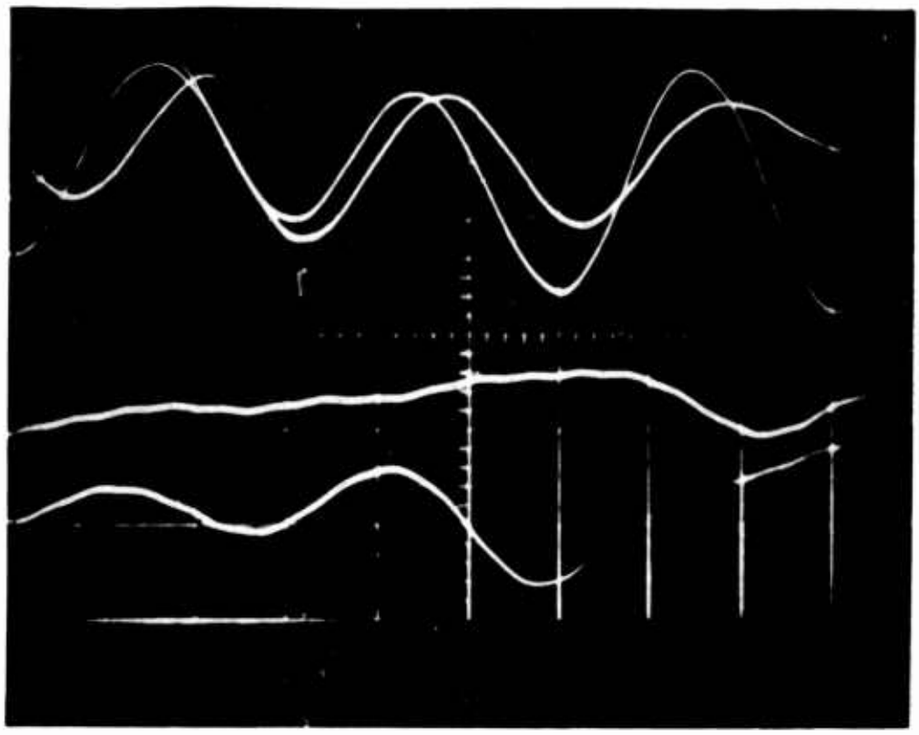

Fig. 46 - Oscilloscope traces. Current 3μa, q = 1. Upper trace just ahead of maximum cylinder width and lower trace just aft. Vertical scale 2mv/cm

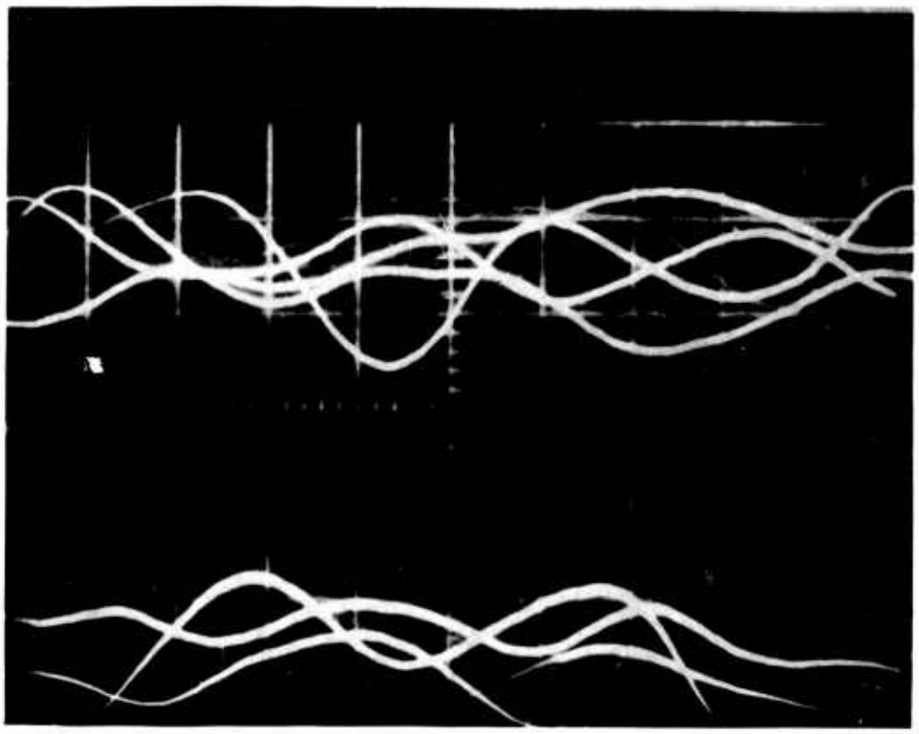

Fig. 47 - Cylinder with splitter plate. Current 10μa. Upper trace from forward position on cylinder. Lower trace from rear of cylinder. 5mv/cm scale. q = 1.0

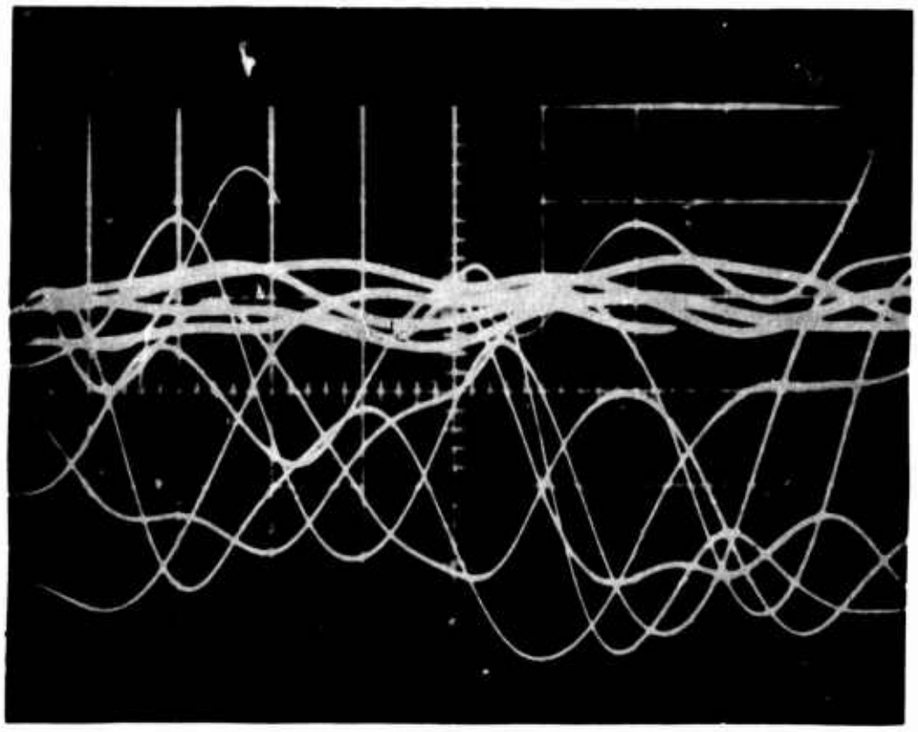

Fig. 48 - Cylinder with splitter plate. Current 10μa. Upper trace from nose cylinder. Lower trace from aft edge of splitter plate. 10mv/cm scale. q = 2.0